Role of toughness in abrasion, and impact-abrasion wear
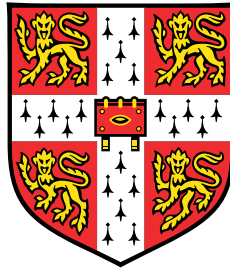
Appa Rao Chintha

Department of Materials Science and Metallurgy
University of Cambridge

This dissertation is submitted for the degree of
Doctor of Philosophy

Darwin College   November 2020

To Swathi . . .

Declaration

I hereby declare that except where specific reference is made to the work of others, the contents of this dissertation are original and have not been submitted in whole or in part for consideration for any other degree or qualification in this, or any other university. This dissertation is my own work and contains nothing which is the outcome of work done in collaboration with others, except as specified in the text and Acknowledgements. This dissertation contains fewer than 65,000 words including appendices, bibliography, footnotes, tables and equations and has fewer than 150 figures.

Some part of the work has been published in the following academic journals:

- Role of fracture toughness in impact-abrasion wear **A. R. Chintha**, K. Valtonen, V.-T. Kuokkala, S. Kundu, M. J Peet, H. K. D. H. Bhadeshia *Wear 428, 430-437* https://doi.org/10.1016/j.wear.2019.03.028

- Metallurgical aspects of steels designed to resist abrasion, and impact-abrasion wear **A. R. Chintha** *Materials Science and Technology 35 (10), 1133-1148* https://doi.org/10.1080/02670836.2019.1615669

<div align="right">

Appa Rao Chintha

November 2020

</div>

Acknowledgements

It gives me immense pleasure to take this opportunity to express my deepest sense of gratitude to my supervisor Professor Sir Harshad Kumar Dharamshi Hansraj Bhadeshia for his stimulating guidance and encouragement during the research and in composing this thesis. Frequent interactions with him and his 'never say no but prove it' attitude helped me refine my ideas. His sense of humour and cycling activities with him made me feel comfortable in the group.

I acknowledge and sincerely thank Tata Steel Ltd., India, for financially supporting this project. I would also like to acknowledge and thank my collaborators Dr K Valtonen, Prof V T Kuokkala for their kind support in facilitating impact-abrasion wear in Tampere University. My special thanks to Dr Chiradeep Ghosh and Dr Subrata Mukherjee for their help in conducting experiments in India.

I am particularly grateful to Dr T. Venugopalan, former Technical adviser to the Managing Director, TATA STEEL, for keeping his faith in me. My journey to the best university in the world would not have been possible with out the help and support of Dr Sanjay Chandra, ex-Chief, R&D of TATA STEEL. I express my sincere gratitude to him. I am greatly indebted to Dr Saurabh Kundu, Chief of Product group, R&D, TATA STEEL, for his valuable suggestions. Many thanks to Dr Monideepa Mukherjee for her guidance in pursuing Ph.D.

I wish to thank the technical staff of the Department and faculty members for their encouragement and support throughout the study. My special thanks to Ms. Mary Vickers for her guidance on analysing the XRD spectra. My sincere thanks to Dr Giorgio Divitini, Mr Andrew Moss, Mr Simon Griggs and Mr Chris Dolan for their assistance in using the sophisticated characterization equipment. I also thank Mr Paul Stokes and Ms Susan Rhodes for their help in processing samples.

I am very grateful to past and present members of the PT group. I would like to thank Mathew Peet, Steve Ooi, Subhankar Das Bhakshi, Chris Hulme-Smith, Wilberth Solano, Arunim Ray, Guo Lei, Neel Bhattacharya, Joachim Dias, Zixin Huang, Gebril M. A. M. El-Fallah, Shaumik Lenka, Ailsa, Wendy, Dominik and

Abstract

Despite the significant progress in understanding the wear mechanisms and associated factors, steels for components susceptible to wear are developed primarily based on their hardness. The hardness often is achieved by martensitic transformation. Increasing the carbon concentration and substitutional solute content may also help. Hardness certainly helps to improve the wear properties, but it is known in the context of lifting and excavation equipment that other properties, such as toughness, may also play a role. In any event, it always is necessary to optimise a basket of properties rather than a single parameter, because the manufacture of a component requires a combination of performance criteria.

It also is clear that a variety of microstructural features can influence the overall wear properties, although the results are not quantitative and the relationships claimed can be uncertain.

The aim of work presented in this thesis is to study of role of toughness in increasing wear resistance in impact-abrasion conditions, in an experiment that, for the first time, decouples toughness from microstructure- and hardness-induced effects.

The relevant literature has been critically examined to highlight the roles of properties other than hardness, such as fracture toughness, the work hardening rate and microstructural considerations in determining wear resistance of steel.

In the work presented in the thesis, a remarkable new steel has been studied to reveal the role of toughness on a particularly dramatic wear scenario involving both abrasion and impact. The steel has very high toughness, $(72.0 \pm 1.5)\,\mathrm{MPa}\sqrt{\mathrm{m}}$, and yet is hard, 561 ± 23 HV. The same steel was heat-treated to produce another variant with poor toughness but similar microstructure. It is demonstrated with clarity that the toughness becomes incredibly important in impact-abrasion, though not during abrasion on its own. The steel with high fracture toughness performed better during impact-abrasion wear tests compared to the other variant with poor toughness but high hardness and similar microstructure. Detailed microscopy and other characterisation techniques have revealed explanations for these observations. Based on the laboratory

test results, full scale trials were undertaken in an integrated steel plant and the performance of a novel steel has been satisfactory thus far.

Table of contents

List of figures

List of tables

Chapter 1

Introduction

Abrasive wear is a complex phenomenon because it is not an intrinsic material property, but depends on the tribo-system which includes a solid in relative motion with the other component and the environment in which the system is being operated [1, 2]. Although there is a huge volume of research to prove that hardness alone will not increase abrasion wear resistance monotonically, hardness is the key parameter used to market various commercial abrasion-wear resistance steels [3–10]. Loss of material depends on the failure mechanism during wear and hence microstructure must play a role in determining wear resistance as it is influential on all the mechanical properties. For example, steels with different microstructures have similar wear resistance despite a large difference in their hardness in three body abrasion wear tests [11].

Nevertheless, the rationales for a particular microstructure or a combination of microstructures and mechanical properties to determine the wear resistance are inconclusive. For instance during abrasive wear, removal of material from the surface takes place when the strain on the surface reaches a critical value. The local fracture strain may be achieved by a single or multiple abradant strikes at the surface. While some material is being removed from the surface, material beneath the surface deforms plastically [12]. It therefore can be expected that steels with high fracture stress and work hardening rate should have a high wear resistance. Therefore, a microstructural combination that can withstand not only the high stresses, but also plastic flow, should increase wear life. For example, it is established that in rails, the work hardening capacity plays a key role in determining the wear rate in pearlitic steels and hence they perform better than martensitic steels with superior hardness [6]. Triaxial stress conditions are common in field applications so the material may also experience other damage mechanisms such as impact, fatigue, high strain rate loading. Hadfield steel

has excellent high wear resistance due to its high work hardening capacity. But when used for ore crushing in which the crusher liner suffers impact-abrasive wear, it has a short service life [13]. Impact wear resistance requires not only high work hardening capacity and fracture stress but also toughness.

Another challenge in developing abrasion wear resistant steels is in cheaply producing the steel on conventional hot rolling mills using the existing process of hot rolling and a separate heat treatment. A further challenge is weldability for the manufacture of mining equipment. Therefore, an in-depth study is required to understand the role of various microstructural combinations on increasing wear life of steels as well as to develop an economical process route to produce weldable, wear resistant steels.

In Chapter 2, a holistic examination of current literature is presented for the identification of factors such as phases, grain size, various mechanical properties other than hardness, and alloy composition to assess how a combination of microstructure and mechanical properties which affect a specific alloy's wear resistance in a given tribo-environment.

Based on the conclusions of the critical review, a novel alloy, which is extremely tough and hard, has been identified to study its wear resistance under complex wear conditions as in impact-abrasion. The alloy selected for this study, experimental methods and characterization techniques are described in Chapter 3 and 4.

The role of fracture toughness in impact-abrasion and its wear mechanism are explained in Chapters 5 and 6, respectively. For comparative study, abrasion tests were carried out and the results are described in Chapter 7. Based on the outcome of these studies the alloy was taken to address one of the perennial problems in an integrated steel plant. Its application at plant level and performance are described in Chapter 8. Finally, general conclusions and suggestions for future work are given in Chapter 9.

Chapter 2

Scientific background: Steels for abrasion, and impact-abrasion wear resistance

Wear and tear are familiar to most people in their everyday lives. Wear can be defined as a process of removal of material from the surface of a solid when it is in contact and in relative motion with respect to another object, be it a solid or liquid [2]. Alternatively, as damage to the surface of a solid when it is in motion relative to another substance. The damage can be either displacement or loss of material from a surface [14].

A study as long ago as 1803 dealt with the of wear of gold coins to understand whether the softness of the coins determines their susceptibility to friction during economic transactions [15]. In 1833, a simple experiment established that hard metals have less friction and hence lower wear [16]. In the same study, it was stated that steel has a remarkable capacity to harden, and hence should 'render it preferable to outperform every other substance yet discovered in reducing the friction of delicate instruments'. It was well-recognised even in those days that wear involves contact between at least two substances, so the behaviour of steel rubbing against ice would be different from when it abrades against brass. In other words, wear is not an intrinsic material property, and the environment in which it occurs must also play a role [1, 2].

Though the wear damage rarely results in catastrophic failure, it reduces operating efficiency and the economic loss can be huge [2]. For example, displacement of material on the surface of a component changes its dimensions and results in misalignment and vibrations of the equipment [17]. According to one estimate, the cost due to wear can be as high as 4 per cent of the gross domestic product of an industrialised country

[18]. Typical values due to wear in various mining activities are given in Table 2.1. The figures are for the USA but may be representative of the general scenario. It is clear from Table 2.1 that wear features prominently in ore processing operations of the mining industry.

Based on the damage mechanism, wear can be classified broadly into (1) adhesive; (2) abrasive; and (3) other forms which include, impact, fretting, fatigue and corrosion [19]. Abrasion wear is commonly observed in mining, lifting and excavation industries where it contributes to about 60% of total wear losses [20, 21]. In these industries, steels are used extensively as wear resistance material due to their availability, ease of manufacturing and phase transformation that can be exploited to control mechanical properties and microstructure.

Table 2.1 Annual wear economic consequences of various industrial activities. Reproduced from [20].

Industry	Operation	Loss mass[a] 10^6 MW h
Mining	Ore processing	6.68
	Surface mining	3.89
	Shaft mining	3.14
	Drilling	1.64
Agriculture	Tillage	4.94
	Planting	0.73
Primary metals	Hot rolling	4.19
	Cold rolling	0.04

[a] Assumes 5.62 MW h per ton of energy represented in lost weight of steel.

2.1   Types of wear

In general, all wear processes involve one or more wear mechanisms. Important wear types and their mechanisms are described in the following section.

2.1.1   Adhesive wear

Adhesive wear takes place when two bodies are pressed together, with resulting normal or shear forces. Surfaces are never smooth and contain asperities, which can weld when bodies come in contact. Subsequent fracture of these bonded asperities generates wear debris on continued relative motion, as illustrated in Fig. 2.1. It can been seen
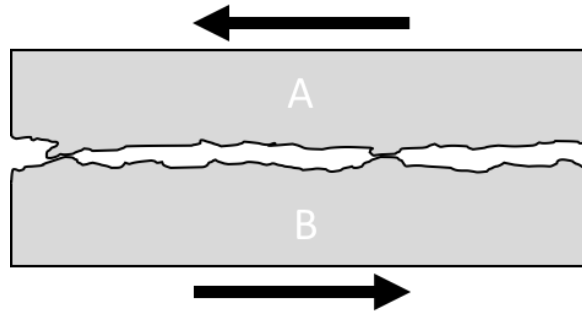
Fig. 2.1 A schematic illustration of adhesive wear, reproduced from [21].

that the asperities of bodies 'A' and 'B' are bonded at two regions and on further motion results in plastic deformation and finally breakage of the asperities from the surface. New asperities of the bodies come into play after the existing asperities have formed wear debris. The wear of bicycle brakes is a good example of adhesive wear. This type of wear can also take place in planar bearings when they are inadequately lubricated [21].

Mechanism of adhesive wear

Adhesive wear is one of the less understood wear phenomena. Several possible mechanisms can explain the detachment of asperities. Shearing can occur at the contact interface and also where the asperities are bonded. According to Archard, the asperities can just slide without any removal of material when the bonds between them are weak [22]. Such sliding leaves smooth surfaces. On the other hand, the asperities may break from the original surface due to frictional forces and resistance due to other asperities. Based on these assumptions, an empirical model was developed by Archard to estimate the loss of material during adhesive wear [22].

The model considers two surfaces in sliding contact under an applied normal load P. It is also assumed that the contact surfaces of asperities are circular with radius a and hence the area of the contact is equal to πa^2. Some asperities would breakdown under shear force. Now assume that its probability to form debris is K. If debris is formed, its volume would be a half hemisphere ($2\pi a^3/3$), so the wear volume, W per unit sliding distance $2a$ is given by

$$W = K \frac{\text{Volume of the debris}}{\text{Sliding distance}} = K\pi a^2/3 \tag{2.1}$$

It is known that the mean contact pressure at the asperity is equivalent to the surface hardness of the wearing material and is given by

$$H = P/\pi a^2 \tag{2.2}$$

Combining Eq. 2.1 and Eq. 2.2 results in the following classical equation for wear loss prediction

$$W = kP/H \tag{2.3}$$

where $k = K/3$ and is known as a wear coefficient, and $1/k$ is sometimes referred to as "wear resistance". It is evident from the equation that wear loss decreases on increasing the hardness, increases on increasing the load but is independent of the apparent area of the contact.

The assumptions in the model are that only one body wears and that wear particles are equivalent to the size of the asperity contact. In a wear process, there is a probability that asperities of the hard material also removed. The probability of removal at each contact may not be the same. The removal of asperities may depend on other mechanical properties, the microstructure of the materials in contact, the shape of the contact, other particles surrounding the asperities, etc. However, the role of these variables can be incorporated through the constant k or the equation can be modified further based on the experimental results [23].

Though the above equations are based on the phenomenological model and provide some insights on wear mechanism and wear volume estimation, it is not clear under what circumstances wear takes place nor the conditions for sliding which leaves polished asperities. Among various mechanisms proposed in the literature, two are accepted widely with supporting experimental evidence [24–26]. Holm proposed that that wear takes place by the gradual removal of atoms as the two surfaces slide under plastic contact, while Archard argued that lumps of particles form by the fracture of asperities [27]. Both the ideas have been confirmed extensively by experimental observations at different length scales [28, 29].

2.1.2   Abrasion, and impact-abrasion wear

Abrasion involves the removal of material from a solid object when loaded against hard particles which have equal or greater hardness [30]. These particles may originate externally or from debris created by the fracture of asperities. Examples of systems

subjected to abrasive wear include chutes, hydraulic systems with dirt, extruders and rock crushers [25].

Based on the type of contact with hard particles, the wear process can be categorised into two-body or three-body abrasion. In the former case, the hard particles remain rigid while in three-body abrasion they move during the wear process. Polishing a metallic sample on paper impregnated with hard particles (sand paper) is an example of the two-body mechanism, while polishing the metal using a hard particle suspension on polishing cloth is an example of three-body abrasion.

It was found that the wear rates are an order of magnitude less in three-body as opposed to two-body abrasion, because the abrasive particles spend about 90 % of the time rolling on the contact surface without causing much damage and only 10 % of the time in abrading the surface [31].

Shear stresses at the surface for sliding and rolling contact must naturally differ, as shown in Figure 2.2. Two-body abrasion is similar to sliding contact whereas three-body abrasion involves a certain amount of rolling contact as well [32]. Therefore, significantly different wear mechanisms apply in the these two modes of wear.
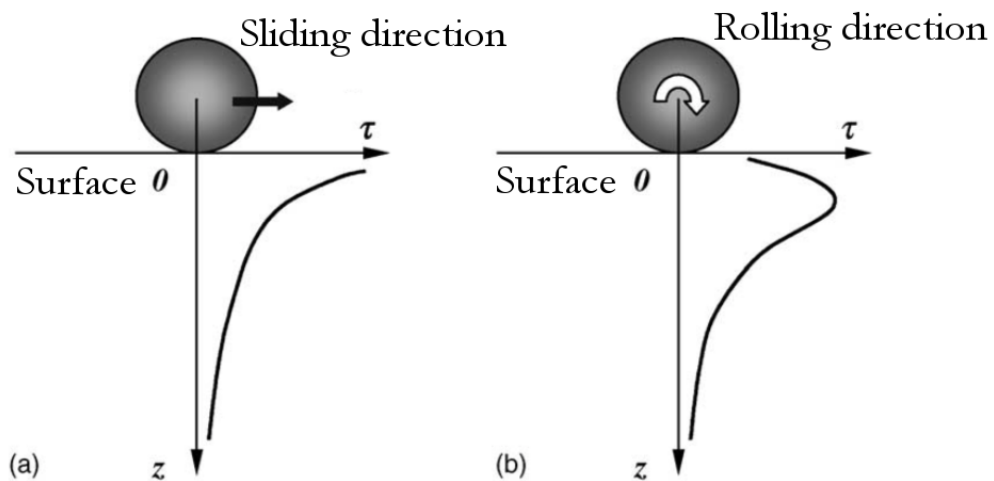
Fig. 2.2 Schematic of the shear stress (τ) as a function of depth below the free surface, (a) for sliding, (b) for rolling particles [33], reproduced with permission of Elsevier.

Other damage can be associated with wear. Corrosion, erosion, fatigue and impact are the common during wear and can accelerate the process. Impact by abrasives occurs in addition to abrasion in the classical lifting and excavation activities common in the mining industries, for example during the loading/unloading of buckets, conveyors, crushers and dump-truck liners [34]. Wear and material loss due to repetitive collision

with abrasives is called impact-abrasion. Under repeated impact, macroscopic spalling and fine-scale surface loss mechanisms occur and the damage can interact with abrasion wear [35]. Impact with an energy as small as 1 J can enhance wear loss in cast iron [36].

(a)   (b)

Fig. 2.3 Transportation of material. (a) The tipper body exposes to impact loading during loading causing impact wear, and (b) the same body exposes to abrasion during off-loading the material causing abrasion wear.

A simple example of impact-abrasion is illustrated in Fig. 2.3 in the context of the loading and unloading of solid materials. Loading of solid material such as ores and minerals, and granite causes impact loads on the tipper body as shown in Fig. 2.3a, while the same body exposes to abrasion damage during the unloading of the material as shown in Fig. 2.3b. Other operations such as digging, drilling and earth moving can be even more complex. Therefore, impact-abrasion wear deserves special attention when steels are designed for such applications.

A great deal of research has been done on the abrasion of metals including steels, important work on experiments, modelling and field tests can be found here [1, 2, 16, 19, 21, 22, 32, 37–48]. However, it has recently been identified that impact-abrasion is a real problem in equipment used in mining, lifting and excavation industries, and it needs to be addressed. The work so far has been devoted mainly on developing and designing of test methods, testing of steels under such conditions, and ranking the steels based on their mechanical properties, mainly hardness [34, 49–53]. There is some work on understanding the role of various metallurgical and microstructural aspects influencing the impact-abrasion wear of steel [34, 54–59]. Before, assessing the published literature on impact-abrasion, it is important to compare and contrast the damage mechanism involved in abrasion, and impact-abrasion.

Wear mechanism in abrasion, and impact-abrasion
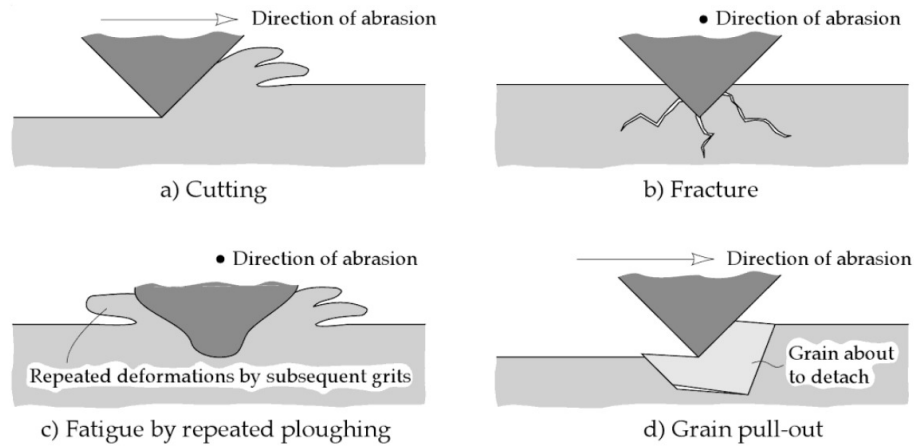
Fig. 2.4 A schematic illustration of mechanisms of abrasion wear: (a) micro-cutting, (b) fracture, (c) fatigue, and (d) grain pull-out [30]. Produced with permission of Elsevier.

Material removal happens in abrasion mainly through ploughing, cutting, and wedge formation or grain pull-out depending on loading, and abrasive properties as shown in Fig. 2.4 [32, 60–62]. Micro-cutting is a classical mode where a hard particle or asperity cuts the softer surface. The material removed as wear debris is proportional to the volume of the groove formed. On the other hand, when the abrading material is brittle, for example ceramics, fracture of the worn surface may take place. However, when the abraded material is ductile, the blunt grit or asperity is unlikely to cut and remove the material in one strike. After multiple strikes the deformed area breaks down due to fatigue. The last mechanism, grain pull-out, takes place in ceramics with weakly bonded grains. Wear in the latter case occurs through a mechanism of delamination [63].

In impact-abrasion, in contrast, abrasive particles impact wear component at different angles from 0 to 90° and also at varying velocities. Near 0°, the damage is abrasion, while at other angles of impact, the material is displaced or removed from the site of the impact depending on the impact energy of abrasives, and properties of the resisting material and abrasives as shown in Fig. 2.5 [49, 64, 65].

In ductile materials such as metals and alloys, material removal is caused by the micro-cutting at an oblique angle of impact and micro-ploughing at normal impact of the abrasives. In brittle materials such as ceramics and high hardness steels, the impacts induce material deformation, crack initiation and propagation which can result in fragmentation as shown in Fig. 2.5. As evident from the foregoing discussion, in
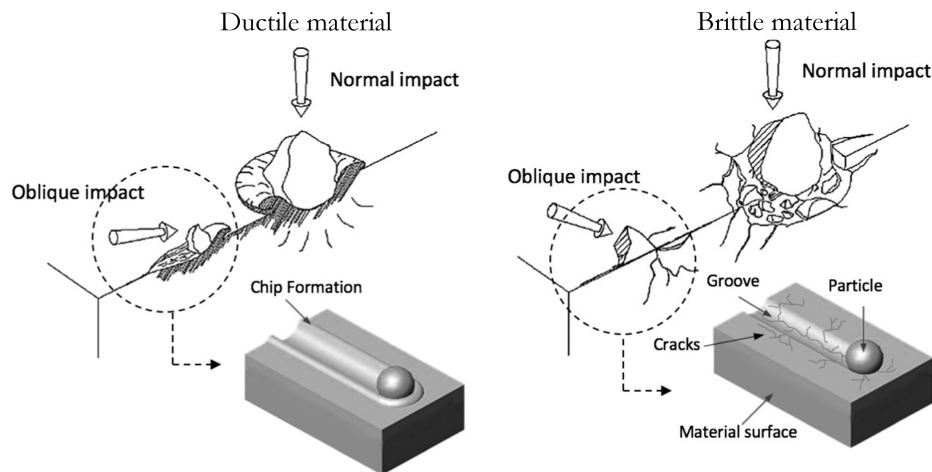
Fig. 2.5 Illustration of impact damage mechanism of ductile, and brittle materials during erosion [64, 65], reproduced with permission of Elsevier.

impact wear, the wear rate depends on impact angle of the abrasive and whether the resisting material is ductile or brittle as shown in Fig. 2.6 when all other parameters are kept constant.

Though mechanisms in abrasive wear, and impact wear in the form of erosion have been studied to a certain extent, the material removal mechanism when they both take place simultaneously is still not clear. The individual roles of abrasion and impact are with respect to the deterioration and material loss from the active surface. For example, Fig. 2.7 shows major differences below the affected surface of abrasion, and impact-abrasion. The cross-sectional microstructure of abrading surface under impact-abrasion revealed a severely deformed sub-surface region. The surface of abrasion wear does not show mixing or craters as in case of impact-abrasion. Heavily deformed material with the presence of embedded abrasive particles can be noticed in Fig. 2.7b [67].

In some applications, abrasion wear resistance may be improved by increasing hardness but to address impact-abrasion, other mechanical properties need to be improved. For example, material tested under only abrasion conditions usually has a strong correlation with hardness, i.e., decrease in wear loss with increase in bulk hardness of the material [51, 68]. However, with impact-abrasion wear the loss data exhibit scatter [69, 70] as shown in Figure 2.8 [70].
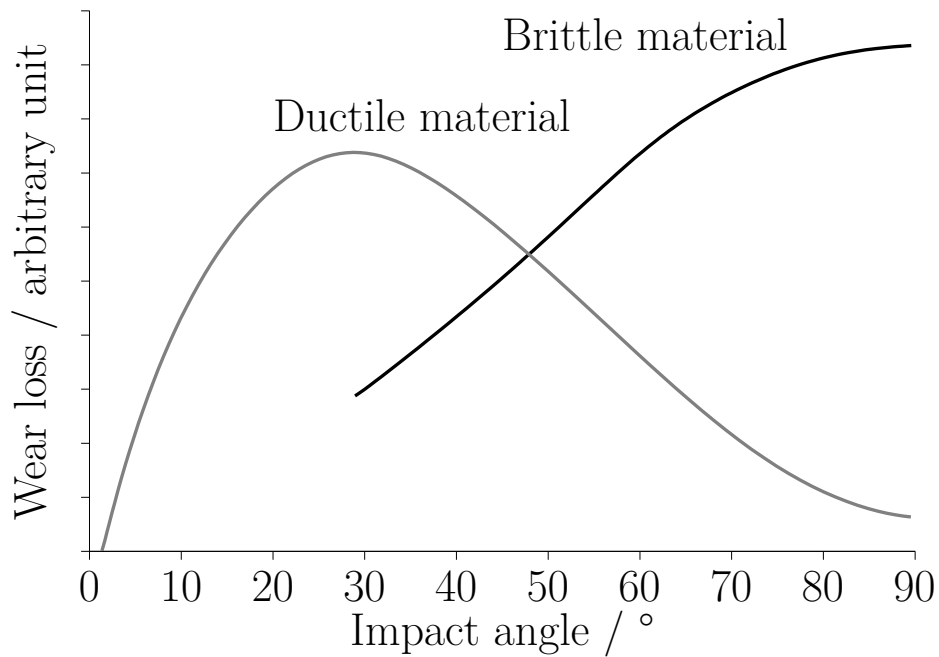
Fig. 2.6 Effect of impact angle on ductile and brittle material, reproduced from [66].

(a) (b)
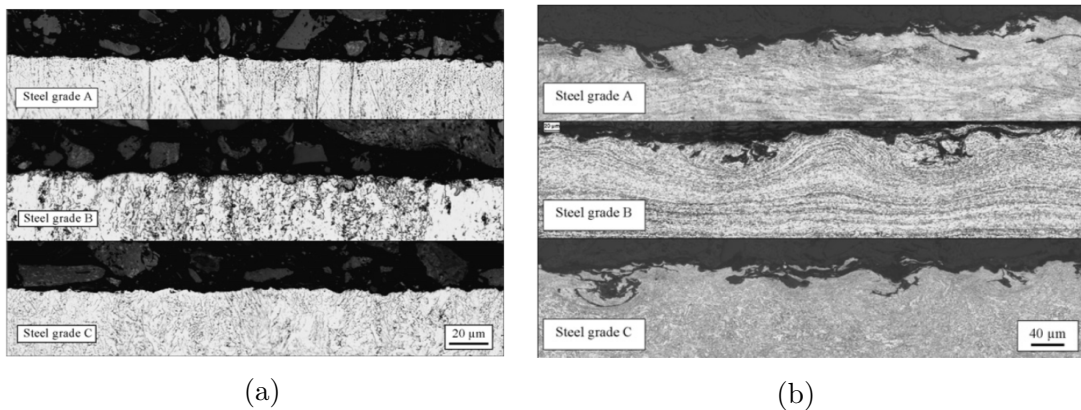
Fig. 2.7 Microstructure of worn subsurface of the steel grades investigated in (a) two-body abrasion, and (b) impact-abrasion. Steel A containing 0.03 wt% C with 190 VHN, steel B containing 0.17 wt% C with 320 VHN, and steel C containing 0.19 wt% C with 390 VHN [67]. Reproduced with permission of Elsevier.

Material removal mechanism in impact-abrasion needs further study.

(a)   (b)
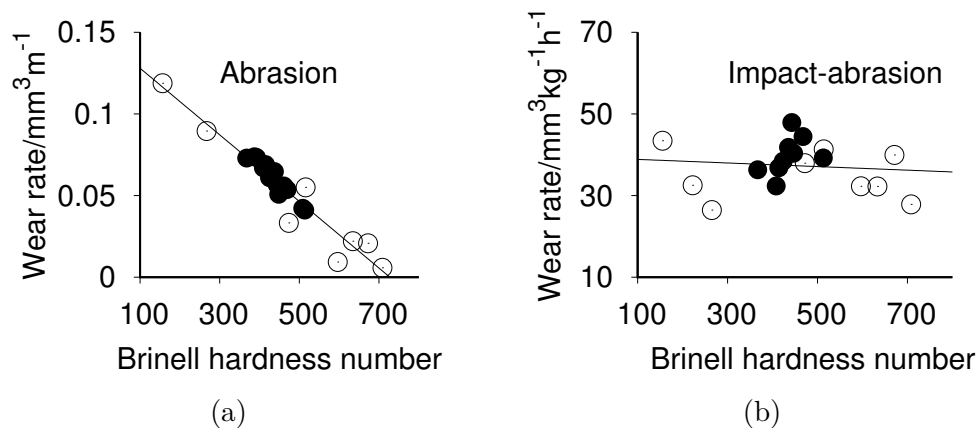
Fig. 2.8 Wear rate as a function of Brinell hardness in (a) three-body abrasion wear test with silica particles of size 200-300 µm. The wear rate is given as a volume loss per unit distance $(\text{mm}^3\,\text{m}^{-1})$, where the abrasion distance is equal to the lineal distance traversed by the rubber wheel during the test, and (b) impact-abrasion in Impeller-in-drum laboratory wear test with high silica quartz particles of size 19-25 mm. The wear rate is given in terms of the volume of material removed in 1 h and for comminuting 2.4 kg of the rock $(\text{mm}^3\,\text{kg}^{-1}\,\text{h}^{-1})$. Linear relationship between hardness wear rate can be noticed in abrasion, while there is no such correlation in impact-abrasion [71]. Filled circles represent commercial wear resistant steel, while open circles represent generic steels like AISI 1040. Reproduced with permission of Elsevier.

2.2   Wear equipment

Components used in mining, lifting and excavation industries are referred as *yellow goods* [72, 73]. The components such as excavator buckets, dumper and truck skips, crushers, demolition claws, auger screw blades and the blades of levelling machines are constantly subjected to wearing work. Low or high alloy martensitic steels, either in the quenched or quenched and tempered condition, are commonly used and identified with their bulk hardness measured on the Brinell scale. For example, HARDOX 400 stands for the steel plate with Brinell hardness number (BHN) 400, while HARDOX is the brand name [73].

There are no internationally approved material specifications for the components. For instance, either HARDOX 400 or HARDOX 500 can be used for any of the components mentioned above. The material is selected based on the wear system. Other than hardness, the components are expected to have impact energy 30 to 40 J at $-40\,^{\circ}\text{C}$ measured using a Charpy-V specimen cut in longitudinal direction of the plate. Welding of the plates is also required during fabrication of components and its weldability measured is in carbon equivalent value (CEV) in wt% as given in Eq. 2.4.

An increase in CEV decreases the ease of welding the plates as susceptibility to cracks in heat-affected zone increases [74].

$$\text{CEV (wt\%)} = \text{C} + \frac{\text{Mn}}{6} + \frac{\text{Cr} + \text{Mo} + \text{V}}{5} + \frac{\text{Cu} + \text{Ni}}{15} \tag{2.4}$$

Fig. 2.9 An excavator bucket used in lifting, excavation and mining industries. The average diameter of such buckets is about 2 m. Courtesy of H. K. D. H. Bhadeshia [75].

A typical excavator bucket used for digging and lifting is shown in Fig. 2.9. For low wear environment and smaller buckets, low hardness (400 BHN) wear resistance steels are used. From the figure it is evident that plates are welded after bending to the required shape and hence bendability is also required for specific applications. Bending to 90° is required for such applications [76].

2.3 Metallurgical aspects of steels designed to resist abrasion, and impact-abrasion wear

2.3.1 Mechanical property-wear relationships

Hardness

Considerable research, as well as field tests, indicate that both abrasion and impact-abrasion wear-rates correlate linearly with hardness [4, 34, 70, 77]. Indeed, commercial steels mostly are developed assuming that wear resistance increases with bulk hardness, Fig. 2.10. However, this may not be the full explanation and it would be interesting to examine the roles of other mechanical properties, microstructure and the steel

composition in determining wear resistance. These relationships may lead to a better insight into the mechanisms involved, and hence the possibility of better steel design [78].
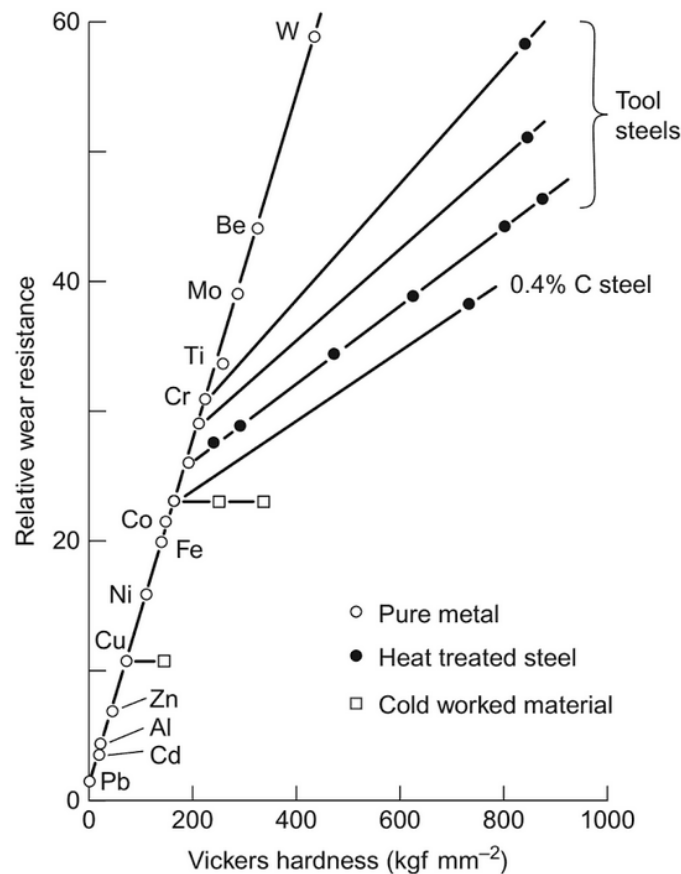
Fig. 2.10 Illustration of relative wear resistance of different materials measured in the pin abrasion test as a function of their bulk hardness [4, 79]. The relative wear resistance is expressed as the ratio of linear wear (change in length of pin) of a standard material to that of the test specimen. A Babbit type lead-tin material was used in this study. Reproduced with permission of Elsevier.

An exaggerated example illustrates the possible role of factors other than hardness – field test data for wear resistance steel tools used in ceramic industry show huge scatter when plotted against hardness, Fig. 2.11 [80]. Similarly, during wet abrasion, Figure 2.12 [81, 82] the dependence of wear on hardness is certainly not linear.

The wear loss data do not show a linear relationship may be due to possible impact loads in the application of the tools. Further, wear rate changes considerably with change in surface hardness. An increase in wear resistance takes place only if there is a sufficient depth of hardening to resist cracking [83]. The ratio of surface hardness
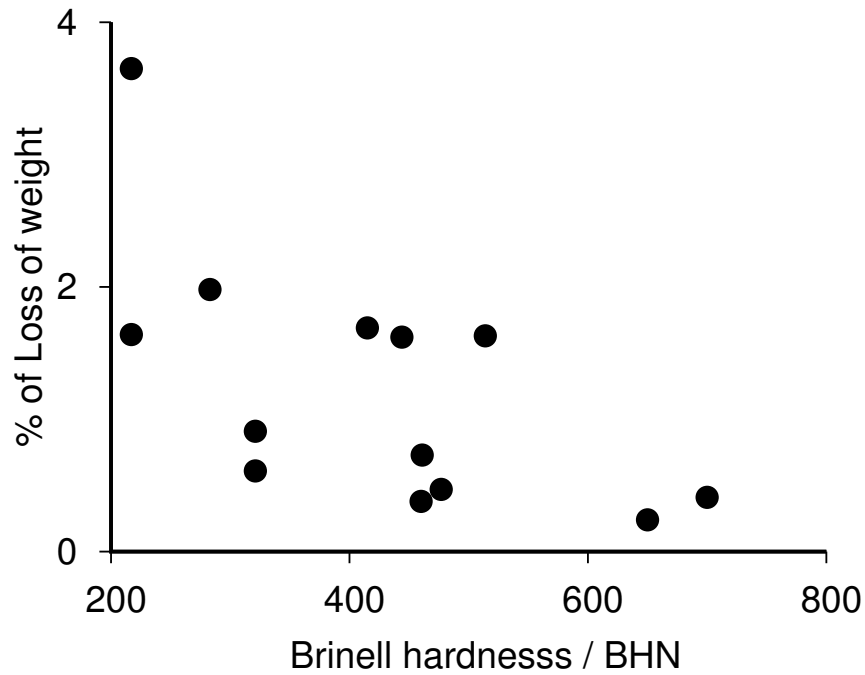
Fig. 2.11 Data for field performance of wear resistance steel tools in ceramic industry. Data from [80].

| (a) | (b) |
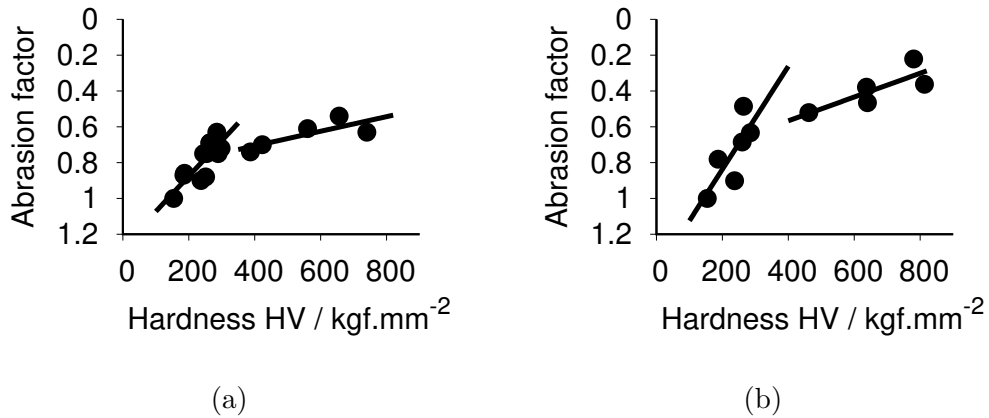
Fig. 2.12 (a) Effect of hardness on abrasion factor in a pot with abrasive and water test, and (b) in test with water jet flow with abrasives. Abrasion factor is defined as wear loss (in grams) of a sample to a reference sample (mild steel). Data from [81, 82].

(H_s) of the wear material to the hardness of the abrasive (H_a) is a rate controlling parameter in abrasive wear. According to Tabor, surface is scratched by an abrasive only when $H_a \geq 1.2 \times H_s$ [84].

The change in wear rate due to the ratio results from a change in the nature of the contact mechanics. At H_s/H_a ratios between 0.6 and 0.8, the fracture mode is dominated by micro-ploughing or cutting due to plastic deformation, while at higher H_s/H_a ratios, the material is removed by fragmentation [18]. However, the increase in surface hardness will increase wear resistance only if the material retains its toughness in the deformed layer [85].

The wear of hard steel subjected to a complex wear environment which involves impact or gouging, correlates badly with hardness [4, 71, 86]. J. Rendón *et al.* tested commercially available steels under purely abrasion and impact-abrasion conditions. Pure abrasion results were found to have strong dependence on hardness, while wear loss in the latter case depended on hardness as well as toughness.

For instance, Miyoshi *et al.* [45] studies on wear loss with hardness in sand abrasion test states that the wear loss decreases with increase in hardness but at decreasing rate. The decrease is small once the hardness exceed 500 VHN which corresponds to about 0.3 wt% C.

Therefore it is evident that the hardness alone cannot increase wear resistance of steels for high impact-abrasion resistance applications which require high hardness components. Wear particles are removed by plastic deformation followed by fracture from the impact/abrading surface and hence other mechanical properties must play a vital role in determining wear resistance of steels of high hardness.

> It is apparent from the totality of results that harder steels in general wear less, but there are diminishing returns once the hardness exceeds about 500 VHN. Why is this?

The commercial steels are marketed based on their BHN, while hardness measurements in scientific reports are mainly VHN as the bulk hardness measured by Vickers machine is independent of applied load [87]. An attempt was made to convert hardness values in different scales to Vickers wherever possible.

Work hardening

In some interesting experiments, Richardson [46] deformed the surfaces of a variety of
materials by shot peening, by wear in stony soil and by burnishing with a tool. His
data are analysed here by plotting the *increment* in surface hardness due to the variety
of deformations, against the initial hardness, Figure 2.13. It is evident in hindsight that
steels that begin hard, harden less during surface deformation, explaining why the wear
rate seems to become insensitive to hardness beyond a certain point. This is consistent
with independent studies, for example a recent study on high-stress abrasion, which
showed that the surface hardness of steels with an initial hardness of 500 to 700 HV
increased to a much lesser degree than when soft, zone-refined steel was deformed [85].
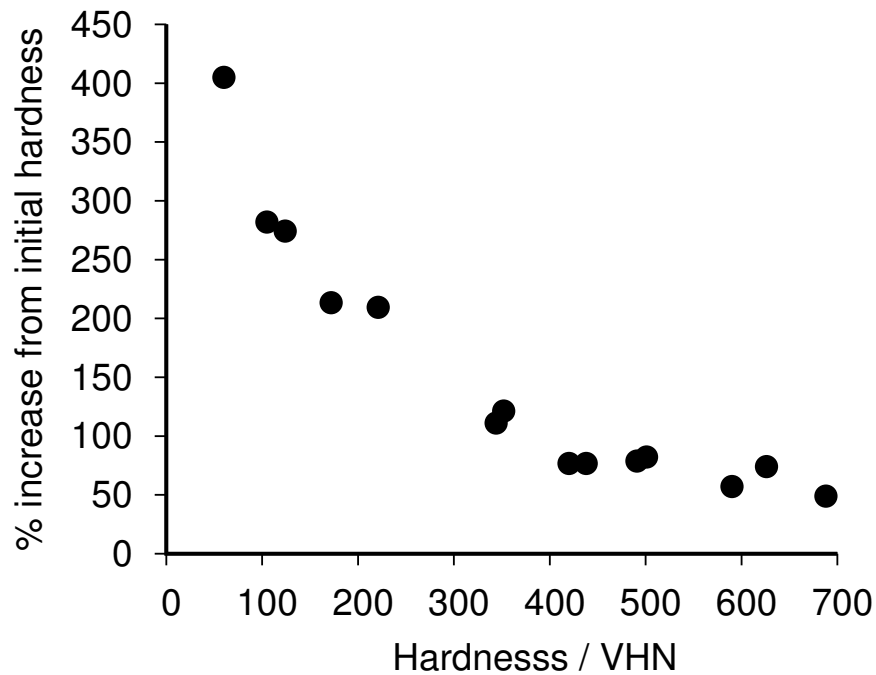
Fig. 2.13 Maximum percentage increase in hardness against initial hardness. Data
from [46].

It is known that a strain-hardened layer increases the ability of the steel to resist
further wear. It has also been reported that that wear resistance correlates better with
abraded surface hardness than with the bulk hardness [46, 88, 89].

> The ability of a steel to work harden is important in enhancing the wear resistance, because it is the surface hardness that determines the interaction between the abrasive and the steel.

Fig. 2.10 may appear to show contradictory results to those discussed above. It seems that in spite of the increase in hardness due to cold working, there is no improvement in abrasive wear resistance. However, this is because the plastic strains involved in the cold-working are much smaller than those associated with abrasion [83]. Similar observations are reported for pure nickel where cold work does not have much of an influence on the wear rate (Table 2.2).

Table 2.2 Effect of cold work on abrasion. Nickel was tested under a normal load of 39.2 N on 60 grit abrasive, Data from [90].

Condition	Hardness / MPa	Wear rate / $\mathrm{m^3\,m^{-1}}$	Hardness after test / MPa
Annealed	870	8.07×10^{-10}	2350
Fully cold worked	2370	8.66×10^{-10}	2370

It is known that retained austenite does play a role in work hardening rate and will be discussed in a later section.

Fracture toughness

Fracture at various length scales is an integral part of most wear mechanisms, beginning with asperities to larger debris formation. It is obvious then that fracture toughness must, in some circumstances, play a role. As pointed out earlier, in very brittle materials such as ceramics, fracture toughness is particularly prominent in determining the wear rate [91–94].

Based on experiments on ceramics and tool steels, a generalised relation between wear resistance, hardness and fracture toughness is given in Fig. 2.14, although it is assumed that the fracture toughness increases monotonically as the hardness decreases. The wear resistance is low either at low or high toughness, with a maximum in-between. It at first increases with fracture toughness in spite of decreasing hardness, presumably because detachment by fragmentation is reduced. Cutting or ploughing dominate at
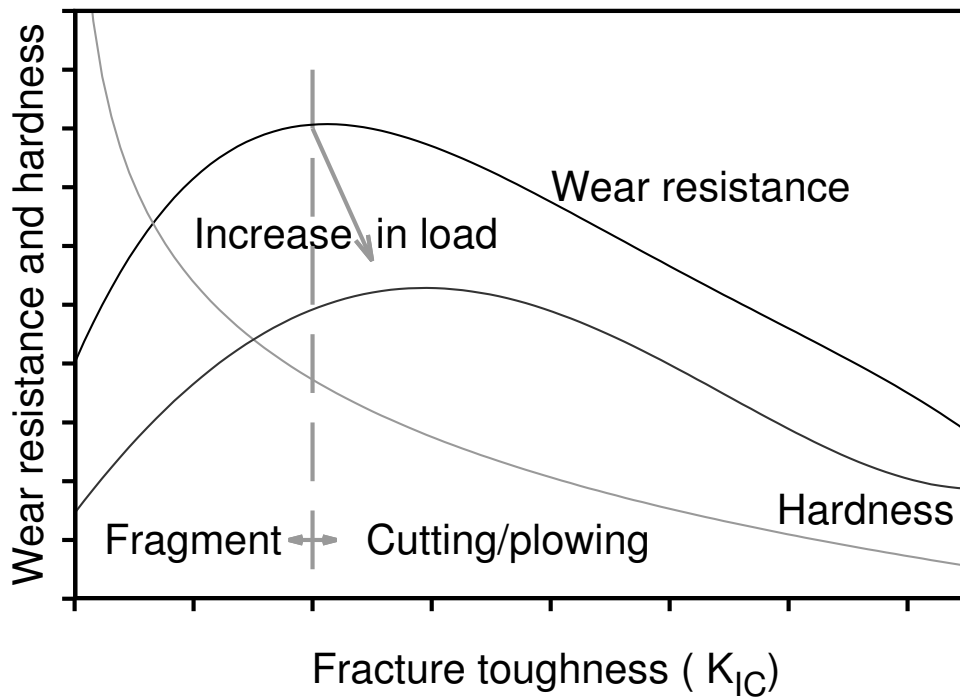
Fig. 2.14 Relation between wear resistance, bulk hardness and fracture toughness of the wear resistance materials [83].

combinations where the toughness is high but the material is soft, again leading to poor wear resistance [95]. Increasing the applied load will of course lead to more rapid abrasion [96]. These trends are consistent with actual data, as illustrated in Fig. 2.15.

Hornbogen modified Archard's model to explain the dependence of abrasive wear resistance on toughness [98]. His model postulates three regimes: I - ductile range where wear takes place by plastic deformation or subcritical crack growth as in high fracture toughness metals in their annealed conditions, II - transition range in which wear rate starts to increase when the critical strain, ϵ_c, of material becomes smaller than the applied plastic deformation ϵ_d, and III - brittle range where the ϵ_d is much larger than ϵ_c.

The wear volume per unit sliding distance ($\dot{V}$), varies with hardness in regimes I & III, but in regime II, toughness plays a crucial role:

$$\dot{V} \propto \frac{W^{3/2}n^2 E \sigma_{\mathrm{y}}}{H^{3/2}K_{\mathrm{IC}}^2} \qquad (2.5)$$
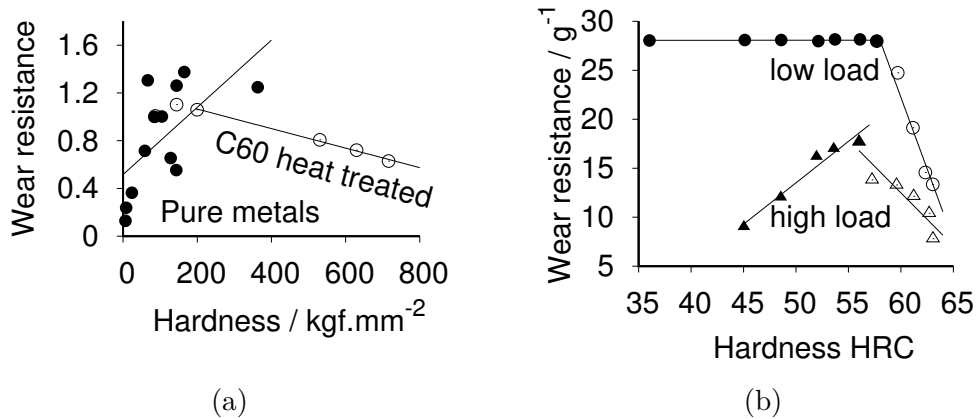
Fig. 2.15 Wear resistance of (a) Pure metals and of steel containing 0.6 wt% C (C60) as a function of material hardness under impact-abrasion conditions at an impingement angle of 90°, (b) Steel with its hardness under two variants of impact energy. Wear resistance in Fig. 2.15a is in relation to Fe. Data from [4, 97].

where E is the Young's modulus, n is exponent of work hardening, σ_y is yield strength, K_{IC} is plane strain fracture toughness, W is the applied load, and H is the hardness of the abrading material.

The model assumes that crack growth determines the wear behaviour in transition range II where fracture toughness play a key role. A sharp contact between an abrasive particle and the substrate would result in an elastic-plastic indentation. Fracture then does not occur until the indentation reaches a critical length. Microcracking occurs above the critical length which increases with fracture toughness [92]. In conventional steels, toughness decreases as hardness increases. It is evident from Fig 2.15a in impact wear that the wear resistance of the pure metals increases with material hardness but it does not apply in the case of hardened steel and in Fig. 2.15b increase in hardness beyond certain value decreases wear resistance.

The model can explain the observations qualitatively in Figure 2.15. However, all mechanical properties of different materials and corresponding wear data are required to evaluate the model quantitatively. Further, the model was developed based on Archard's equation which was based on asperity contacts/junctions and hence further investigation is required to study if the model is valid beyond asperity length scale (order of micrometres), and also under impact loads.

In circumstances where a steel is not too brittle, nor too tough, the wear rate varies inversely with the square of the fracture toughness.

Ductility

Moore *et al.* have shown theoretically that plastic deformation accounts for the major part of the energy absorbed in the abrasive wear of a ductile material [99]. They argued reasonably that the work of creating new surfaces during debris creation is very small and about 10^{-4} times the plastic work contribution. The definition of 'ductile' in this context must therefore mean that the steel is well above its ductile-brittle transition temperature. Another calculation based on conservation of energy reaches a similar conclusion, that around 95 % of the energy during abrasive wear is consumed in structural changes and deformation at the surface [100]. Structural changes include phase transformation, for example that of retained austenite [101, 102]. Uetz *et al.* also argued that plastic deformation consumes major amount of input energy [97].

Indeed, the correlation of wear resistance with hardness can, for a ductile material, be interpreted in terms of ductility alone, as shown in Figure 2.16 [103]. Rendon *et al*[67] also found that the wear resistance of commercial steels tested in abrasion is related to both hardness and strain to fracture.

(a)   (b)
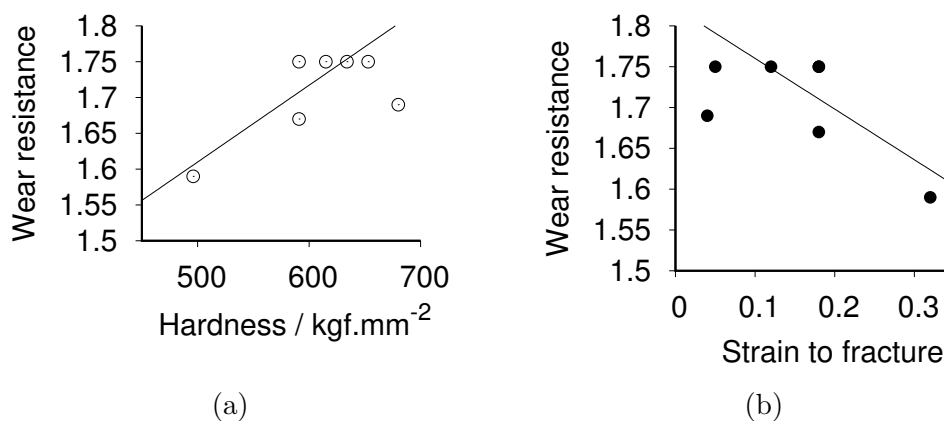
Fig. 2.16 Variation of Two-body wear resistance of D2 steel with its (a) hardness, and (b) strain to fracture [103]. Wear resistance is not strong function of either hardness or strain to fracture. Reproduced with permission of Elsevier.

> It is difficult to identify the independent effects of hardness and ductility with the sort of correlations presented in the literature. A neural network model of the experimental data would almost certainly be more revealing.

2.3.2   Microstructural constituents

Conventional wear resistance steels are mainly medium carbon (about 0.2 - 0.4 wt%) martensitic in either quenched and tempered or auto-tempered condition [104]. Microstructure is one of the key factors in abrasion, and impact wear resistance of alloys as it affects how load influences the wear rate, and changes in subsurface microstructure influences wear behaviour [55, 105–107], but it is difficult to assign an effect of structure that is independent of mechanical properties [108]. For instance, the role of retained austenite on wear resistance is inconclusive as some reports claim improved wear resistance due to work-hardening [56, 109–116], while others show harmful or no effect of retained austenite on wear resistance depending on loading conditions [53, 114, 117, 118].

Its role is important to study because the conventional steels can contain about 10 - 15 % retained austenite. Further, high austenite containing Hadfield steel crusher liners show short service life when exposed to impact wear in the field of ore crushing [119].

The improvement in abrasion wear resistance is related to both the hardening effect of the retained austenite and/or the strain induced transformation of austenite into martensite. Such transformation also leads to compressive stresses at the surface which enhances the local ductility and hence permit the wear surface to achieve higher hardness [110, 115].

In shot peening studies on Hadfield Mn steels, it was shown that surface hardness increased greatly due to formation of refined microstructure at subsurface [120]. In the same study it was found that three-body wear resistance of the steel after shot peening increased when subjected to soft abrasives, but failed to show any improvement when exposed to hard abrasives in two-abrasion wear due to severe plastic deformation caused during the test. It was also reported that in impact wear, material loss increases

under heavy impact energy where wear is caused mainly by plastic deformation as the local ductility improvement due to transformation is small [114].
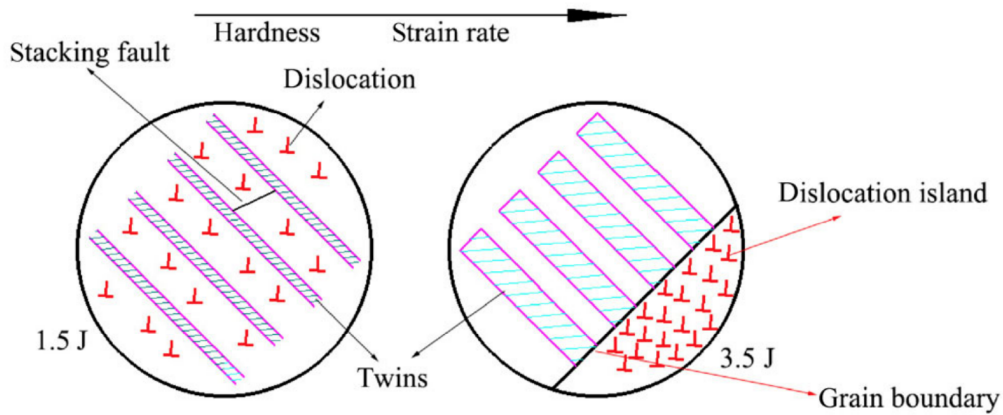
Fig. 2.17 Schematic illustration of formation of twins and dislocation at different impact energies in impact wear [121], reproduced under the terms of the Creative Commons Attribution 4.0 International License.

Increase in hardness not only depends on the amount of austenite transformed but also the work-hardening mechanism. For example, when tested under impact wear, a medium manganese steel showed different hardness values, 467 HV and 579 HV, despite similar amount of martensite produced by two impact loads 1.5 J and 3.5 J, respectively [121]. Lower impact energy caused formation of dislocations cells and fine twins, while at higher energy the density of dislocations increased steeply causing to form islands and wider twins as shown in Figure 2.17. The high dislocation density increases resistance to plastic deformation, while a twin structure cuts the matrix and increases the strength [121, 122]. Therefore, the role of retained austenite in impact-abrasion can be very complex depending on wear component and loading conditions.

However, retained austenite films are special in this context, they are known to have complex interactions with abrasives, by enhancing toughness *during deformation*, and by absorbing load prior to any transformation into martensite [102].

Nanoscale bainite or carbide-free bainite and high toughness martensitic steels have recently become relatively prominent in wear investigations and demonstrated an excellent wear resistance in different types of wear environments [102, 123–134]. The abrasive wear resistance is very high in carbide-free bainitic steels when compared to conventional quench and tempered steels, largely due to the relatively stable retained austenite and the absence of any carbides [102, 124, 135, 136]. It was also suggested

that the increased wear resistance is due to increase in hardness and introduction of compressive residual stresses during decomposition of retained austenite in worn layer [126].

The wear loss is controlled by micro-cutting and ploughing in these steels [135]. While in conventional steels containing carbides, it was observed that the carbides can increase hardness but enhance wear rate by causing disruption of plastic flow during particle impact. The inhomogeneous nature of the plastic flow results in very high strain gradients which can lead to void formation near to and cracking of the carbides [137]. It was also showed that large carbides can also act as abrasive and increase wear rate during abrasion[138]. Therefore, it is possible to increase the wear resistance of the commercially available steels by refining its microstructure and increasing the austenite in the film form.

Carbide-free bainite steels may be future wear resistance steels. However, the challenge is the commercial viability of the mass production of this steel.

Precipitation

Commercial wear resistance steels are produced by quenching followed by tempering. Tempering results in formation of iron carbides and/or other metallic carbides depending upon the tempering temperature and alloy composition. Usually they are tempered below 300 °C to avoid temper embrittlement. Role of precipitation of iron carbides in steels on wear resistance depends on the particle size, morphology, and their hardness. Hard and randomly distributed fine carbides resist micro-cutting more efficiently than the large and low hardness precipitates [139].

For example, in Figure 2.10, precipitation strengthened alloys show no increase in wear resistance with hardness. Abrasion resistance increases if there is an increase in strength at high strains. It is possible with fine precipitation in steel on tempering at low temperature but this is not the case in at high temperature tempering [23, 79]. Abrasive wear resistance of steels with carbon ranging from 0.04 to 1.23 wt% in quenched and tempered (between 300 to 600 °C) did not increase substantially. However, the wear resistance increased when tempered between 20 to 200 °C [23, 140].

Deng *et al.* [141] work on 0.32 wt% C steel in quenched, and then tempered at
different temperatures showed that wear resistance increase if the drop in hardness is
compensated by improved toughness properties at low temperature tempering below
190 °C. However, wear resistance dropped when both hardness and impact energy are
decreased [141, 142].

> Precipitation has limited role in increasing wear re-
> sistance of commercial steels containing 0.25 to 0.4 wt%
> C.

Grain size

Fine grain size in metals increases hardness at low strains but after sufficient strain the
mechanical properties and energy stored during plastic deformation become similar
to that of a large grained material [143]. Work on brass showed that the strain levels
reached at abrading surfaces are extremely high compared with those reached under
conventional cold working processes [144]. Therefore, a change in grain size may not
improve wear resistance [145].

Experimental results of Kashcheev showed no increase in wear resistance with change
in grain size [146]. He proposed that non-strengthened boundaries, and dislocations
walls, as in cold worked metals, with a higher degree disorientation are not effective
against abrasive wear.

However, Sundstrom *et al.* [34] claimed that a decrease in grain size increased
the wear resistance. But when the data are looked at carefully, it seems that the
interpretation is not well founded as the steels compared were of different compositions
and also, the changes in grain size did not correlate with changes in their hardness [34,
147]. Therefore, there is no strong evidence to show that grain size effects abrasion or
impact-abrasion wear resistance.

Nevertheless, the grain size of prior austenite in steel has an indirect effect on wear
resistance. Change of prior austenite grain size from 50 μm to 200 μm changes the
hardness of quenched martensite from 390 to 280 HV in medium carbon steel [148].
Deformed hot-rolled structure exhibit severely pancaked unrecrystallised austenite
grains, which contain deformation bands with increased number of defects such as

sub-grain boundaries, and dislocations cells. These defects ensure a fine martensite structure, consisting of packets, blocks and laths, which are conducive to good toughness since the tendency to crack under load decreases with lath size [149, 150]. It was experimentally proved that decrease in prior austenite grain size decreases the packet size and the block length of transformed and hence strength-ductility combination and toughness were significantly increased by refining packet/block size [150–153].

> Fracture toughness of commercial wear resistance steels can be improved by severe thermomechanical treatment to refine prior austenite grain size and hence increasing their performance under impact-abrasion damage.

2.4   Effect of alloying elements

Commercially available steels for wear resistance are listed in Table 2.3 and in [154], marketed based on their bulk hardness and carbon equivalent (an indication of weldability). These steels are either in the quenched or quenched and tempered martensitic condition with hardness in the range 300 to 550 BHN and carbon from 0.15 to 0.4 wt %. These steels are alloyed with Mn, Mo and Cr for hardenability, Si for solid solution strengthening and microalloying elements like Nb, V, Ti added for austenite grain refinement during hot rolling. Their impact energy is about 20 - 40 J at $-40\,°C$ and this is relevant for low temperature applications.

Medium carbon steels, containing about 0.3 to 0.4 wt% are most commonly used for wear resistance applications possibly due to its weldability and ease of processing in steel plants. It is important that steels produced by thermomechanical processes without any complementary heat treatment make them more cost effective compared with quenched and tempered steels or high carbon carbide-free bainitic steels which require long heat-treatment schedules [34]. However, there are no specifically designed commercial steels for impact-abrasion wear applications.

The narrow carbon range not only helps to have martensite start temperature about $300\,°C$ to develop a heavily dislocated lath martensite matrix with retained austenite interlath films as the second phase [155], but also possible to produce in conventional

hot rolling mills. It was also suggested that microstructure with martensite and finer precipitates enhances wear resistance in steels due to quenched martensite and fine precipitates [156].

Table 2.3 List of various commercially available abrasion wear resistance steels. Composition and CEV are given in wt %

Grade	CEV	C	Si	Mn	P	S	Al	Cr	Mo	B	Ni	BHN / kgf mm^{-2}	YS / MPa	TS / MPa	EL /%	Charpay impact energy / J	Ref.
MAS500 AR	-	0.3	0.7	1.7	0.025	0.015	-	1	0.5	0.005	0.7	500	1250	1450	8	20 at −30 °C	[157]
MAS450 AR	-	0.26	0.7	1.7	0.025	0.015	-	1	0.5	0.005	-	450	1200	1450	8	20 at −40 °C	[157]
MAS400 AR	-	0.25	0.7	1.7	0.025	0.015	-	1.5	0.5	0.005	0.7	400	1000	1250	10	20 at −40 °C	[157]
DUROSTAT 400	0.5	0.13	0.35	1.4	0.02	0.005	0.03	0.5	0.1	0.002		400	1000	1250	10		[158]
DuROSTAT 400	0.55	0.27	0.35	1.2	0.02	0.005	0.03	0.4		0.003		500	1200	1500	8		[158]
AR400		0.2	0.7	1.7	0.03	0.015	0.06	0.5	0.5	0.004	0.4	400	1000	1250	10		[159]
AR450		0.26	0.7	1.7	0.03	0.015	0.06	1	0.5	0.004	0.7	450	1200	1450	8		[159]
AR500		0.3	0.7	1.7	0.03	0.015	0.06	1	0.5	0.004	0.7	500	1250	1600	8		[159]
BISPLATE320	0.4	0.15	0.2	1.1	0.01	0.003		0.2	0.2	0.001		340	970	1070	18	60 at 20 °C	[160]
BISPLATE400	0.4	0.16	0.2	1.1	0.01	0.003		0.2	0.2	0.001		400	1070	1320	14	55 at 20 °C	[160]
BISPLATE500	0.61	0.29	0.3	0.3	0.015	0.003		1	25	0.001		500	1400	1640	10	35 at 20 °C	[160]
BISPLATEHHA	0.61	0.32	0.35	0.4	0.025	0.005		1.2	0.3	0.002		500	1400	1640	14	20 at −20 °C	[160]
DILLIDUR325 L												325					[161]
DILLIDUR400 V												400					[161]
DILLIDUR450 V												450					[161]
HARDOX450	0.47	0.21	0.7	1.6	0.025	0.01		0.5	0.25	0.004	0.25	450				40 at −40 °CC	[162]
HARDOX500	0.49	0.27	0.7	1.6	0.025	0.01		1	0.25	0.004	0.25	500				30 at −40 °C	[162]
XAR300		0.2										300					[163]
XARHT		0.25										350					[163]
XAR400		0.15										400				40 at −40 °C	[163]
XAR400W		0.25										410					[163]
XAR450		0.19										450					[163]
XAR500		0.25										500					[163]
XAR550		0.3										550					[163]
XAR600		0.35										>550					[163]
QUARD400	0.36	0.16	0.6	1.4	0.025	0.01		0.5	0.25	0.005	0.1	400	1160	1300	10	40 at −40 °C	[164]
QUARD450	0.41	0.2	0.6	1.4	0.025	0.001		0.2	0.25	0.005	0.1	450	1250	1400	10	35 at −40 °C	[164]
QUARD500	0.57	0.3	0.8	1.6	0.025	0.01		1	0.5	0.005	1	500	1500	1700	8	30 at −40 °C	[164]
Abrazo																	[165]
RQT																	[166]
SAILMA 450 HI		0.25	0.4	1.5	0.055	0.055	0.01						300	560	20	27 at 0 °C	[167]
ABREX400	0.35	0.21	0.7	2	0.025	0.01		1.2	0.6	0.005	1	360					[168]
ABREX450	0.4	0.23	1.2	2	0.025	0.01		1.5	0.6	0.005	1	410					[168]
ABREX500	0.45	0.35	1.2	2	0.015	0.01		1.5	0.6	0.005	1	450					[168]
ABREX600	0.54	0.45	0.7	2	0.015	0.01		1.2	0.6	0.005	1	550					[168]
ABREX500LT	0.45	0.35	1.2	2	0.015	0.01		1.5	0.6	0.005	1	450				21 at −40 °C	[168]
EVERHARD-C500LE	0.55	0.29	0.55	1.6	0.02	0.01		0.8	0.35	0.004		500	1203	1681	17	21 at −40 °C	[166]

In steels, carbon is the most effective in increasing hardness and hence abrasion resistance. Not surprisingly, the wear resistance of pearlitic steels increases with its carbon content [169, 170]. The rate of increase of wear resistance is low in hypereutectoid steels where networks of carbides can embrittle the steels. Similarly, the wear resistance of quenched martensitic, and quenched and tempered steels also increases with increase in carbon content. The hardness of bainitic steels increases linearly with carbon by about 190 VHN per wt% [171].

Other alloying elements, like Mn, Cr, Mo, B, etc., are added to steel to enhance hardenability so that fully a martensitic structure can be obtained on quenching from the austenite phase field to room temperature. In general the wear resistance steels are produced in thick sections and hence addition of alloying elements are required to increase the hardenability. Though Si is a strong solid solution strengthening element, its addition is restricted to 0.5 wt % to avoid red scale formation during hot rolling [172]. Microalloying elements, Ti, Nb, V are added to control the austenite grain size during hot rolling.
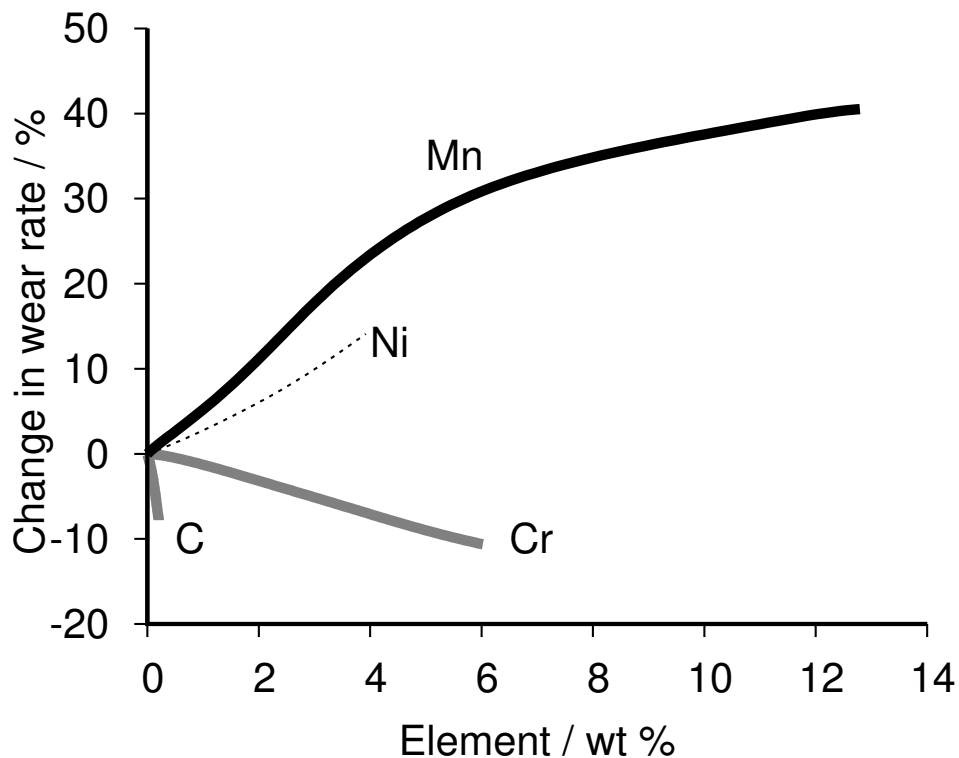
Fig. 2.18 Effect of alloying elements on the wear rate of 1 wt% C steel. Reproduced from [38].

Ojala *et al.* studied 15 commercially available abrasion steels with 400 BHN to understand the role of chemical composition on wear properties. The steels were in the quenched condition with similar amount of carbon, carbon equivalent and alloying additions. Samples were tested using a crushing pin-on-disk wear test. It was found that steel containing high amount of boron and combined Ni and Mo contents performed better than other samples. The wear loss difference is minimum 20 % to the next best sample. However, B is added in very small concentrations that are difficult to control during steel making. Ni increases ductility and toughness while Mo promotes secondary hardening during tempering [104].

Besides microalloying elements, rare earth metals can be added to refine the austenite grain size. Fu *et al.* reported that the addition of rare earth metals improved impact energy and also the material performance against wear for a particular application. It was also found that the elements acted as deoxidizers and desulphurisers which results in clean steels [173]. However, rare earth metals are expensive to use on a large scale and are sparsely distributed in the world.

Bhakat *et al.* studied three-body abrasion resistance of steels containing different amounts of C, B, Cr for agricultural tools and found that steel containing 0.3 wt% C with either 0.4 wt% Cr or 25 ppm B in quenched condition performed better than other combinations due to combination of martensite and fine carbides in the steels[174, 175]. Effect of C, Cr, Ni and Mn on change in abrasion wear of line pipes by sand is shown in Figure 2.18. It seems that Cr is most effective element to increase wear resistance after carbon. Further, from Table 2.4 it is evident that addition of at least 2 to 5 wt% Cr enhances wear resistance. Cr increases hardenability, it can form a variety of carbides along with carbon and can replace part of Fe to form composite cementite (complex carbides) which play a significant role in increasing wear resistance of steel [176, 177].

Table 2.4 Effect of Cr on sand abrasion of 0.3 % C steel. Tempered martensite with 500 VHN, Data from [45]

Amount of Cr / wt%	Wear loss / arbitrary units
0.57	0.904
2.00	0.888
5.13	0.856
13.19	0.822

Previous work on developing very high wear resistance steel suggest that high strength medium carbon steels (0.3 to 0.4 wt% C) that are alloyed with up to 2 wt%

Mn, 2 to 4 wt% Cr and 0.5 wt% Mo in quenched and tempered condition have high wear resistance in high stress abrasion. The steel also has high fracture toughness compared to commercially available steels and hence it is expected that this material should perform better when exposed to impact damage besides abrasion [35, 142, 155]. For example AISI 4340 steel with 52 HRC and fracture toughness of 49 MPa$\sqrt{m}$ showed sliding wear resistance of 3.7×10^{-6} mm mm^{-3}, compared to 7.9×10^{-6} mm mm^{-3} with 48 HRC and fracture toughness of 129 MPa$\sqrt{m}$ in case of the newly developed steel [142].

2.5   Role of abrasives

Wear obviously must depend on the physical properties of abrasives as discussed in Section 2.3.1. One of the captivating phenomena during either two or three-body abrasion and erosion wear is the existence of a critical size of abrasive particle at which wear rate changes. It was established that wear loss increases steeply with particle or grit size below the critical size, while the loss is independent of particle size, or either increase or decrease at lower rate above the critical size [32, 48, 90, 178–193]. Fig. 2.19 from the past data shows existence of such trends as a function of the critical particle size.
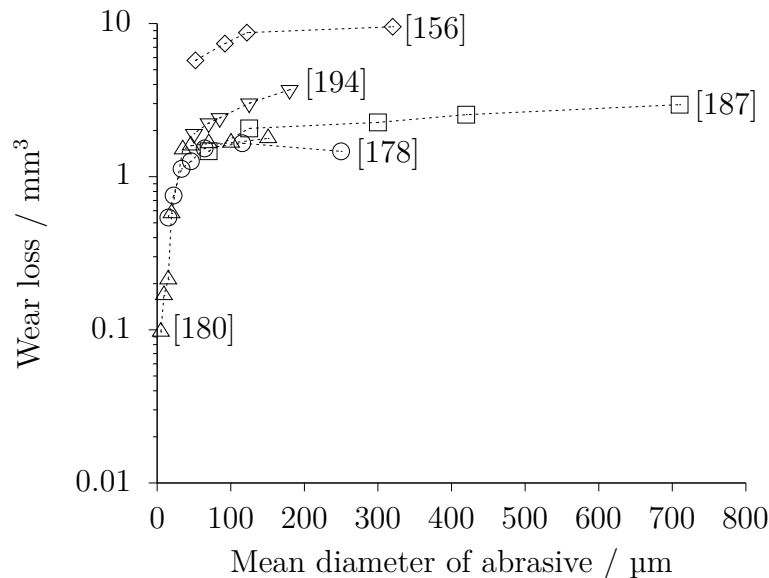
Fig. 2.19 Effect of size of abrasive particle on wear volume. There exists a critical size, d_c, at which wear behaviour changes. Data from [156, 178, 180, 187, 194].

Misra *et al.* reviewed about a dozen studies and argued that the shallow surface layers exhibit a higher flow stress than that of the bulk material during wear [186]. Some more new insights are discussed and important arguments are presented below:

1. **Pick-up of the abrasive particles:**

   It was argued that the clogging of the interstices between the finer abrasive grains by wear debris is responsible for the size effect while working with relatively large samples on abrasive papers. The clogging or pick-up of the abrasive particles decreases the number of abrasive grains which contact the surface and remove material, thus decreasing the wear rate. The pick-up increases with the abrasive particle size and reaches maximum or equilibrium at the critical size and hence further wear loss is independent of the particle size [32, 48, 178, 195, 196]. The critical radius found to be about $70\,\mu m$ for the pure metals.

   However, this explanation fails for a critical size in three-body or erosion wear where clogging does not occur.

2. **Minimum wear particle size:**

   Rabinowicz proposed that that there is a minimum wear particle size which hinders abrasion when the abrasive particles are smaller than the particles of abrasion debris which restrict contact between the two surfaces [32]. However, later it was proved that the groove width and cutting fragment is proportional to load and hence the wear particle size changes.

3. **Rapid deterioration of fine abrasives:**

   Moore *et al.* and Mulhearn *et al.* proposed that the shapes of the abrasive particles are different for different sizes and the fine particles contain high proportion of cracks which make them break up easily whereby their ability to remove material is greatly reduced [61]. The abrasive paper deteriorates during repeated usage (shown in Fig. 2.20).

   They proposed the following equation to determine mass loss with number of traversals:

   $$M_n = M_\infty(1 - \exp(-\beta n)) \tag{2.6}$$

   where where M_n, is the total metal removed up to n traversals, M_∞, the ultimate metal removed, β the deterioration factor and n the number of traversals.
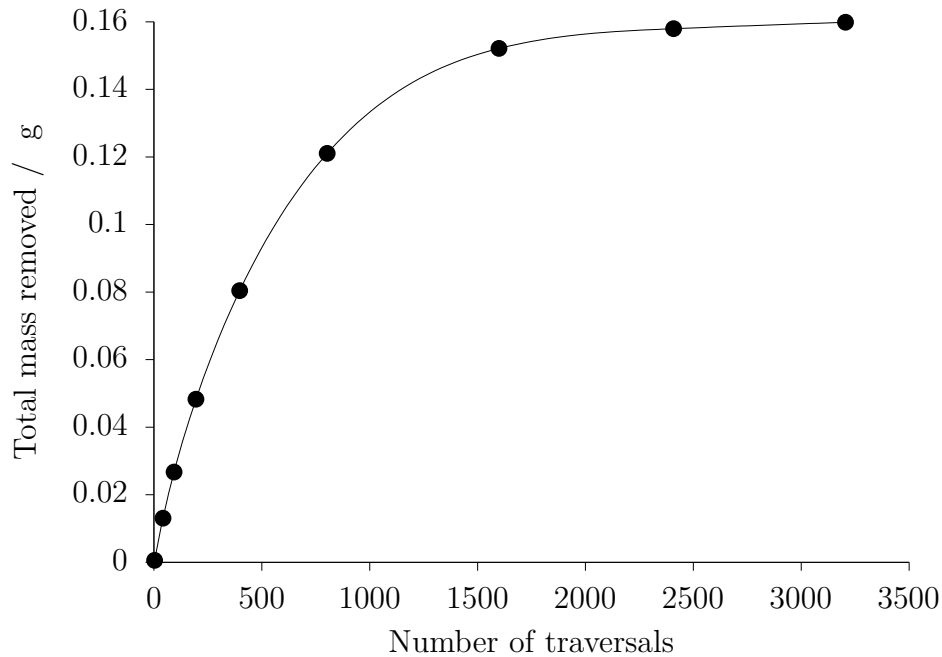
Fig. 2.20 Variation in total mass removed from steel specimen with number of specimen traversals on the same track of 220-grade of SiC abrasive paper. Data from [61].

However, Larsen-Badse had shown that the abrasive particles of the various sizes act in the same manner [181]. The number of grains forming grooves on the metal surface is a function of the applied load, while the average width of the grooves varies only slightly with load [90]. Further, fine particles require more energy to split into parts to increase in surface energy as the particle size decreases.

4. **Elastic contact theory:**

Larsen-Badse proposed an elastic contact theory based on their studies of abrasion of Cu under various loads and abrasive sizes. It was proposed that many fine abrasives have only elastic interaction with the metal and play a part in supporting the applied load without contributing to material removal. The fraction of the load carried by the abrasives in elastic contact increases with decreased abrasive size [181].

It was further confirmed in later experiments that the smaller initial abrasion rate with finer abrasives is due to abrasive grains making elastic contact with the metal specimen at loads insufficient for cutting [184, 197]. However, Date *et al.* observed that rapid deterioration of fine particles with continued use and clogging due to particles of wear and abrasive becoming stuck between the grains [184].

5. Thakare proposed that the existence of critical size is due to change in wear mechanism from ductile to fracture dominated failure mode owing to the increase in the severity of contact with increased abrasive size [198] .

A study on a work hardening model of the abraded surfaces revealed that surface layers of about 50 to 100 µm work harden more than the bulk of the material. Therefore, the smaller particles continuously encounter the harder surface and hence low wear rate [186]. Though this has addressed the problem in materials which work harden but failed to explain for the metals which form soft layers during wear. A study on single-crystal of copper revealed that the depth of the soft surface layer is about 2 mm.

Sasada *et al.* showed experimentally that there are three stages of wear with particle size in three-body abrasion as shown in Fig. 2.21. If the abrasive size is below a transition size (d_t), the wear mode changes to two-body or adhesion as the abrasives are smaller than the wear debris. However, if the abrasive is above the transition size but below a critical size (d_c), then the wear rate increases with increase in abrasive size as found in many investigations, If the particle size is above the critical size, then the wear rate remains constant. The transition and critical abrasive size depends on various factors like abrading material, abrasives, load and speed of the test [189].

The size effect is also noticed in impact or erosion wear and the reasons are inconclusive [137, 183, 199–202]. It can be fairly argued from the above discussion that like wear the size effect is a system property.

> The size-effect is a system property similar to wear.

2.6   Predicting wear rate

When it comes to predicting the wear resistance, it is commonly assumed that that the wear resistance increases with increasing hardness of the component in application. In general, the resistance to wear increases with increase in hardness when applied load is low. Rabinowicz *et al.* proposed a simplified model in abrasive wear and is given by

$$\frac{dV}{dl} = \frac{W\overline{\cot\theta}}{\pi H} \tag{2.7}$$
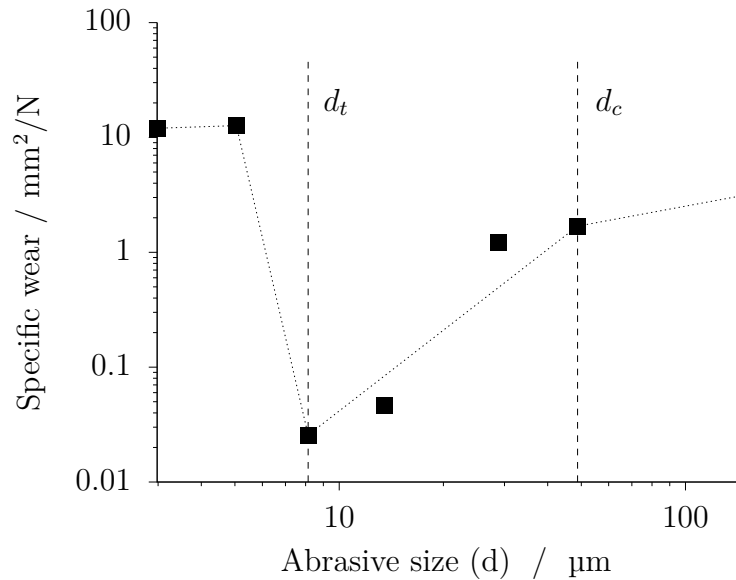
Fig. 2.21 Effect of size of abrasive (SiC) on unlubricated thee-body abrasion: iron on iron with the abrasives at a load of 15.7 N and speed of 52.8 mm s^{-1}. Adhesive wear below the critical transition size, d_t, while abrasion wear above the d_t. Above the critical size, d_c, the wear rate may remain constant or increases at decreased rate with the abrasive size. Dotted line over the data points denotes a possible trend. Data obtained from [189].
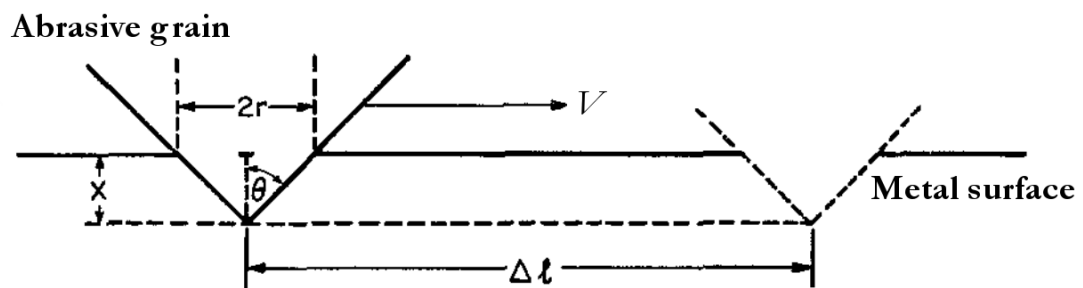
Fig. 2.22 Schematic illustration of a conically-ended abrasive grain which is removing material from a metal surface [32], reproduced with permission of Elsevier.

where l is the length of a groove, W is the load, V is the volume swept by a sharp edged abrasive fragment, H is the hardness of the abrading material and $\overline{\cot\theta}$ is the average cotangent of the angle of penetration of all the abrasive particles [32]. This equation is similar to Archard's equation (Eq.) for an adhesive wear [22].

$$\frac{dV}{dl} = \frac{kW}{3H} \qquad (2.8)$$

The models predict the wear behaviour of pure metals reasonably well but Sin *et al.* evaluated Eq. 2.7 experimentally and found that the observed wear rates were at least an order of magnitude lower than the calculated using the equation. Further, effect of the particle size on wear could not be predicted using the equation. For instance it was observed that the wear resistance is not linear with annealed hardness but depends strongly on the abrasive particle size and speed of the test [180] [187].

One study correlated room temperature wear resistance with fracture toughness and uniform elongation of the material at high temperature. It was found that room temperature properties handicapped in predicting wear resistance as during wear the local temperature increase and hence high temperature properties are important to consider [203]. Nevertheless, the study established a linear relationship between wear rate, and fracture toughness (U_T) and elongation (ϵ_u). The equation is given blow.

$$\text{Wear rate} = 1/U_T\epsilon_u \qquad (2.9)$$

As stated earlier, the material undergoes tremendous amount of plastic deformation and fracture toughness is an important property to capture wear resistance. The reason given by authors why uniform elongation should be included to an equation was that uniform elongation is equivalent to strain hardening exponent based on Holloman relationship [204]. However, it is known that steels with the microstructure predominantly containing the austenite and the martensite or the bainite have high elongation but with negligible work hardening. Therefore further study is required to develop a mathematical model to predict abrasion loss.

2.7   Modelling

A single or multi-pass scratch tests using diamond or ideal indenter were used to model two or three-body abrasion to determine conditions of cutting and ploughing under given circumstances [42, 47, 67, 205–207]. Attacking angle is one of the important
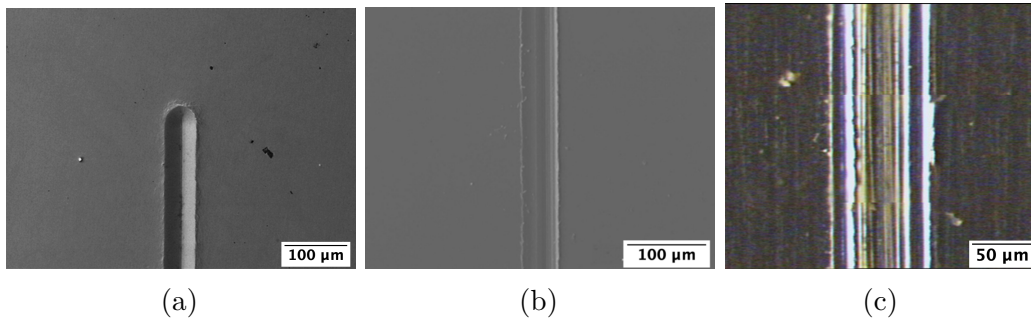
Fig. 2.23 Scratch tests on a hard steel alloy. (a) Scratch formed at at an attacking angle of 10° using a conical diamond indenter with a microscopic hemispherical tip. (b) Scratch formed at an attacking angle of 80° using a prismatic blue corundum grain (length ≈ 10 mm, width ≈ 1.5 mm, and height ≈ 1 mm) under the similar condition of (a). (c) Multiple scratches under the prismatic blue corundum due to higher velocity, $1\,\mathrm{m\,s^{-1}}$, compared to (b) at $0.1\,\mathrm{mm\,s^{-1}}$ under similar conditions [207]. Reproduced with permission of Elsevier.

parameter that determine the mode of wear. It is defined as included angle between the moving indenter/abrasive and the abrading surface. From the various models and controlled experiments it was deduced that cutting takes place if the attacking angle of the abrasive is above 30°, while ploughing below that angle.

Khellouki *et al.* studied the effect of attacking angle and speed on the wear mechanism with a typical abrasive and an indentator [207]. It was found that there is huge difference between the scratch made by the indenter and the real abrasive particle. In contrast to the previous investigation, it was found that ploughing was observed during scratching at 80° when tested using a prismatic abrasive particle as shown in Fig. 2.23b. The scratch resembles the one produced at 10° using a diamond indenter under similar conditions as shown in Fig. 2.23a. Multiple scratches formed by the abrasive at higher velocity is shown in Fig. 2.23c. The individual scratches in this case resemble the one produced by the diamond indenter.

Further, the coefficient friction using the real grain is around 0.25 which is very low for an acute attack angle of 80°. For instance, the coefficient of friction is about 0.2 at 10° and 0.9 at 45° attacking angle when using the diamond indentator under the similar conditions of load and velocity. So the coefficient could be well above 1 when the attacking angle is 80°.

The large difference between the diamond indentator and the real abrasive can be attributed to the roughness and irregularity of the real abrasive surface compared to the polished surface of the diamond indentator. The surface of the real abrasive

enhances material adhesion at the expense of plastic deformation. Another reason could be that the broken pieces of the abrasive locked in the rough surface decreases the abrasiveness [207]. It was also found that the damage mechanism changes from cutting to ploughing in an abrasion test when very hard abrasives (SiC > 3000 HV) are replaced with relatively low hardness abrasives (ZrO2 ≈ 1100).

One of the major limitations of a scratch test is that small noticeable differences in the scratch widths for a comparatively great difference in hardness, mainly in high hardness alloys [208]. Shetty *et al* also observed that wear debris and surface features developed in scratch test by irregular abrasive particle resemble to those observed in abrasion test, where as the features by diamond indentator do not [209].

Nevertheless, models developed using indentator like diamond can cautiously be applied to understand and quantify abrasion wear under relatively soft abrasives. Sedriks *et al.* developed conditions of ploughing and cutting in two-body abrasion by using pyramidal indenter as an abrasive particle. A typical configuration of the indenter and the abrading surface is shown in Fig. 2.24.

Under equilibrium conditions the forces parallel and normal to the abrasive face may be resolved as follows:

$$F_T = F_H \sin b + F_v \cos b$$

$$N_T = F_H \cos b - F_v \sin b$$

$$\mu = \frac{F_T}{N_T} = \frac{F_v + F_H \tan b}{F_H - F_v \tan b} \tag{2.10}$$

where, μ is the coefficient of friction between the chip and the abrasive face. F_V is equal to the applied force and if F_H is expressed as the product of the cross-sectional area of the groove, A, mean pressure required to displace the metal, p, and a geometric constant, c, then by rearranging and substituting Eq. 2.10:

$$A = \frac{W}{cp} \left(\frac{1 + \mu \tan b}{\mu - \tan b} \right) \tag{2.11}$$

Similarly, an expression for the cross-sectional area of the groove during ploughing is given below:

$$A = \frac{W \mu'}{cs \cot a + cp} \tag{2.12}$$
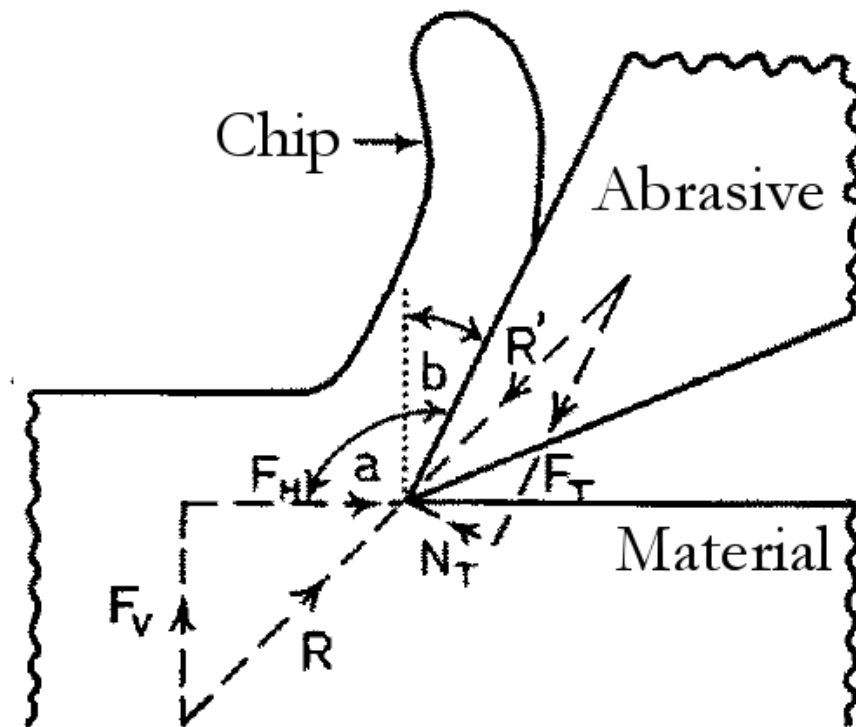
Fig. 2.24 Force system acting at the abrasive face. F_H is the horizontal force, F_v is the vertical force, F_T is the force parallel to the abrasive face, N_T is the force normal to abrasive face, a is attack angle, and b, the rake angle, is $a - 90°$ [210], reproduced with permission of Elsevier.
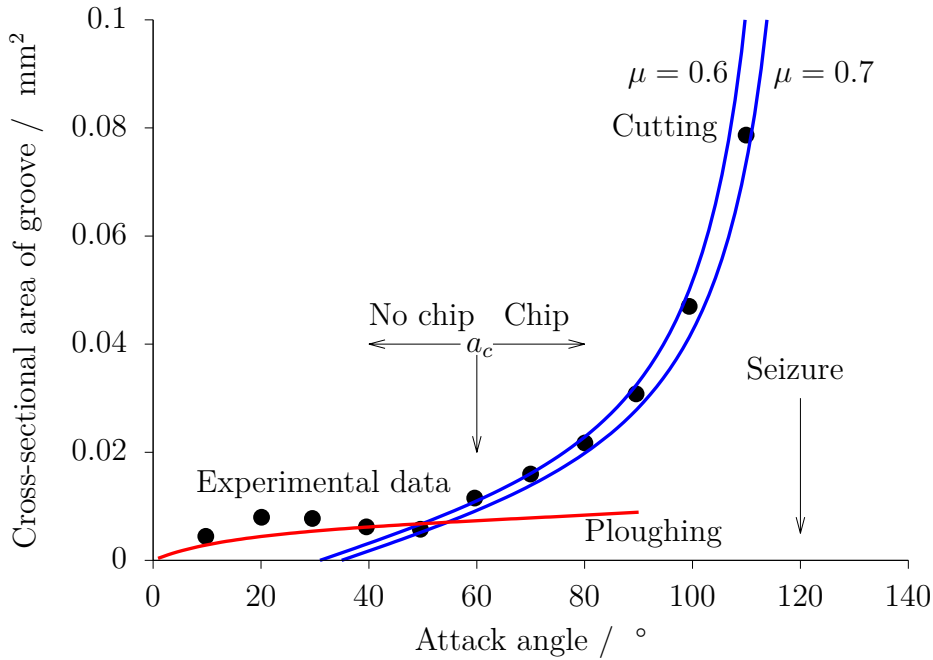
Fig. 2.25 Variation of the cross-sectional area of groove with attack angle. Blue curves are calculated from Eq 2.11 using values of $\mu = 0.6$ and 0.7. Red curve is calculated from Eq 2.12. The experimentally measured values of lead are represented by filled circles. It can be observed that critical attach angle a_c is about 60°. Data from [210], reproduced with permission of Elsevier.

where, μ' is the coefficient of friction during ploughing, and s is the shear strength of the material. The results and experimental data are plotted in Figure 2.25.

The results indicates that ploughing occurs below a critical attack angle, while cutting that causes chip formation occurs above the critical angle but below 120°. Above 120°, frictional force doesn't support the abrasive and hence rolling of abrasive takes place. In these calculations work-hardening was ignored and it is also assumed that μ remains same throughout the cutting or ploughing process.

Interestingly, calculations and experiments on fully work-hardened, and annealed metals showed that the critical attack angle, a_c, remain same for a given metal. It was observed that the critical attack angle of the cutting face, at which a chip is cut first, determined primarily by the coefficient of friction between the contacting surfaces. It was suggested that the chip which is in contact with the cutting face must be highly deformed irrespective of whether it is cut from annealed or fully worked materials [211]. This is possibly another reason why prior cold-work of metals do not increase their wear resistance.

2.8   Way forward

1. It is evident that fracture toughness plays a role in high intensity impact-abrasion wear. However, careful quantification of the extent of improvement due to increased fracture toughness is still needed. Due to work of Peet *et al.*[212], it is possible to produce steel that has very high toughness, $(72.0 \pm 1.5)\,\mathrm{MPa}\sqrt{\mathrm{m}}$, and yet is hard, 561 ± 23 HV with yield strength of 2.1 GPa. The steel can be heated to a fully austenitic state in order to destroy the elegant thermomechanically processed microstructure that is responsible for its high toughness. After quenching, the martensite will therefore not be as refined, and hence should have a lower toughness but identical hardness. This will allow the role of fracture toughness, for example in Equation 2.5, to be evaluated based on wear results and mechanical properties of the steels.

2. Similarly, role of retained austenite in carbide-free bainitic or quenched martensite steels in increasing wear resistance need to be quantified when all other parameters are maintained similar. For instance, retained austenite in the steels [11, 132] can be eliminated by tempering and hence its wear properties with and without retained austenite can be obtained.

3. There is a huge amount of laboratory and field test data of wear of various steels available against many operating parameters. A neural network model of the data would assign relative importance of the parameters and steel properties which can assist in developing high wear resistance steels.

4. From the survey of various laboratory and commercial steels, medium carbon steels (0.3 to 0.4 wt% C) that are alloyed with up to 2 wt% Mn, 2 to 4 wt% Cr and 0.5 wt% Mo in quenched after thermomechanical treatment and then tempered at below 200 °C condition can achieve a combination of high hardness and fracture toughness [23, 38, 45, 141, 142, 149, 155, 212]. The steels can be mass produced economically and may be an alternative to many commercially available wear resistance steels to both abrasion as well as impact-abrasion damage.

2.9   Conclusions

Several factors influence the wear resistance of steel under impact-abrasion conditions, including hardness which is a primary parameter. Nevertheless, other factors such as

toughness, work-hardening capacity and ductility play a role although clear evidence is needed. From the critical review of the published work, the following conclusions can be reached:

- Wear resistance of steels of hardness above 500 VHN of steels is limited by work-hardening capacity, and fracture toughness. Increasing the base hardness perhaps reduces the ability to dissipate impact energy, and the depth of deformation also decreases. An ability to spread deformation to a greater depth can increase the wear resistance at a given hardness.

- As the hardness of the base steel increases, or loading conditions change, the wear damage mechanism changes from ductile to brittle. Therefore, toughness should play a role by delaying microscopic fracture events. The fracture toughness of the steel can be increased by refining martensite and retaining some amount of austenite to enhance fracture toughness.

- There is hardly any published literature to quantify either the role of fracture toughness or work hardening rate on the wear resistance of steels when all other parameters including composition, hardness and microstructure are kept at similar level.

- It is possible that increasing hardness reduces the ability to dissipate impact energy, and the depth of deformation also decreases. An ability to spread deformation to a greater depth may increase the wear resistance at a given hardness. Retained austenite may be useful in this context. Carbide-free bainitic steels have proved to be successful due to their high work hardening rate.

- Alloying additions such as Cr, B, Mo, Ni and Cu contribute to the combination of hardness and toughness if added in right quantities. It is possible that appropriate adjustments to these or other solutes should result in a commercially viable wear resistance steel.

Chapter 3

Alloys and Experimental methods

Based on the critical literature review in the previous chapter, it was decided to study specific role of toughness in improving the wear resistance in high-hardness steels when they are exposed to complex wear environments as in impact-abrasion. This chapter gives details of alloys selected for the study, heat-treatments carried out to change their mechanical properties, and an experimental plan to evaluate the wear resistance of the selected alloys.

3.1   Alloys

A new steel (Table 3.1) with a unique combination of properties in the hot-rolled condition, has been designed, mass produced, and tested [212]. The steel has a hardness of 561 ± 23 HV and a tensile strength of 2.00 ± 0.01 GPa, while maintaining a fracture toughness of $(72.0 \pm 1.5)\,\mathrm{MPa}\sqrt{\mathrm{m}}$. It was thermomechanically processed to obtain severely pancaked austenite and then naturally cooled in ambient conditions to room temperature to generate a martensitic microstructure (Figure 3.1). It also has a high hardenability and hence it can transform into martensite at cooling rates as low as $1\,\mathrm{K\,s^{-1}}$. The final thickness of the hot-rolled plates was $6\,\mathrm{mm}$. The steel was commercially produced by M/s Mishra Dhatu Nigam Limited, Hyderabad, India for Tata Steel Limited, India.

Table 3.1 Composition of the steel in wt%

C	Si	Cr	Ni	Mo	V	Al	S	P
0.34	1.45	1.5	3.53	0.39	0.3	0.01	0.005	0.005
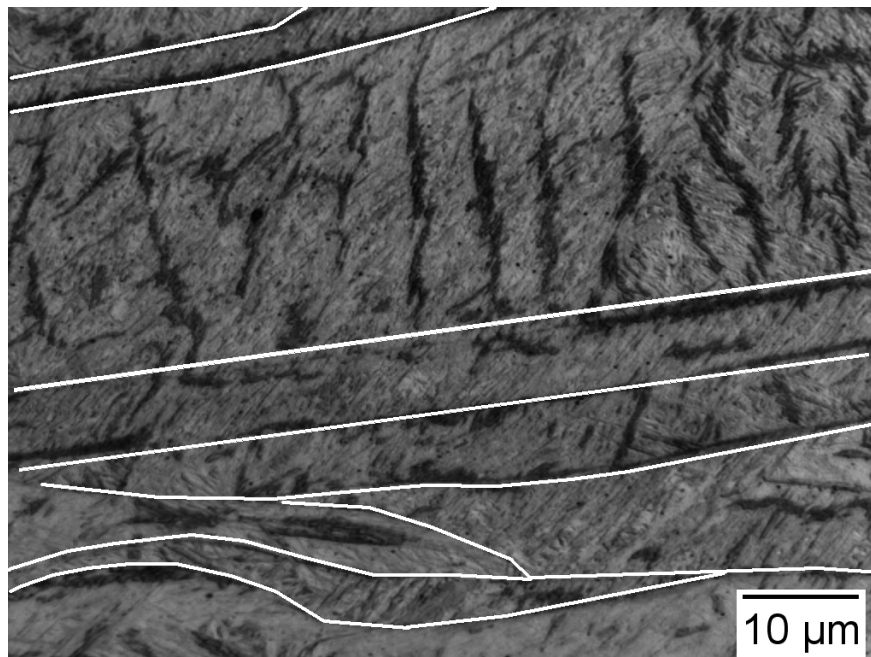
Fig. 3.1 The hot-rolled steel showing pancaked prior-austenite grains, which transform into fine martensite during cooling. Prior austenite grain boundaries are marked white.

There are a number of applications envisaged for the alloy, but of particular interest is its use in conditions where it would sustain damage from a combination of impact and abrasion. In this study the steel is used to evaluate role of fracture toughness during abrasion, and impact-abrasion wear. For this reason, some of the steel was heat treated such that its hardness was maintained, but the toughness was not. To do this, the steel was reaustenitised at 900 °C for 1 h to destroy the hot-rolled microstructure followed by quenching to room temperature. The steel was also tempered at 190 °C and 300 °C for two hours to reduce the hardness in order to match that of the as-rolled steel. The hot-rolled steel was also tempered for two hours at 190 °C and 300 °C to study its wear resistance in a mildly tempered condition. The microstructures, and mechanical properties of the rolled, quenched, and their tempered variants are discussed in this chapter. In the discussion that follows, the hot-rolled steel will be referred to as 'rolled' , rolled and tempered at 190 °C referred as 'R+T190 °C', rolled and tempered at 300 °C referred as 'R+T300 °C'. Similarly, the reaustenitised steel is referred as 'quenched', and 'Q+T190 °C' and 'Q+T300 °C' notation are used to refer quench and tempered at 190 °C, and 300 °C respectively as given in Table 3.2.

Table 3.2 Tested samples and their reference.

Sample details	Designator
Hot-rolled	Rolled
Hot-rolled and tempered 190 °C for 2 h	R+T190 °C
Hot-rolled and tempered 300 °C for 2 h	R+T300 °C
Reaustenitised 900 °C for 1 h and quenched	Quenched
Reaustenitised and quenched and tempered 190 °C for 2 h	Q+T190 °C
Reaustenitised and quenched and tempered 300 °C for 2 h	Q+T300 °C

3.2 Sample preparation

Samples were cut to the required size using an ATM Brillant cutting machine. The rotation rate of the cutting blade was set to $600 \, \text{s}^{-1}$ to achieve the cut at a slow speed of $0.015 \, \text{mm} \, \text{s}^{-1}$ in order to minimise damage. For optical micrography and hardness measurements, the samples were hot mounted (at around 200 °C) followed by curing for 20 min using a mounting press. Then the samples were ground using silicon carbide emery papers followed by fine polishing using diamond paste according to standard procedure.

Samples for X-ray diffraction analysis and scanning electron microscopy were polished using an electrolytic technique. The electrolyte consisted of 80 % methanol, 15 % glycerol and 5 % perchloric acid. The polishing was carried out at 5 to 10 °C at the applied voltage of 10 V for 2 to 5 min depending on the sample dimension.

3.3 Microstructural characterization

3.3.1 Optical microscopy

After electrolytic polishing of the samples, the polished surfaces was etched with 2 % Nital etchant to reveal microstructure. Optical microscopy was carried out on a Leica Microsystems DM2500M microscope with a DFC295 camera. The Leica Application Suite was used to obtain and process the images.

3.3.2 Scanning electron microscopy

Scanning electron microscopy (SEM) was carried out using FEI Nova NanoSEM, fitted with Everhart-Thornley, through-the-lens secondary electron detectors, for microstruc-

tural characterisation. A voltage of 10 to 15 kV and working distance of 4 to 5 mm were used to obtain images. Abraded surfaces of the samples were studied using a Phenom Prox desktop SEM with a back-scatter detector with an accelerating voltage of 10 to 15 kV. To obtain 3D microstructure of the damaged surface, ZEISS CrossBeam 540 combining a field emission SEM and advanced FIB were used.

3.3.3   X-ray diffraction

X-ray diffraction (XRD) analysis was done to obtain volume fraction of retained austenite, crystallite size and strain. The XRD spectrum for 2θ range of 35 - 135° with a step size of 0.02 obtained from Bruker D8 DAVINCI diffractometer using CuK$_\alpha$ radiation. Ni foil of thickness 0.012 mm was used to maximize Kα_1 incident radiation. Quantitative phase fractions were determined by fitting the full XRD spectrum by Rietveld refinement. High Score plus 4.0 was used to fit the full spectrum by refining specimen displacement, background, peak profiles and lattice parameters of both the phases.

3.3.4   Transmission electron microscopy

To investigate the damage at the surface, a thin foil sample from the damaged area for transmission electron microscopy was prepared using a dual-beam FEI Helios Nanolab equipped with a FEG-SEM and a focused ion beam. The thin foils were examined using a FEI Tecnai Osiris FEGTEM transmission electron microscope operated at 200 kV and selected area electron diffraction patterns using a 40 μm were obtained at different locations of the foil.

3.3.5   X-ray tomography

X-ray computed tomography (X-ray CT), Henry Moseley X-ray Imaging Facility, The Manchester University, was used to study 3D microstructure at larger volume of the damaged surface. In order to obtain high-resolution imaging, high photon energies of 120 keV and 10 W power were used in this study.

3.4   Mechanical testing

3.4.1   Hardness measurements

The bulk hardness was measured using a Vickers indentor with $30\,kg$ and $10\,s$ dwell time on a Qness automatic hardness testing machine.

3.4.2   Tensile test

Tension tests were conducted on sheet specimens of standard size of $25\,mm$ gauge length, $6\,mm$, and $5\,mm$ thickness as per ASTM E8 method. All the tests were conducted by using Instron 8032 universal testing machine at a crosshead speed of $1\,mm\,min^{-1}$, which corresponds to an initial strain rate of 3.3×10^{-4} s^{-1} and the resultant strain was measured with an external strain gauge.

3.4.3   Impact tests

The ASTM E23-93a method for impact testing of metallic material allows the use of subsize samples when standard test samples cannot be obtained. The impact test was conducted using a ZwickRoell HIT $50\,J$ machine operated at pendulum velocity of $3.8\,m\,s^{-1}$. Subsize $5 \times 5 \times 55$ mm notched-bar samples were used for all conditions. Shear fracture appearance is one of the key parameters to determine relative impact toughness of the materials. The shear fracture appearance is calculated as total shear area divided by the total fractured area, times 100.

3.4.4   Bend testing

Bend tests were conducted to evaluate ductility of hot-rolled, reaustenitised and quenched steels. The ASTM E290-14 standard provides method to conduct the tests. The test was conducted by supporting the sample near each end on rollers and applying a force through another roller between two supports, as shown schematically in Figure 3.2. $75 \times 10 \times 5$ mm polished bar samples were used for all conditions. The tests were also conducted by using Instron 8032 universal testing machine at a crosshead speed of $1\,mm\,min^{-1}$.
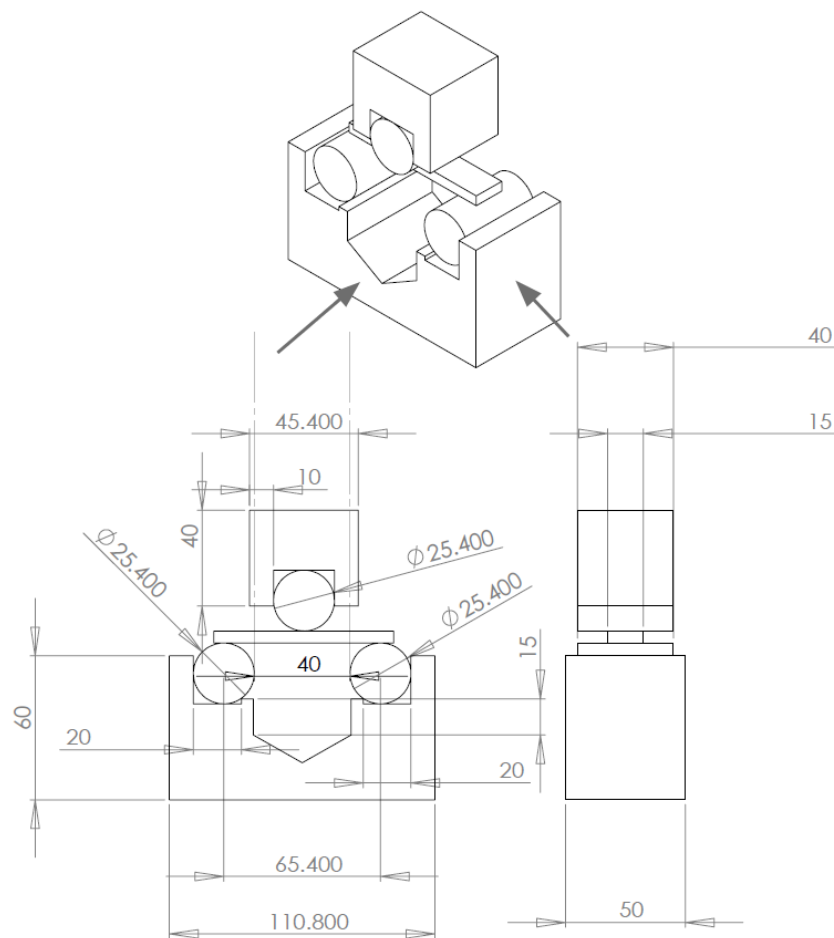
Fig. 3.2 Pictorial view of a standard bend test and two of its projects. A test specimen is placed between the rollers. All the dimensions are in mm.

3.4.5   Surface roughness

Surface roughness is measured as an arithmetic average (R_a) of the profile height deviations in either direction from the mean line of the profile. It was measured using a single scan surface profilometer, DEKTAK 6M. A load of 10 mg was applied. A total of six profile readings were obtained for each tested condition. The length of each profile was 10 mm with scan time of 120 s.

3.5   Wear tests

The abrasion wear test conditions can be gouging, high stress and low stress [83, 213]. Gouging occurs when the coarse abrasive of the size of a football impacts, this results

in shattering of the abrasive into small pieces. Gouging conditions are commonly noticed in earth digging teeth (Fig. 2.9) and material handling truck bodies. In high stress conditions, the abrasives are crushed during the process, while in low abrasion conditions the abrasive particles do not fracture. An ore or granite crusher is an example of high-stress abrasion, while crusher teeth digging in sandy soil is an example of a low stress condition.

Most common wear tests methods are dry sand / rubber wheel test for low stress three-body abrasion (DSRW), Pin on drum or disc for low or high stress two-body abrasion, Jaw crusher gouging abrasion test to simulate high-stress impact-abrasion, and Impeller-tumbler for impact-abrasion wear testing [70]. DSRW is an ASTM approved test and hence this test method is selected for the new alloys. Impeller-tumbler methods expose the samples to both abrasion as well as impact and hence this method is selected to decipher the influence of toughness in controlling wear loss. These tests are summarized below.

3.5.1 Dry sand / rubber wheel test

The dry sand, rubber-wheel (DSRW) is an ASTM approved test used to grade materials for low stress three-body abrasive wear and to simulate conditions of low wear in joints, pivot pins and ropes in the mining industry [70, 214]. Under these conditions, where wear arises from the sliding and rolling action of broken pieces of material that is being handled trapped between metal surfaces, the test helps evaluate the alloys [70]. Field tests to evaluate actual conditions can be expensive, but some work has demonstrated a correlation between field and laboratory tests in low-stress abrasion in which wear loss is a linear function of hardness and hence performance is mainly determined by hardness [71, 98].

The test consists of a rubber wheel of diameter 228 mm that rotates at a specified rate depending against on a test specimen, $76.2 \times 25.4 \times 12.7$-3.2 mm. A certain size range (200 to 300 µm nominal particle size) silica sand flows between the rubber wheel and the specimen. The specimen is held against the rubber wheel using a lever arm with a specified force, for example 130 N.

3.5.2 An impeller-tumbler wear test

Abrasive wear and impact loading occur during transportation, lifting and excavation operations as discussed earlier [71, 215]. An impeller-tumbler wear test method to

simulate such conditions is illustrated in Fig. 3.3. The test is also called as a continuous impact-abrasion test [216]. It is used widely in recent years to test steels developed for mining industry [51, 67, 216]. Further, the stresses in these conditions are neither as severe as in grinding and crushing nor as low as in the case of dry sand rubber wheel (DSRW) test conditions. Therefore, the test not only fits between DSRW and pin on disc but also complements other wear tests in ranking the wear resistance of materials. As discussed above it was used in this study to interpret the role of toughness in impact-abrasion wear.

Impact-abrasion tests were carried out using an impeller-tumbler testing machine available at Tampere University, Finland. The machine consists of an impeller shaft carrying samples in a rotating drum containing abrasives. Multiple samples can be mounted at different angles relative to the sample holder tangent. The abrasive media in the drum can be ore or granite of a specific size range, 8 mm to 20 mm [34, 52], consistent with wear in mining scenarios [70]. Increase in abrasive size increases wear loss. Similarly, the weight of the abrasive can vary but it usually is 400 to 900 g [34, 118]. Abrasive size, charge weight, and number of abrasives in the drum are limited by its volume. The salient features of the impeller-tumbler wear test are given below.

3.5.3   Main features of the impeller-tumbler wear test

- The variance in wear loss with the test is typically 10 % [70].

- Three different materials or identical samples can be tested simultaneously.

- In a study, the test was recorded using a high speed video to distinguish impact and abrasion events. It was found that abrasion to impact ratio is 1 to 100. Therefore, the test is an impact-abrasion wear in nature [34]. In the same study it was estimated that impact energies can be about 0.1 J depending on the size and area of the impact.

- The sharp edge of the sample is exposed to potentially frequent interactions with the charge and hence edges wear rapidly. The uneven wear reflects real life scenario associated with mining equipment. The edges of bucket plates and scraper blades interact quite frequently with the abrasive environment and hence the sharpness of the edges decreases affecting the efficiency of the machine [52].

- The test is non-standard and there are many parameters to study. For example, wear loss using one sample in the test will obviously be greater than multiple

samples. Similarly, change in size range and weight of the charge changes the results. Furthermore, speed of the drum and shaft can also can be varied.

- The test reaches a steady state when wear loss is proportional to the run time [52]. Though the wear loss is not representative of real-time wear loss in real components, the test can rank the materials based on weight loss per hour.
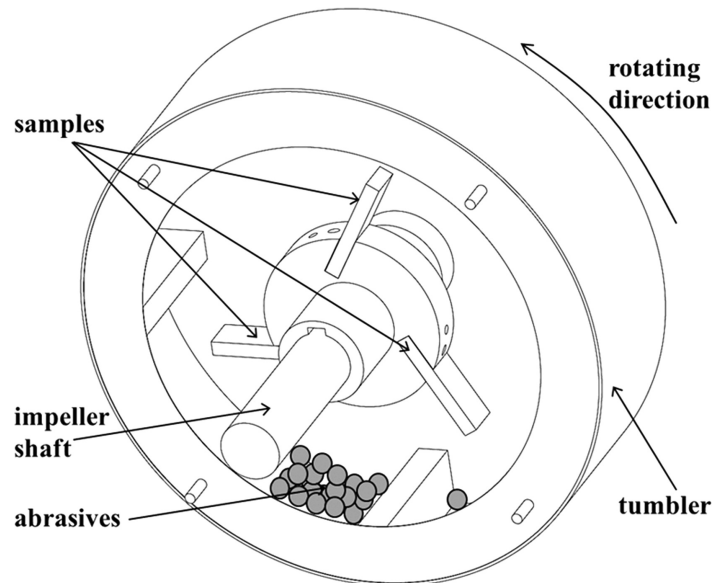
Fig. 3.3 Diagram of the impeller-tumbler wear testing machine describing various components [118]. The diameter of the tumbler is about 300 mm. Produced with permission of Elsevier

The entire assembly is enclosed and both the drum and impeller shaft are allowed to rotate in the same direction. A typical sample in the form of a pedal has the dimensions 75×25 mm. The shaft with samples attached is rotated at 620 ± 5 rpm [71], while the drum is rotated in the same sense at 60 rpm. There is a simultaneous application of impact from different angles by the charges and abrasion from sliding of the charges on the sample surface. The charge breaks during the test so the conditions can change with time. To avoid this, the abrasives are changed after every 15 or 20 min of testing. The procedure is repeated for a total time of 1 h or more. The weight loss is measured at hourly intervals.

The parameters for the tests carried out at Tampere University are given in Table 5.1. The conditions were chosen to be similar to those in the published literature on commercially available wear resistance steels [51]. The granite abrasive used in the present test is from Kuru with specific gravity $2.64\,\mathrm{g\,cm^{-3}}$ and abrasion index

0.82, while Sorila granite abrasive with specific gravity $2.69\,\text{g}\,\text{cm}^{-3}$ and abrasion index 0.82 was used in the reference work. Abrasion index is a factor used to determine the effective rate of wear of the mining equipment. The wear loss of the equipment increases with increase in the index.

Table 3.3 Wear test parameters of the impeller-tumbler equipment at Tampere Wear Center.

Test parameter	Value
Sample dimension	$75\,\text{mm} \times 25\,\text{mm} \times 6\,\text{mm}$
Rotation speed impeller	$700\,\text{min}^{-1}$
Rotation speed tumbler	$30\,\text{min}^{-1}$
Abrasive size	10 to $12.5\,\text{mm}$
Abrasive mass for every $15\,\text{min}$	$900\,\text{g}$
Test duration	$240\,\text{min}$
Abrasive	Granite (Kuru quarry, Finland)
Sample angle	$60°$

Chapter 4

Microstructure and mechanical properties

4.1 Microstructure

The steel with composition listed in Table 3.1 was thermomechanically rolled to obtain deformed austenite and then cooled to room temperature to produce a martensitic microstructure with small amount of retained austenite less than $5\,\%$ by volume, Figure 4.1. Figure 4.1a shows the banded microstructure with alternative layers of dark and bright regions due to inevitable chemical segregation in this steel produced in a tonnage quantity. The hot-rolled structure with severely pancaked prior unrecrystallised austenite grains, which contain deformation bands can be seen in Figure 4.1b. These defects ensure a fine martensite structure which is conducive to good toughness since the tendency to crack under load decreases with plate/lath size [149]. Further, it is experimentally proven that a decrease in prior austenite grain size reduces the martensite packet size and block sizes [151–153]. The complex structural levels that develop on transforming a prior austenite grain in a lath martensitic steel is illustrated in Figure 4.2. The prior austenite grains are divided into 'packets' that contain a cluster of blocks which share the same one of the four independent $\{111\}_\gamma$ and each block consists of laths of similar orientation [217].

Figure 4.3a shows prior austenite grain boundaries(solid line), martensite packets identified by 'A' and 'B' and separated by dashed line, and blocks are marked with dotted lines. Fine martensite laths $(51 \pm 22$ nm$)$ can be noticed in Figure 4.3b. Such a refined microstructure increases both strength as well as fracture toughness as crack propagation is resisted at each crystallite boundary.

<div align="center">(a)   (b)</div>
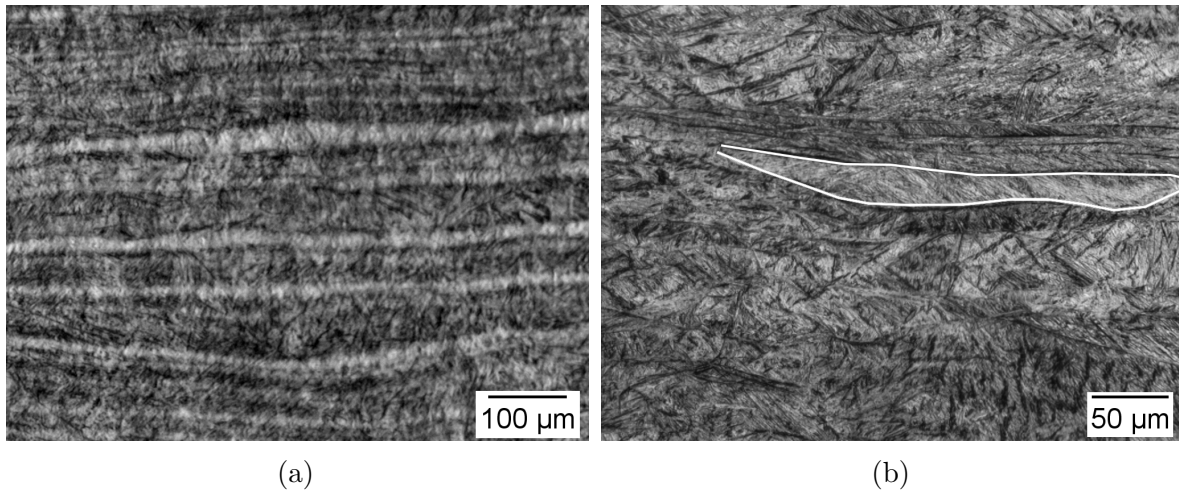
Fig. 4.1 Optical micrograph showing (a) banded microstructure (alternative layers of dark and bright regions) due to chemical segregation. (b) Elongated prior austenite grains (marked white) with martensite in it.
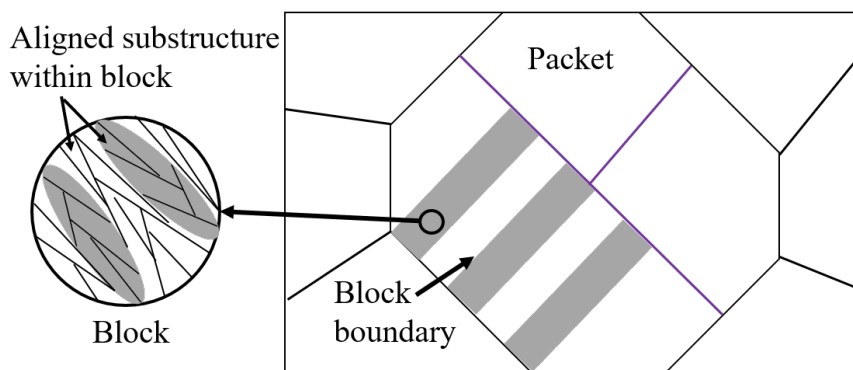
Fig. 4.2 Showing schematic of the microstructure of lath martensite developed on quenching steel from austenite phase. The prior austenite grain is subdivided into packets (represented by blue boundaries). The blocks are further divided into blocks which may contain closely aligned laths [218, 219].

As described earlier, to investigate the role of fracture toughness in impact-abrasion conditions, a simple experiment was designed. The idea was to test steel with same composition, similar microstructure but lower fracture toughness. The rolled steel with its incredibly fine structure was heat treated to deteriorate the microstructure and hence produce the samples with lower toughness. In this process, the steel was heated to 900 °C for 1 h followed by quenching to room temperature in water.

The microstructure of the steel in the reaustenitised and quenched condition is shown in Figure 4.4, with equiaxed prior austenite grains produced during austenitisation, so

<center>(a)</center>

<center>(b)</center>
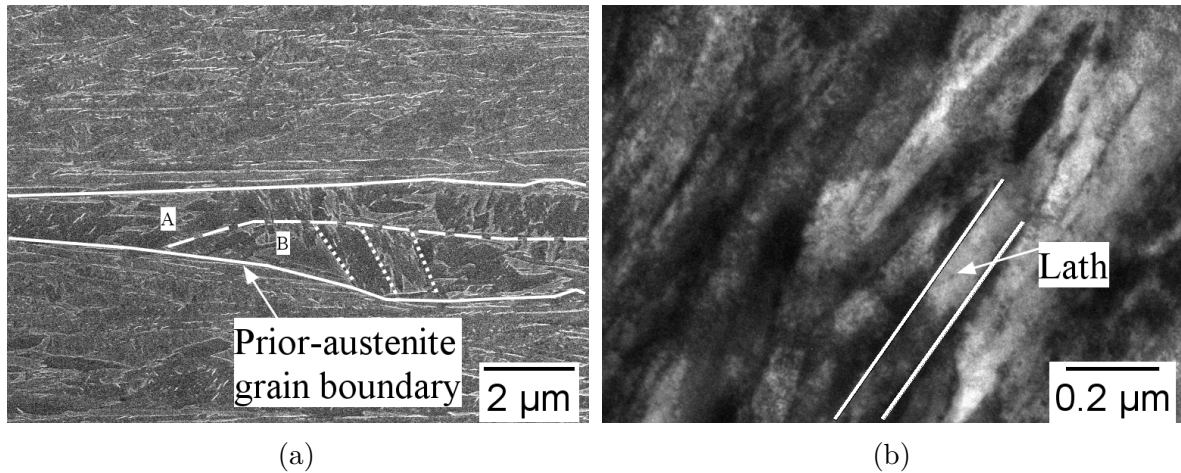
Fig. 4.3 Showing higher magnification images of hot-rolled steel consisting of (a) martensite packets identified by 'A' and 'B'. Continuous while lines indicates the prior austenite grain boundary, while the dashed line marks the boundary between the identified packets. Regions between the dotted line are blocks containing (b) fine martensite laths.

that the scale of the microstructure increases and the toughness decreases. The grain size was measured with the linear intercept method and was found to be 12.3 ± 1.5 µm.

The fineness of the microstructure in both the steels was further studied by EBSD technique. The orientation imaging maps of the hot-rolled, and the quenched steels are shown in Figure 4.5. The {100} pole figure of the martensite from a single parent austenite crystals (Figures 4.5a and 4.5b) for the hot-rolled, and the quenched sample are shown in Figure 4.5c and 4.5d, respectively. The data consist of about 17 000 poles in both the steels. RGB color scheme denotes martensite variants. Each austenite grain in the hot-rolled steel is severely deformed and fragmented, resulted in a large spread of misorientation in the martensite orientations (within a single γ grain) generated on cooling. In contrast, the martensite that formed in an individual γ the undeformed austenite has a much smaller spread in orientations. The martensite in the hot-rolled structure expected to be much tougher, for two reasons. Firstly, the crystallographic grain size, which controls the cleavage mode of fracture [220] and secondly because fine plates of martensite have a reduced tendency to crack [149].

As discussed in the literature review, retained austenite play a role in increasing work-hardening capacity and toughness of the steel. The volume fraction of retained austenite in the hot-rolled and quenched samples was determined by refining the full spectrum by the Rietveld refinement method using HighScore Plus software. The retained austenite fraction is 0.041 ± 0.030 and 0.028 ± 0.030 in hot-rolled, and
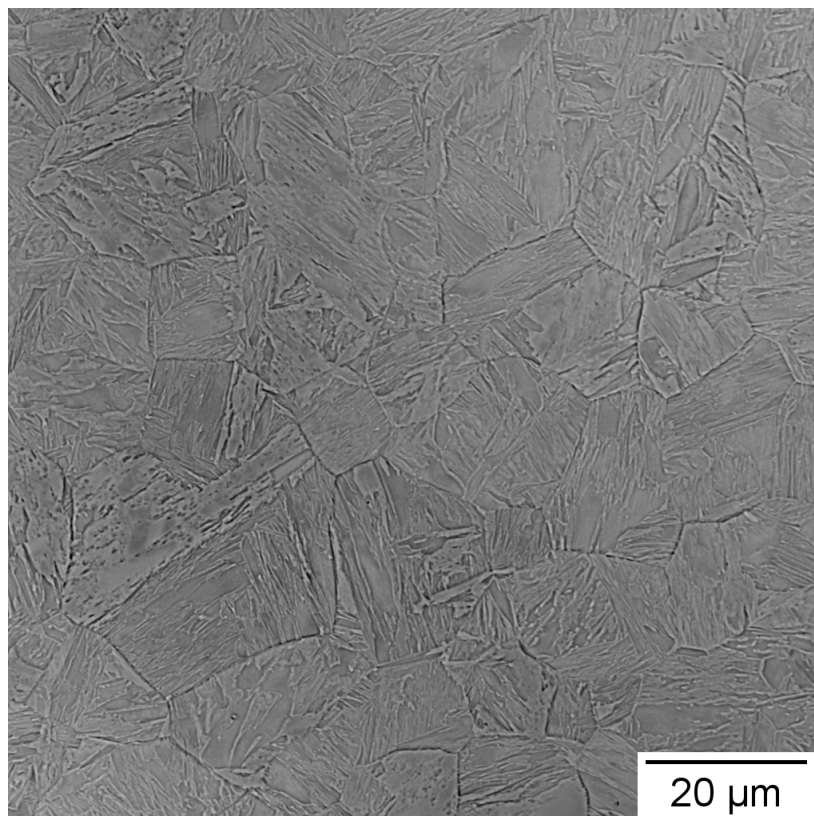
Fig. 4.4 Showing the microstructure of the heat treated sample. Equiaxed prior austenite grains containing martensite can be noticed. The arrows indicates one of the prior austenite grain boundaries. The average prior austenite grain size is $(12.3 \pm 1.5)\,\mu m$

.

quenched steels, respectively. The specific role of retained austenite is not studied in this work as the amount is small with large standard deviation and similar amount in both sample.

(a)   (b)

(c)   (d)
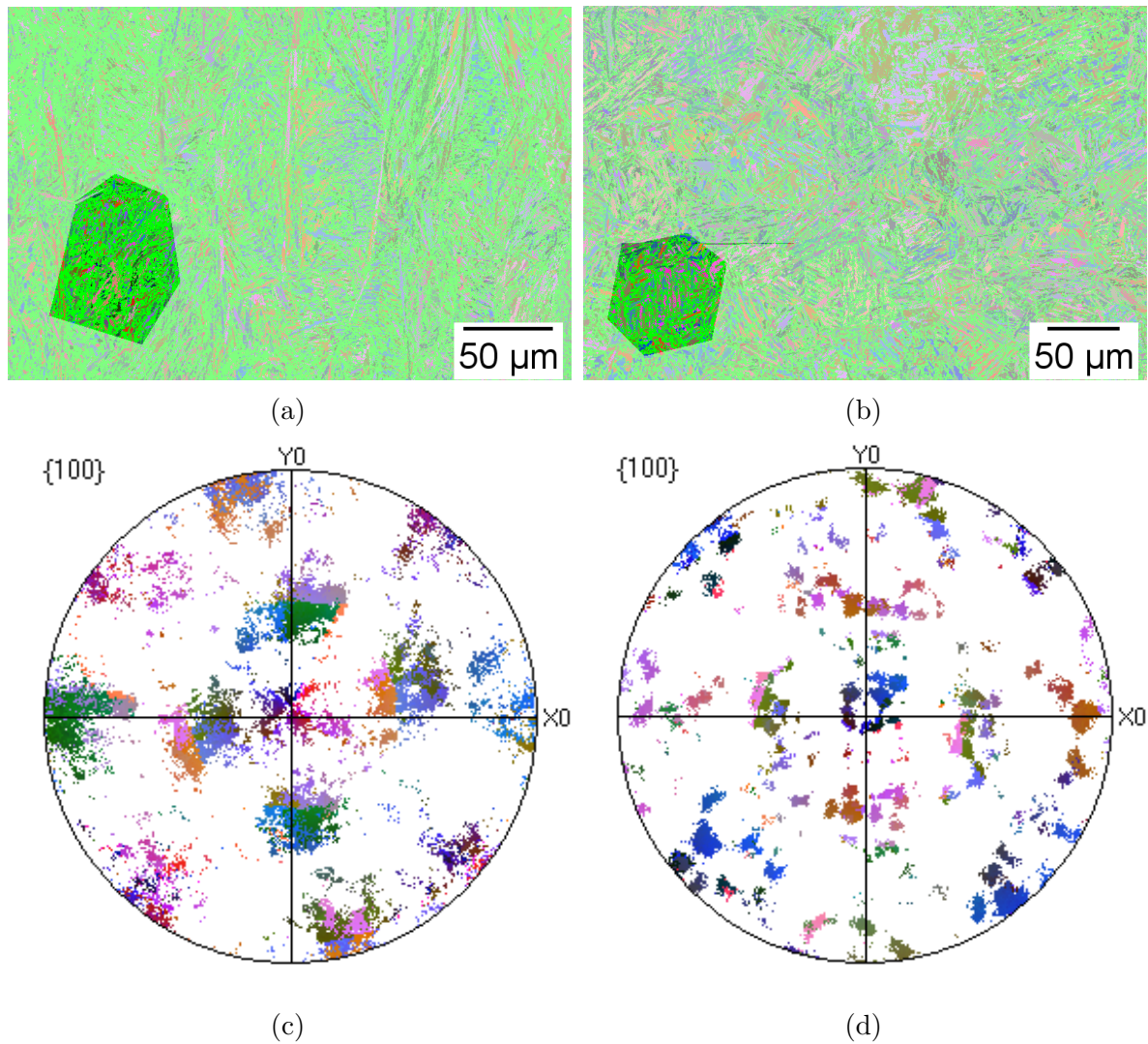
Fig. 4.5 (a) & (b) Inverse pole figure orientation map of the hot-rolled steel, and the quenched steel, respectively. (c) & (d) $\{100\}_\alpha$ pole figure of highlighted prior austenite grain in (a) and (b), respectively. It is emphasized that each pole figure is from a single prior austenite grain.
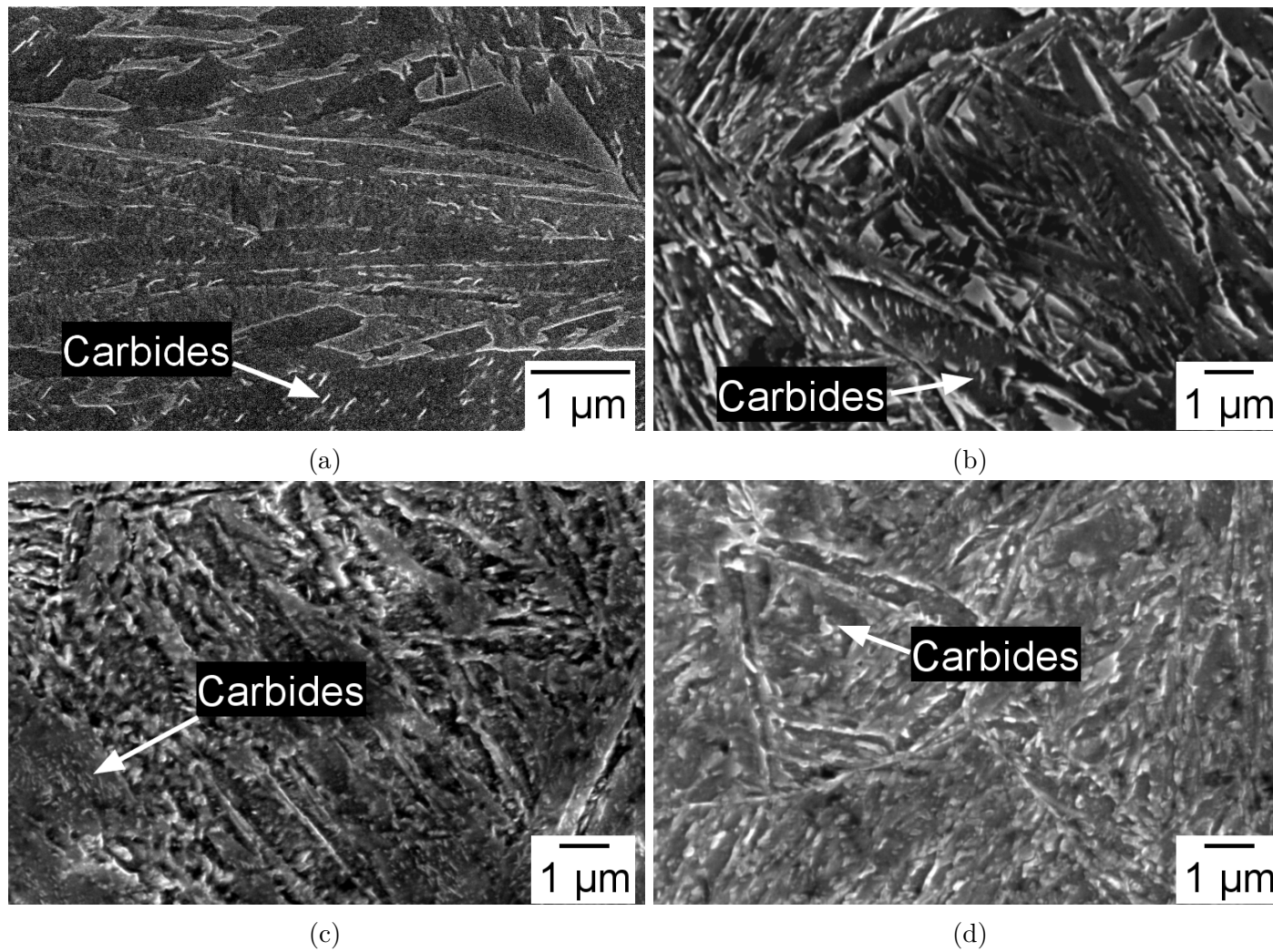
Fig. 4.6 Microstructures of (a) & (b) hot-rolled and tempered at 190 and 300 °C for 2 h, respectively. (c) & (d) Quenched and tempered at 190 and 300 °C for 2 h, respectively.

The hot rolled, and quenched steels were tempered and their microstructures are shown in Figure 4.6. Tempering the martensite causes cementite to precipitate. Figures 4.6a and 4.6b show tempered variants of rolled steel at 190 °C and 300 °C for 2 h respectively, while Figures 4.6c and 4.6d show tempered variants of the reaustenitised and quenched steel. The morphology of cementite is plate-like in all of the samples. The major qualitative difference between the tempered variants of the rolled and of the quenched is that the carbides in latter appear more in number.

4.2   Mechanical properties

4.2.1   Tensile test

Although many mechanical data are available on the hot-rolled steel, it was necessary to characterise the subsequent heat-treated samples. Some samples of the hot-rolled steel were nevertheless tested for reference. The 6 mm plate thickness prevents conventional fracture toughness tests. Tensile tests were therefore carried out to determine the ductility. It is evident from Figure 4.7 that the quenched steel broke in a brittle manner before significant plastic yielding, whereas the hot-rolled steel behaved in a ductile manner. Figure 4.8 shows the mixed mode tensile fracture surface of the rolled sample, consisting of ductile dimples and quasi-cleavage. In contrast, brittle cracks and cleavage facets dominate in the case of quenched samples. Therefore, the purpose of the reaustenitised and quenched condition, i.e., to embrittle the originally hot-rolled steel, was considered achieved.

Tempering the rolled samples naturally weakens them and the ductility was increased only when tempered at 300 °C. Both ductility and strength decrease when the rolled samples are tempered at 190 °C. The fracture surfaces (Figure 4.9) of the samples tempered at 190 °C were nearly flat with narrow shear lips compared to the one tempered at 300 °C. On the other hand, tempered variants of the quenched steel recovered ductility to a maximum of 4 % but insensitive to the tempering temperature over the range studied.
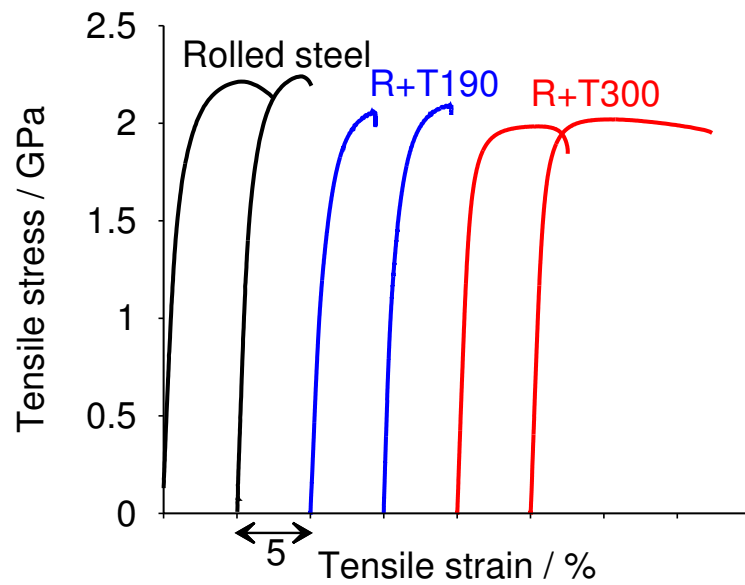
(a) Rolled, and its tempered variants
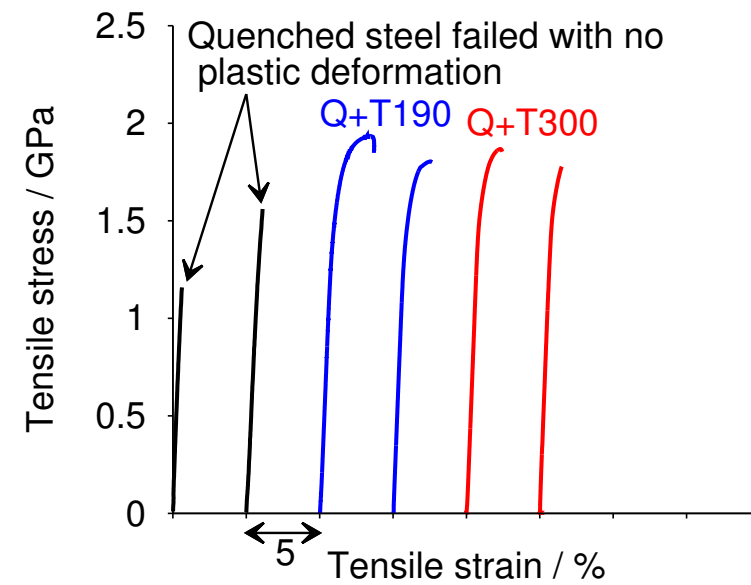
(b) Quenched, and its tempered variants

Fig. 4.7 Engineering stress - strain curves of the rolled steel in black lines in (a), and of the reaustenitised and quenched steel in black lines in (b). The quenched steel fractured at about 1.6 GPa with negligible plastic deformation. Blue lines indicate tempering at 190 °C, while the red lines for 300 °C.

(a)   (b)
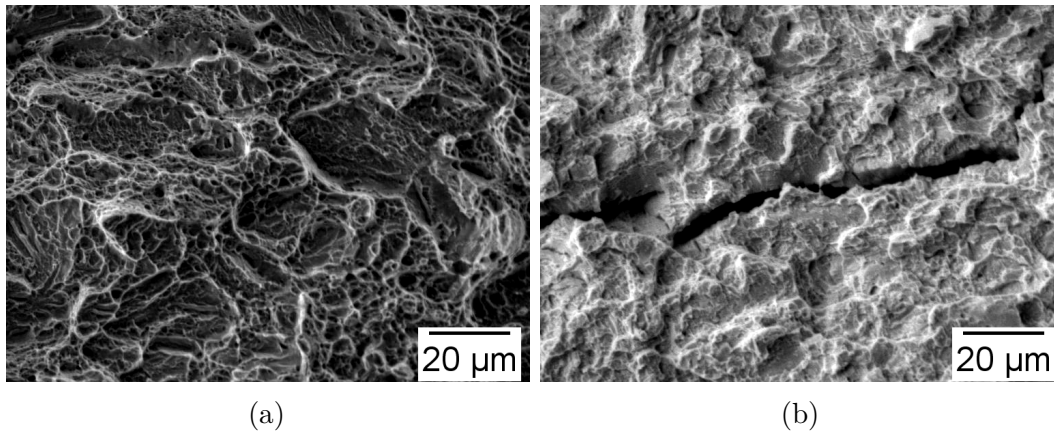
Fig. 4.8 (a) Micrograph of a fractured hot-rolled steel revealing ductile and quasi-cleavage features. (b) Brittle fracture of the quenched steel.

4.2.2 Impact test

The samples were impact tested at room temperature to compare how the rolled steel performs compared to the quenched samples. The impact energies absorbed and fracture surfaces of the tested samples are shown in Table 4.1 and Figure 4.10.

Table 4.1 Charpy impact energy of the samples. Subsize $5 \times 5 \times 55$ mm notched-bar samples were used for all conditions. Three samples are tested for each test condition.

	Impact energy / J
Rolled	12.0 ± 2.4
R+T190 °C	10.4 ± 0.6
R+T300 °C	10.2 ± 1.4
Quenched	2.8 ± 1.3
Q+T190 °C	11.5 ± 0.4
Q+T300 °C	12.2 ± 1.6

(a)   (b)
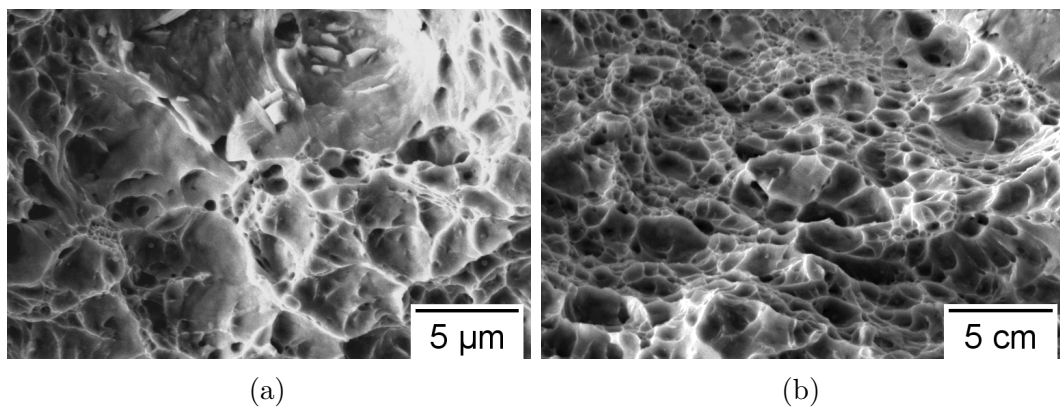
Fig. 4.9 (a) A fractured, tempered rolled-steel revealing quasi-cleavage features in (a) tempered at 190 °C, (b) relatively more ductile features tempering at 300 °C.

(a) Rolled:12.0 ± 2.4 J   (b) R + T190 °C: 10.4 ± 0.6 J   (c) R + T300 °C: 10.2 ± 1.4 J

(d) Quenched: 2.8 ± 1.3 J   (e) Q + T190 °C: 11.5 ± 0.4 J   (f) Q + T300 °C: 12.2 ± 1.6 J
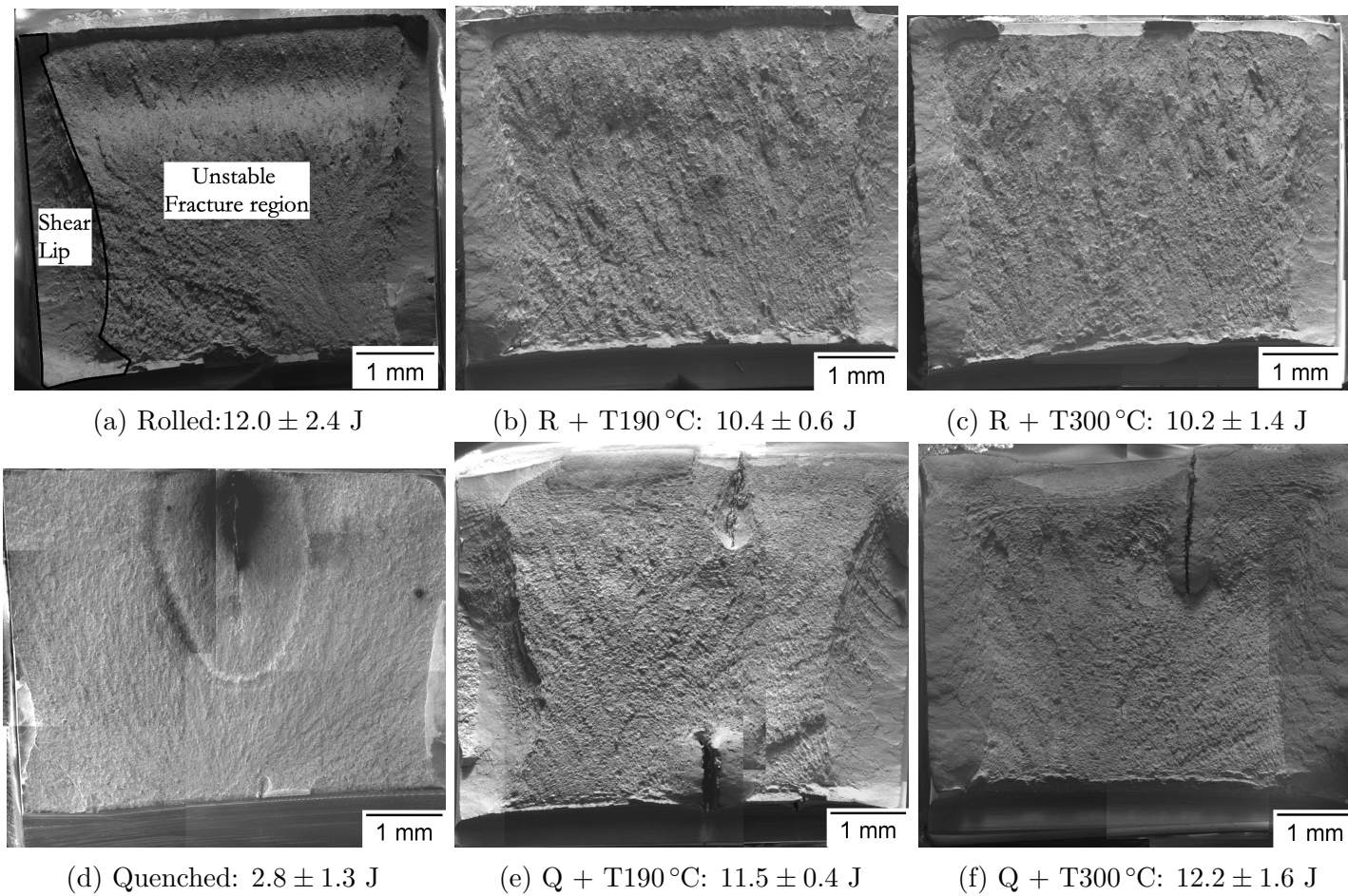
Fig. 4.10 Fractographs of Charpy V-notch impact specimens of (a) hot-rolled steel, (b) hot-rolled and tempered at 190 °C for 2 h, (c) hot-rolled and tempered at 300 °C for 2 h, (d) quenched steel showing equiaxed grains, (e) quenched and tempered at 190 °C for 2 h, and (f) quenched and tempered at 300 °C for 2 h.
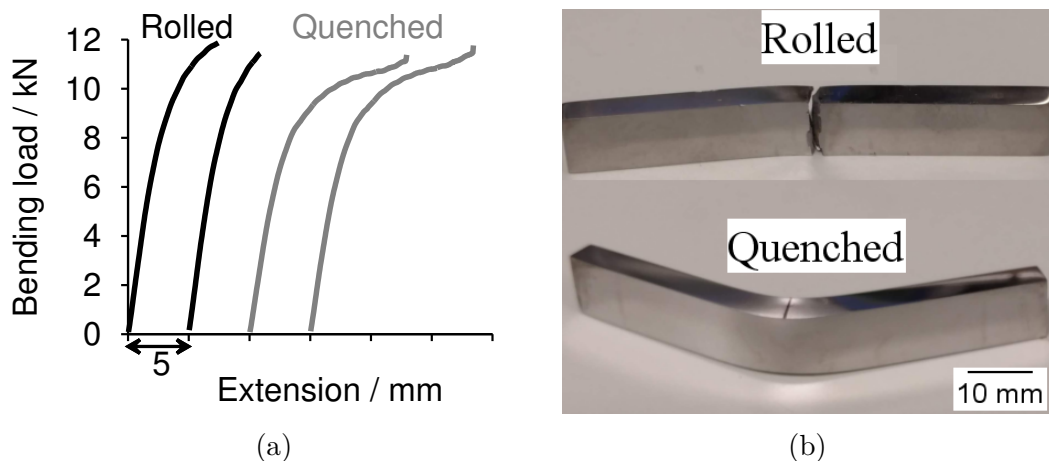
Fig. 4.11 Showing (a) Bending-load versus displacement curves at ambient temperature, and (b) broken pieces of rolled steel, and bent sample of quenched steel.

The impact energy of the quenched sample is low compared to that of rolled samples. Two important features of fracture surface are described in Figure 4.10a. An increase in the shear lip area increases energy absorption, while the region labelled 'unstable' does not contribute to toughness. There was little or no shear lip formation in the quenched specimens.

4.2.3   Bend test

Bend testing is another way of studying the ductility of the materials. Figure 4.11 shows load-extension curves and the appearance of the tested samples. Two samples were tested in each case. The rolled samples broke before the quenched ones despite their higher toughness. The load per unit of extension is large in the rolled sample compared to the quenched sample. Higher loads lead to greater stress at the bottom surface which experiences tension. This may be one of the reasons for the early fracture in the rolled sample.

Figure 4.12 shows longitudinal sections of the fractured surfaces. Surprisingly, the rolled sample has a similar amount of shear fracture appearance as in impact test without any cracks. In contrast, the quenched samples have multiple cracks in both the sections. The cracks in Figure 4.12c suggest that delamination was taking place. Delaminaiton is a mode of failure where a material fractures in layers, thus consuming more energy to clear new surfaces. It is speculated that the existence of quench cracks helped to create cracks perpendicular to the loading direction.
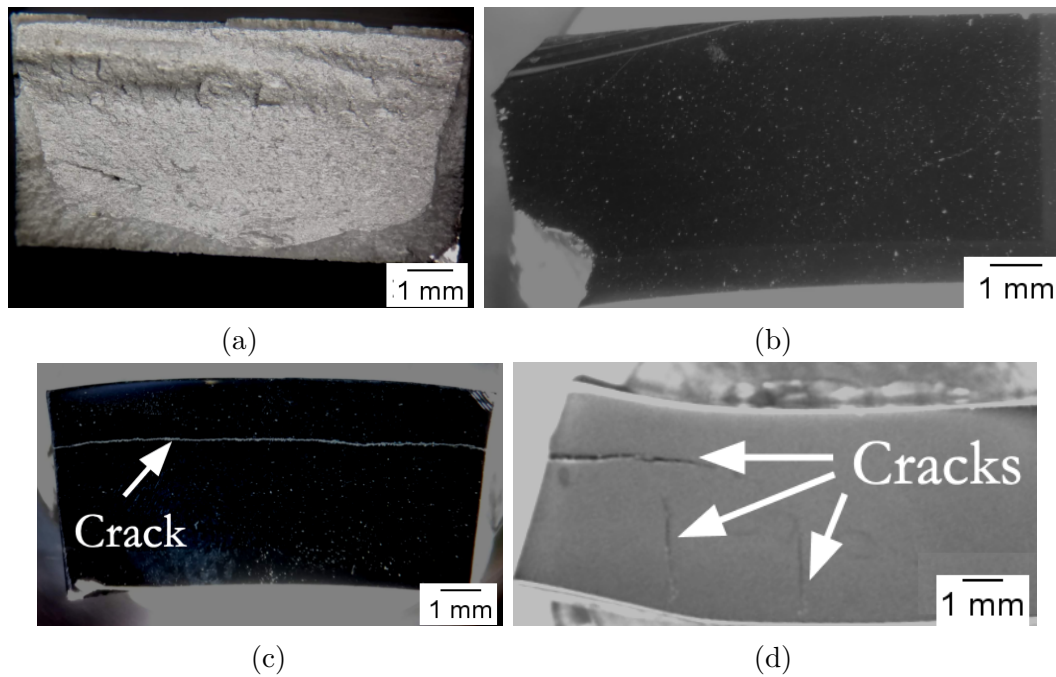
Fig. 4.12 Showing (a) fracture surface of a rolled sample, (b) longitudinal section of the rolled sample, (c) transverse section of the bend in a quenched sample, and (d) longitudinal section of the quenched sample near the bend.

4.3 Conclusions

The martensite in the hot-rolled structure is expected to be much tougher, for two reasons. Firstly, the crystallographic grain size, which controls the cleavage mode of fracture [220] and secondly because fine plates of martensite been shown to have a reduced tendency to crack [149]. Though fracture toughness values are not obtained for the quenched and its tempered variants, it appears that the quenched steels definitely have poor fracture toughness based on other mechanical properties and fracture surface analysis. Therefore, from the {100} pole figures, the tensile test results and fracture surface analysis, it can be assumed that the fracture toughness in the austenised and quenched is lower compared to the rolled steel.

Chapter 5

Role of toughness in impact-abrasion

5.1 Introduction

Impact-abrasion includes the effects of both the collision of abrasive particles with the solid surface, and scratching motions; other factors such as particle size, shape, environment and rate of impact and abrasion, together make this a complex problem [1, 2]. The phenomenon itself is of considerable importance in the wear-resistant steels used in earth-moving equipment such as excavators and loaders, and machines used in mining operations. Abrasion *per se* correlates strongly with hardness, although it is well-established that hardness alone does not always explain the wear behaviour [3–10, 104]. For instance, the abrasion wear resistance of commercially available steels showed sparse correlation with their hardness [104]. Loss of material in a phenomenon such as impact abrasion is likely to have some dependence on the failure mechanism [83].

The purpose of the work presented here was to examine specifically the role of toughness of a newly developed steel on impact abrasion.

5.2 Material and Experimental details

The test parameters implemented in the present study are listed in Table 5.1, chosen to be similar to those in the published literature [223]. The Kuru granite used in this work has the same crushability, about 38 % [224], but relatively lower abrasiveness (1380),

while Sorila granite used in the reference work had 1500 abrasiveness. In both granites, the abrasiveness is clearly in an extreme abrasive range [51]. Although there is a small difference in the abrasiveness measured with the laboratoires des ponts et chaussees, paris (LCPC) method [224], the results from this work can be compared against the reference data which is advantageous in addressing the novel alloy. Kuru granite was originally crushed with a jaw crusher in the quarry and then sieved to the selected 10-12.5 mm particle size.

Table 5.1 Impeller-tumbler test parameters.

Sample dimensions	$75\,\mathrm{mm} \times 25\,\mathrm{mm} \times 6\,\mathrm{mm}$
Rotation speed impeller	$700\,\mathrm{min}^{-1}$
Rotation speed tumbler	$30\,\mathrm{min}^{-1}$
Abrasive size	10 to $12.5\,\mathrm{mm}$
Abrasive mass	$900\,\mathrm{g}$
Test duration	$240\,\mathrm{min}$
Abrasive	Granite (Kuru quarry, Finland)
Sample angle	$60°$

5.3   Results and discussion

5.4   Wear test results

The relative wear loss data, the weight losses relative to that of a reference sample, R400 with 400 BHN, are plotted in Figure 5.1 and listed in Table 5.2. The hardness values reported here were obtained from the surface of the samples. The high standard deviation is attributed to chemical segregation in the industrially produced rolled steel as shown in Figure 4.1a. R400 is commercially available steel with hardness 400 BHN, R is for brand name. The supplier or brand name can not be disclosed under confidential agreement. The tests were done in conditions comparable to those of the published work [223]. Figure 5.1 shows that the wear loss of the reference samples (R400, 450, 500) indeed correlate with hardness, but it is evident that our hot-rolled steel, which is softer than the reaustenitised and quenched version, has better wear performance, confirming that its better toughness prevails. Furthermore, at essentially the same hardness, the hot-rolled steel performs far better than steel R500 [51]. The relative wear loss of the rolled samples is about $17\,\%$ less than that of the quenched

samples. The standard deviation of the many samples tested in the impact-tumbler test was evaluated to be less than 4 % [223], and it is about 2 % for the reference samples in impact-abrasion tests. Therefore, it is evident that the wear loss in the much harder quenched samples is at least 10 % greater than that of the rolled samples.

A novelty of the present work is that it reports experiments where toughness is varied greatly, while maintaining a martensitic microstructure and hardness. The martensite in the hot-rolled sample is in a greatly refined state, reflected in its high toughness and ductility. A previous study could not be conclusive because hardness, toughness, microstructure and alloy composition were not controlled to enable clear comparisons [34].

Table 5.2 Relative wear loss in comparable steels. Relative wear loss is weight loss relative to R400. Minimum ten surface hardness measurements were made on each sample, while for wear loss, two samples were tested and three readings of weight loss were taken for each sample.

Sample	Hardness / HV30	Relative wear loss
Hot rolled	561 ± 23	0.700 ± 0.003
Hot rolled and tempered at 190 °C for 3 h	519 ± 11	0.730 ± 0.003
Quenched	666 ± 8	0.820 ± 0.003
Quenched and tempered at 190 °C for 3 h	582 ± 5	0.900 ± 0.003
R400	395 ± 14	1.00 ± 0.02
R450 [223]	450 ± 15	0.920 ± 0.010
R500 [223]	515 ± 17	0.880 ± 0.010

Surface roughness

Surface roughness of the tested samples as well as comparative data on pearlitic and bainitic steels tested in dry sand rolling / sliding wear tests are listed in Table 5.3. All the impact-tumbler test results shown were generated under identical conditions. Compared to pure abrasion, impact-abrasion exacerbated roughness. Pure abrasion involves material removal through microcutting and micro-fatigue, so it is not surprising that it leads to a lower roughness. Impact-abrasion, in contrast, includes chipping and fragmentation. Figure 5.2 shows that the roughness does not correlate well with hardness for any of the samples. The newly developed steel shows similar roughness values, although the roughness of the rolled sample is marginally smaller. To understand these observations, the worn surface was characterised using a number of techniques.
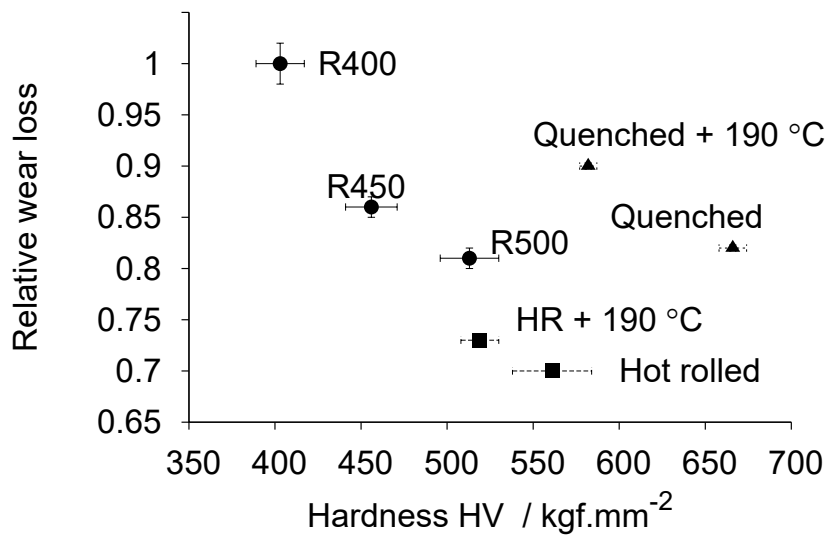
Fig. 5.1 Relative wear loss of different steels plotted against their hardness. The triangles represent the heat treated samples of hot-rolled steel, and the filled squares the hot-rolled steel.
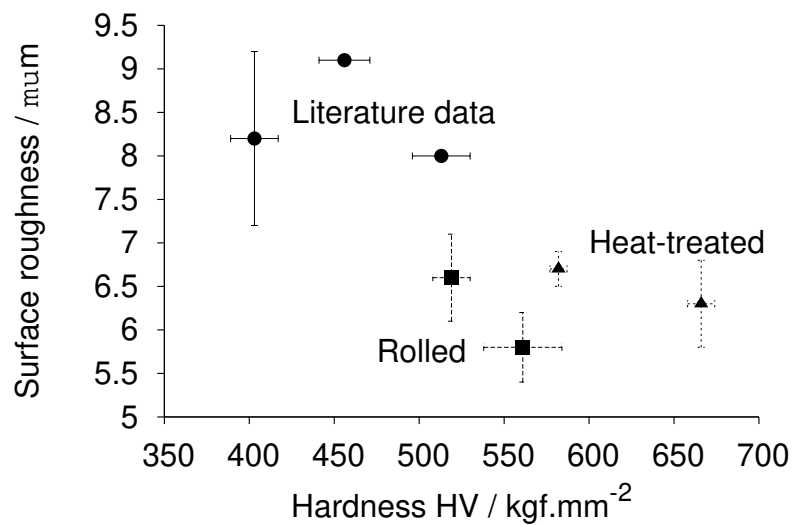
Fig. 5.2 Roughness of the surface of the tested samples. The data for the R450 and R500 samples are from [223].

Unlike in the case of pure abrasion, the wear caused by impact-abrasion is not uniform across the sample surfaces (Figure 5.3). The worn sample edge resembles the rounded tip of the cutting edges of a typical mining loader bucket [225]. Samples for the surface as well as for the cross sectional microstructural studies were cut as marked

Table 5.3 Surface roughness after impact-abrasion testing compared to previous studies, varying steel microstructures, and test methods. Three profiles were obtained for each sample.

Sample	Test type	Surface roughness / μm
Hot rolled	Impeller-tumbler	5.8 ± 0.4
Hot rolled, tempered at 190 °C, 3 h	Impeller-tumbler	6.6 ± 0.5
Quench	Impeller-tumbler	6.3 ± 0.5
Quenched, tempered 190 °C, 2 h	Impeller-tumbler	6.7 ± 0.2
R400	Impeller-tumbler	8.2 ± 1.0
R450	Impeller-tumbler	9.1
R500	Impeller-tumbler	8.0
S355	Impeller-tumbler	15.1
R400	Uniaxial crusher	10.1
R400	Pin on disc	8.0
R450	Uniaxial crusher	7.9
R500	Pin on disc [223]	6.0
R500	Uniaxial crusher [223]	7.0
Pearlite	Dry sand rubber wheel [154]	3.0
Bainite	Dry sand rubber wheel [154]	1.1

in Figure 5.3b. Sample 'A' (10×10 mm) was used to characterise the surface, while sample 'B' (10×5 mm) was used to study the cross section.

A typical surface of the tested sample is shown in Figure 5.4. The back-scatter electron images reveal darker-contrast regions containing granite, which contains silicates and oxides with low atomic number elements, including, Si, Al, and O, as confirmed using energy dispersive X-ray spectroscopy, Figure 5.5 and Table 5.4. The topography of the same area as in Figure 5.4a can be seen in 5.4b. A typical impact crater and abrasion are marked in Figure 5.4b. The abraded regions are relatively bright

(a)   (b)
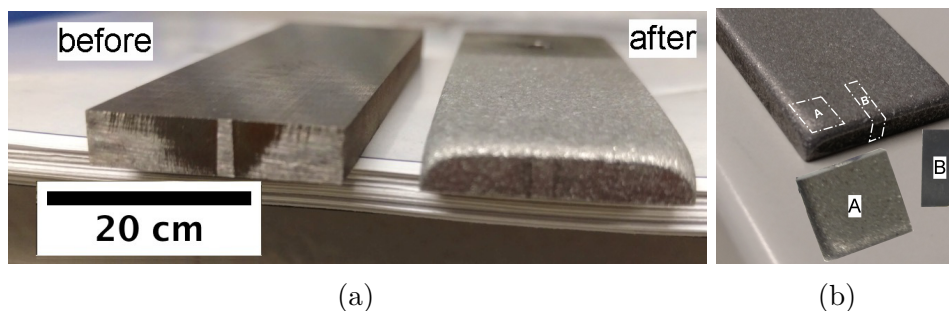
Fig. 5.3 (a) Impeller-tumbler samples before and after testing. (b) The areas marked as 'A' and 'B' were cut for the further characterisations. 'A' (10×10 mm) was used to characterise the surface, while 'B' (10×5 mm) was used for the cross sectional studies.
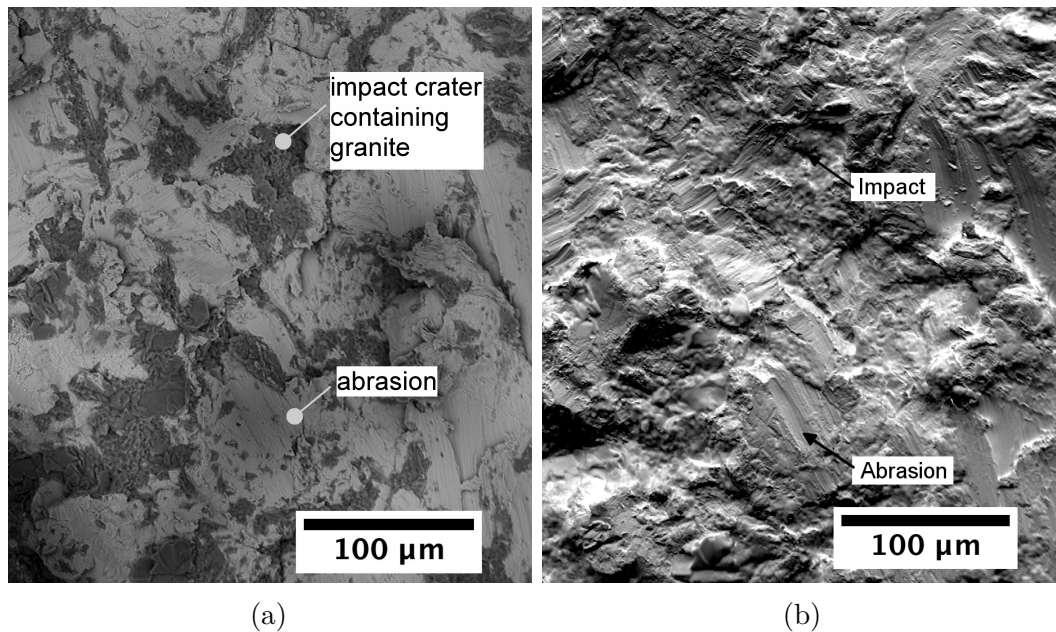
Fig. 5.4 Backscattered electron images of the worn surface of a hot-rolled sample, (a) illustrating two distinctive regions of wear: impact and abrasion. (b) Topography of the same area as in (a). The flat regions in (b) show abrasion in different directions.

compared to the regions of impact, and uniform in their contrast due to their small roughness. The rougher impact regions are darker and less resolved. It is noteworthy that the directions of the abrasion scratches are not constant, as would be expected from three-body or two-body abrasion wear. Some areas indicate delamination, which is one of the key damage mechanisms in sliding or abrasion wear [226].

The damage modes observed in impact-abrasion are shown in Figure 5.6. The test consists of many chaotically moving granite particles impacting the test surface at different angles from 0 to 90° and also at varying velocities. Near 0°, the damage is abrasive, involving microcutting, wedge formation and microploughing. At other angles of impact, the material is displaced or removed from the site of the impact depending on the impact energy, and impact craters are also developed. When the impact occurs approximately normal to the surface, the displaced material from the crater is distributed as a lip around the crater, although some material may also be ejected from the sample, depending on the energy of the impact. An example is illustrated in Figure 5.6a, where the impact was at an acute angle with material piling up on the sides of the crater. The crater itself contains some of the granite responsible for the damage. At the exit side of the impact, small chips of the steel can be noticed, and hence the process of such removal can be classified as microchipping.
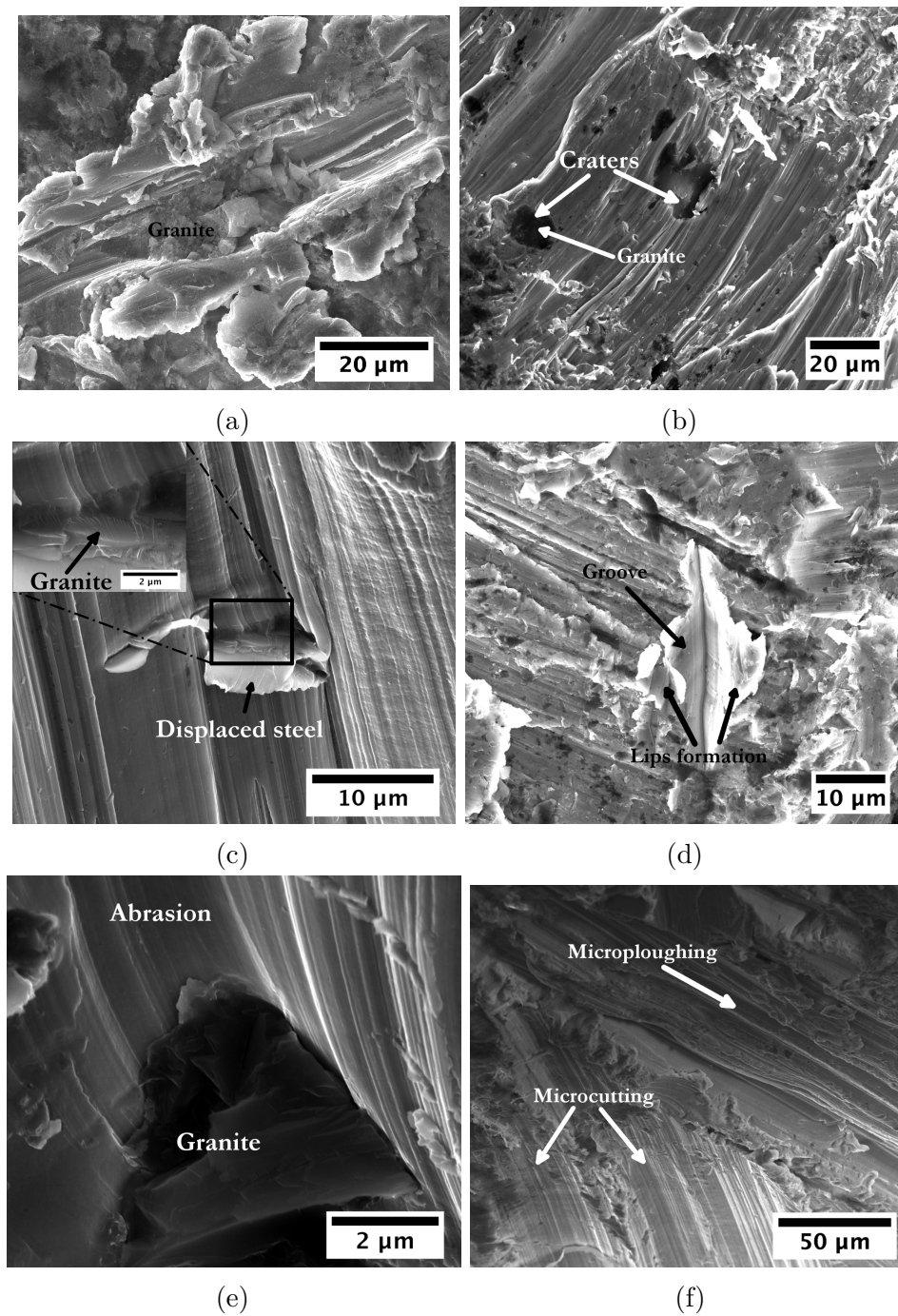
Fig. 5.6 Surface topography of the tested samples after 4 h of testing. The images illustrate the impact-abrasion wear in general, (a) and (b) showing craters formed by impacts, (c) and (d) cutting by the abrasives, and (e) and (f) abrasion due to moving granite particles. (a), (c) and (e) are from the quenched steel, while the rest of the images are from the hot-rolled steel.
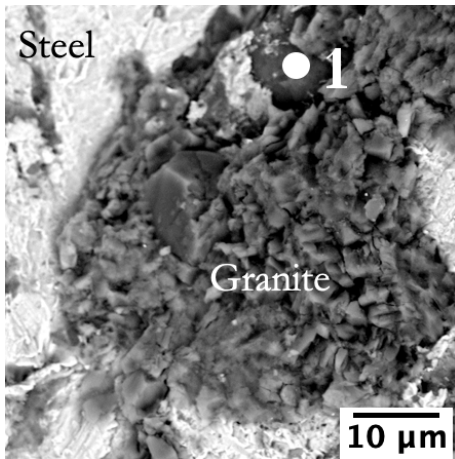
Fig. 5.5 Shows a granite particle in an impact crater. The granite essentially contains oxides of Al and Si.

Table 5.4 Contents (in fraction) of the granite obtained by energy dispersive X-ray analysis from the region marked '1' in Figure 5.5.

Element	At. conc.	Wt. conc.
O	0.50	0.33
Si	0.26	0.31
Al	0.11	0.12
Fe	0.08	0.18
Na	0.03	0.02
Ca	0.02	0.03
K	0.006	0.01

Other impact incidents where the sharp edges of a granite particle has caused the formation of a groove and lips are shown in Figures 5.6c and 5.6d. The removal of material is similar to that of micromachining reported in the previous investigations [227]. However, in the impact shown in Figure 5.6d, in which there is no debris left as in the previous impact example, the lips are severely strained. Any lips that form also act as obstacles for the abrasion by granite and hence can be removed by subsequent action, rather like macroscopic asperities. Intense shear of remaining material can occur during the removal process. A case of abrasion after an impact event is shown in Figure 5.6b. There are two craters, one containing granite (on the left hand side of the image), and another without any debris.

It is possible that the embedding of hard granite particles in the steel during the process of impact abrasion actually enhances its resistance to further damage, by creating in effect a metal matrix composite. It is known that in the case of quartz particles, that their embedding leads to a better pin-on-disc wear resistance when the substrate has a hardness in the range 400-800 HV, but spalling becomes easier when the substrate is soft [228]. The steels characterised in this study fall in a fairly narrow hardness range of 525-675 HV, so the mechanism of embedded particles should be identical and therefore do not affect the ranking in terms of wear loss. There is a caveat to the comparison with the quartz experiments, that the present study involves both severe impact and abrasion, so there are many cracks created in the embedded granite
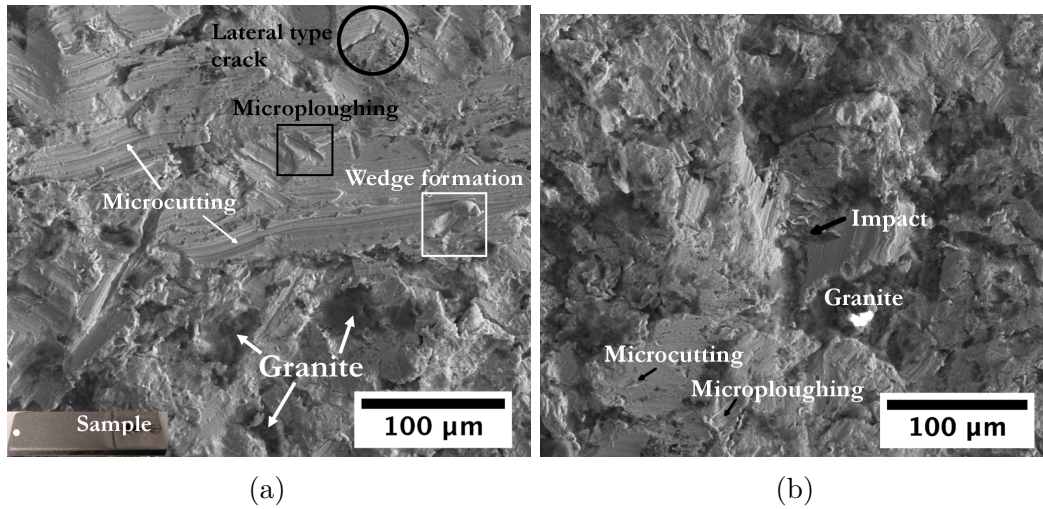
Fig. 5.7 Surface topography following 4 h of testing, (a) a hot-rolled sample, (b) quenched sample.

particles, which may render them liable to detachment. However, these phenomena warrant further studies.

Figure 5.7 shows a comparison between the hot-rolled and quenched samples. Although the same mechanisms of damage are apparent in both samples, the quenched samples show much more brittle behaviour with smaller extents of microcutting regions.

5.4.1 Microscopy of sections

Dominant wear mechanisms in the cross section sample 'B' are shown in Figure 5.8. Representative micrographs from the abrasion and impact dominant mechanisms are presented in Figure 5.9. Data from about ten measurements for the hot-rolled and about twenty measurements for the quenched are listed in Table 5.5. In general, the hot-rolled and quenched steels show similar abrasion resistance, although the material within the abraded regions seems to be more damaged in the latter case (Figure 5.9). On the other hand, the craters in the impact zone, which represent the biggest surface of the impact-tumbler sample, are largest for the quenched steel, and there also seem to be cracks associated with the craters in the steel. This must be consequence of the low toughness in quenched steel compared to the hot-rolled steel, which explains why the wear rate is greater for the quenched steel even though it is much harder than the hot-rolled grade.

Further, the hot-rolled steel strain hardens during wear to a greater extent than the quenched grade (Figure 5.10), presumably because of its greater ductility. It is

Fig. 5.8 The cross section sample 'B' shown in Figure 5.3b of the impact-tumbler sample. Abrasion predominates in region '1', and impact damage in regions '3', with region '2' representing a transition area.

Table 5.5 Depth of the craters in due to impacts on the test surface. Abrasion-dominated and impact-dominated regions are illustrated in Figure 5.8.

Sample	Abrasion dominated region	Impact dominated region
Hot-rolled steel	5.0 ± 1.7 µm	7.5 ± 3.7 µm
Quenched steel	6.5 ± 2.0 µm	15.8 ± 5.5 µm
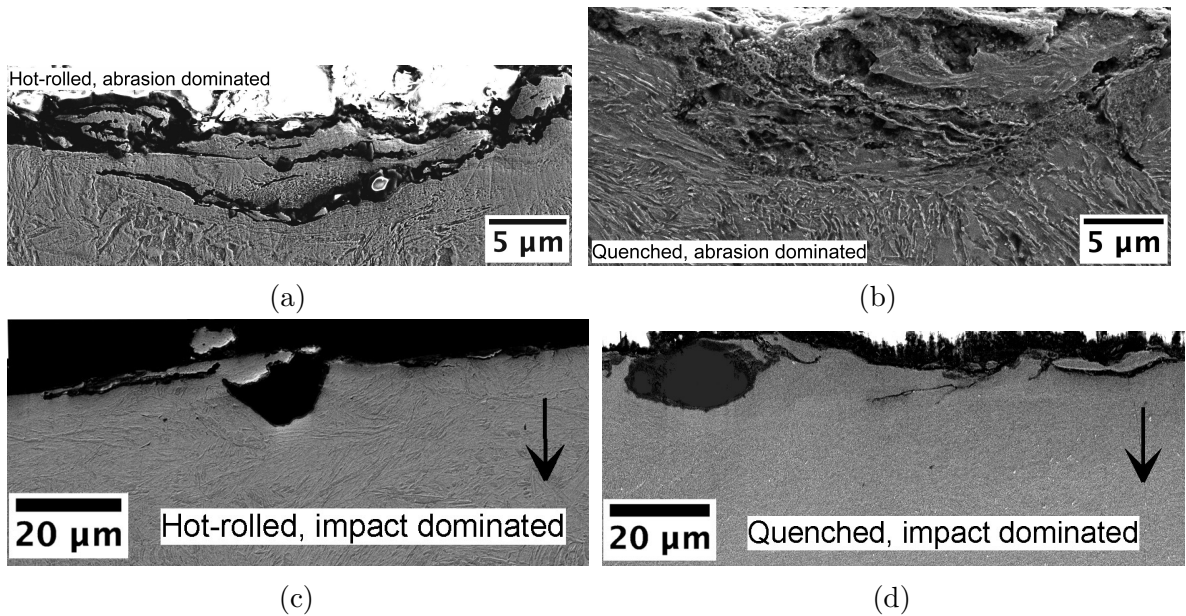
Fig. 5.9 Metallography of the predominantly abrasion and impact resistant regions illustrated in Fig. 5.8. The arrows show the direction of impact in (c) and (d).
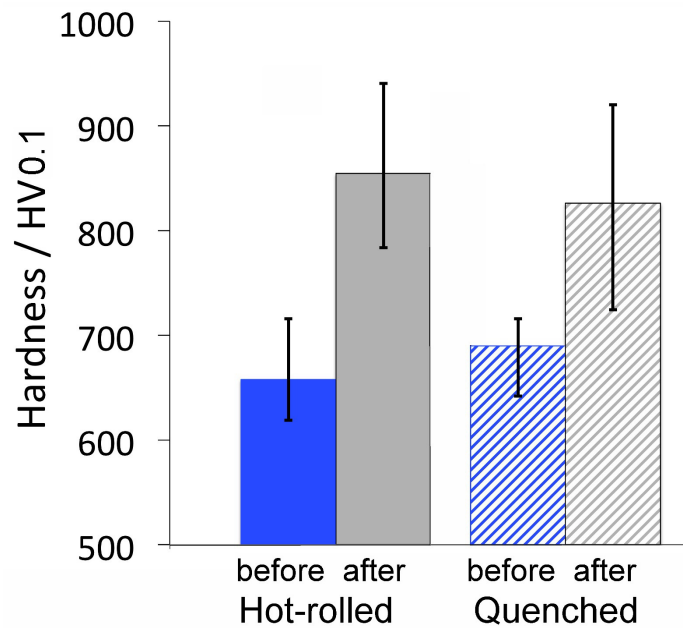
Fig. 5.10 Hardness data obtained using a 0.1 kgf load to assess the surface hardening after wear testing. The "error" bars in this case illustrate the maximum and minimum values recorded.

well known that surface hardening, leads to improved wear resistance in many abrasion scenarios [11, 34].

5.5   Conclusions

This study is the first of its kind to develop steels with two levels of toughness without changing either composition or microstructural phase, and at similar hardness levels. It has been demonstrated here that under the given circumstances, the steel with a better toughness outperforms a harder and relatively brittle steel.

In hindsight, this result may look quite obvious, but the work reveals two mechanisms that rely on toughness and ductility in addition to hardness. The first is that the abrasion wear resistance of the steel is clearly better when it is tougher, because the material that is extruded by the abrasive action is more likely to detach from a brittle steel. On the other hand, and even more interestingly, the wear resistance did not show a significant difference between the two steels, when the impact-dominated regions of the samples were studied. Secondly, the steel with the greater ductility revealed a greater hardness in the vicinity of the wear surfaces after the impact-tumbler tests. Despite the fact that the quenched grade had a greater initial hardness, the hot-rolled steel had a greater capacity to work harden given its much larger ductility.

Further investigation of the damaged surface and subsurface is required to understand the impact-abrasion damage mechanism in general and the role of toughness in changing the wear mechanism. 3D SEM and X-ray tomography may help in revealing the damage mechanism at surface and subsurface level although our attempts with these techniques were unsuccessful. The details are given in Appendix 1.

Chapter 6

Wear mechanism during impact-abrasion wear

The objective of the work presented here was to see whether a set of characterisation techniques can reveal the mechanism of damage during impeller-tumbler testing of the novel steel that has a combination of properties listed in Chapter 5, enabling it to resist weight-loss when compared against commercially available alloys tested in an identical manner.

The samples that were cut as described in the previous chapter (in Figures 5.3 and 5.8) for surface as well as cross-sectional microstructural studies, were characterized using electron microscopy to investigate the damage effects at the microscopic scale, in two- and three-dimensions.

6.1   Cross-sectional microscopy

Typical craters in the rolled, and quenched sample can be seen in Figure 6.1a and 6.1c. Such deep craters are possible when the abrasive impacts occurs normal to the surface. However, these events are not necessarily from a single impact. In Figure 6.1c it can be noticed that abrasive particle is locked under the abraded material. The material might have dragged on the granite either due to abrasion or due displacement caused by previous collisions.

By analogy with abrasion, the affected region can be assessed as consisting of two zones [50, 132]. The contact zone where the granite and steel meets will degrade the most, but the underlying material undergoes plastic deformation to create the work hardened zone (marked '2'); material underneath is unaffected (marked '3'). The width
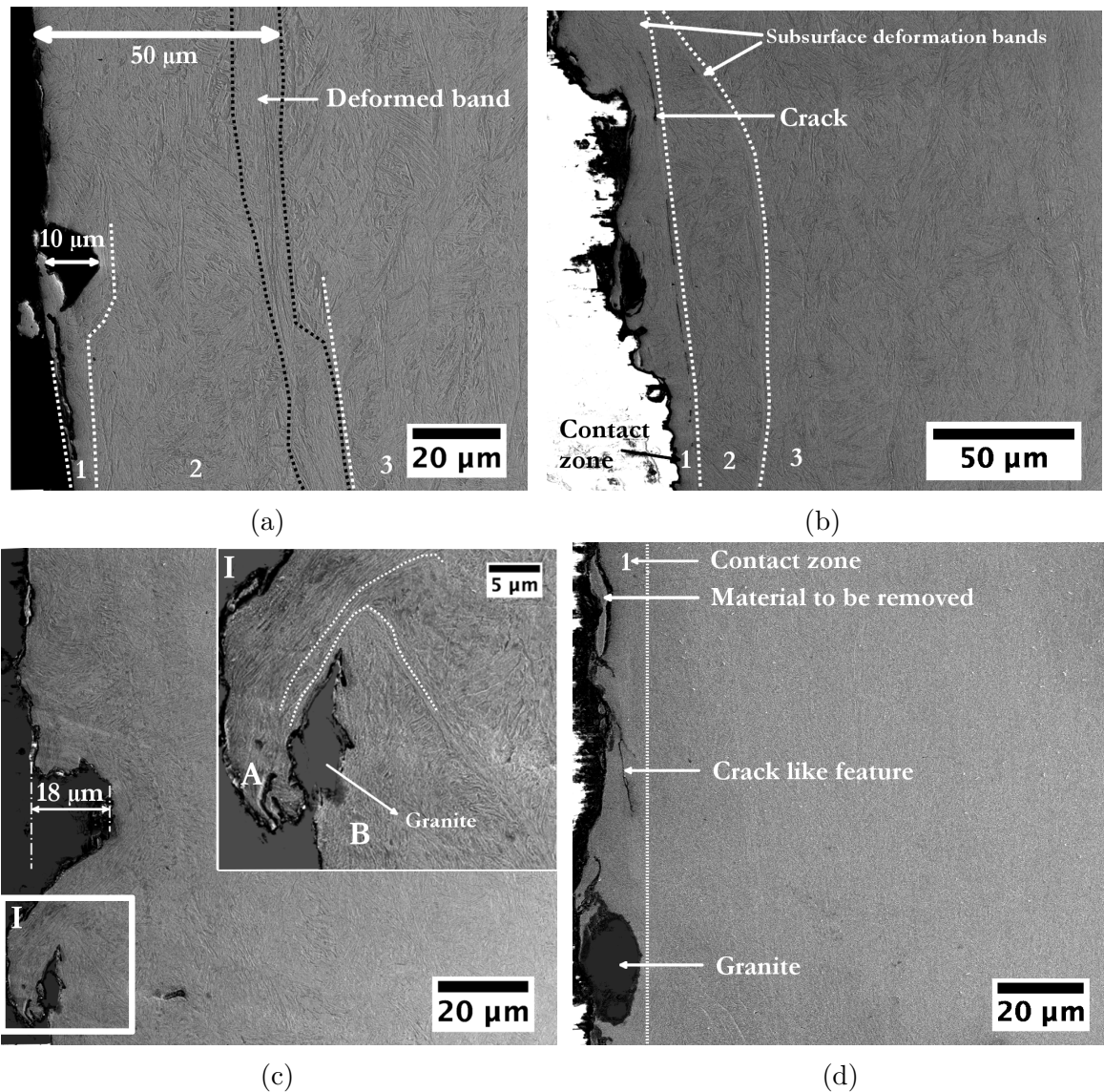
Fig. 6.1 Cross section of the rolled (a & b), and quenched samples (c & d) . '1', '2' and '3' indicate zones due to wear. (a) Locked crater and three different zones. A deformation band can also be seen in the work-hardened zone, '2' . (b) Another region showing subsurface deformation bands. Crack-like features can be seen in one of the bands. (c) Displaced material due to impact on the embedded granite. (d) Embedded granite and damage at the cross-section of the quenched steel.

of the contact layer is assumed to be related to the mean depth of the craters, measured to be about 7.5 ± 3.7 µm and 15.8 ± 5.5 µm in the rolled and quenched samples, respectively. This trend is consistent with the greater toughness of the hot-rolled steel in spite of the fact that the quenched sample is significantly harder.

It may be significant that there are no cracks penetrating from the craters into the interior of the steel, presumably because of the compressive nature of the impact and that plastic flow occurs to lead to the heaping of material around the impact itself.

6.2   Subsurface microscopy

The region below the wear surface was examined as a function of depth. The abraded surface was polished carefully for 10 s to 30 s on 4000-grit SiC paper at 100 rpm followed by diamond polishing with 3 µm paste on a synthetic cloth. The same topographic samples 'A' in Figure 5.3a were used for subsurface characterisation. The surfaces after such polishing for the rolled, and the quenched samples are shown in Figure 6.2.

Impact craters and abrasives penetrated the rolled surface, Figure 6.2a and 6.2c. Cracks associated with the impacts are also seen, often much longer and wider in the quenched than in the rolled sample. Some crack branching occurred, as might be expected from the complexity of the deformations involved. None of the features could be identified with Hertzian type contact in which damage would mostly be initiated below the surface. Another crack marked with black a arrow can be seen connecting two impact regions. Such cracks, invisible on the virgin surface of the abraded surface, are visible after removing a thin layer of damaged surface. Figure 6.2b reveals various damage features after etching the polished surface. Impact followed by abrasion can be seen. The abrasion event that caused to deform the displaced material due to impact can be seen in the figure. The white dashed lines show the abrasion features.

An impact and its crater are shown in Figure 6.2d. The impact was apparently from bottom-left corner to top-right corner as indicated by the black arrow in the figure. The impacted granite is partly locked and also removed the abraded material at the exit side of the impact. The cracks in the granite can cause volumetric expansion which further damages the surrounding deformed material.

To understand the crack like features in the cross-sectional microscopy, 3D SEM was performed to visualise 3D microstructure of the damaged surface. One such section is shown in Figure 6.3, illustrating a crack in sub-surface. After serial sectioning for about 20 µm, the images are stacked and a section perpendicular (direction is marked
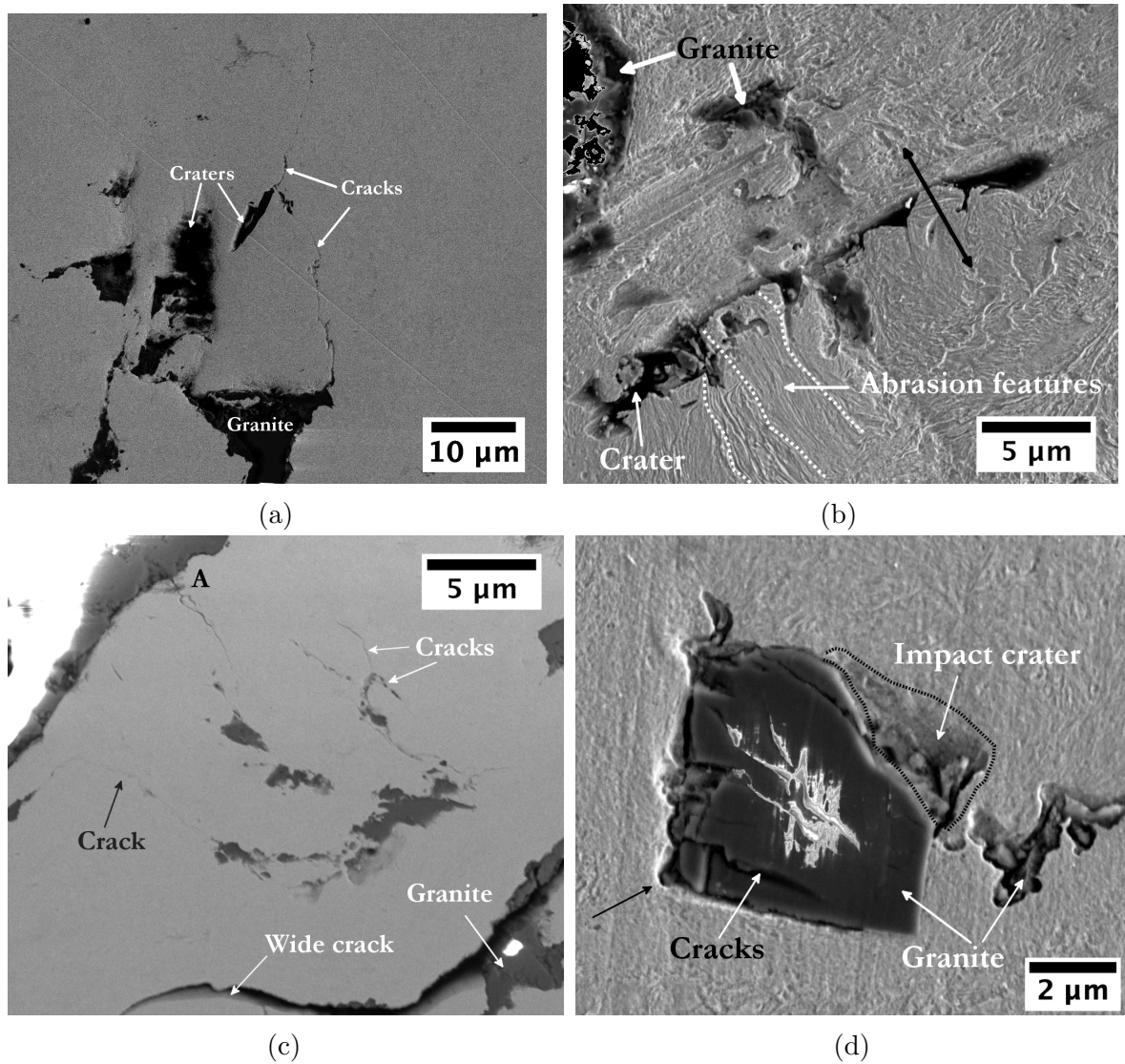
Fig. 6.2 Subsurface damage the rolled steel (a & b), and quenched steel (c &d). (a) Cracks, craters, and embedded granite can be seen. (b) Depicting how granite is locked inside the abraded steel. (c) Wide cracks, multiple cracks and embedded particles in quenched steel. (d) Embedded granite and cracks in it. Black arrow shows possible direction of impact.

with black arrow) to the crack is constructed and is shown in Figure 6.3. A granite particle was discovered inside the material, presumably inserted by impact followed by a welding of the broken surface during subsequent damage. This hypothesis is supported by the fact that incomplete welds were frequently encountered.
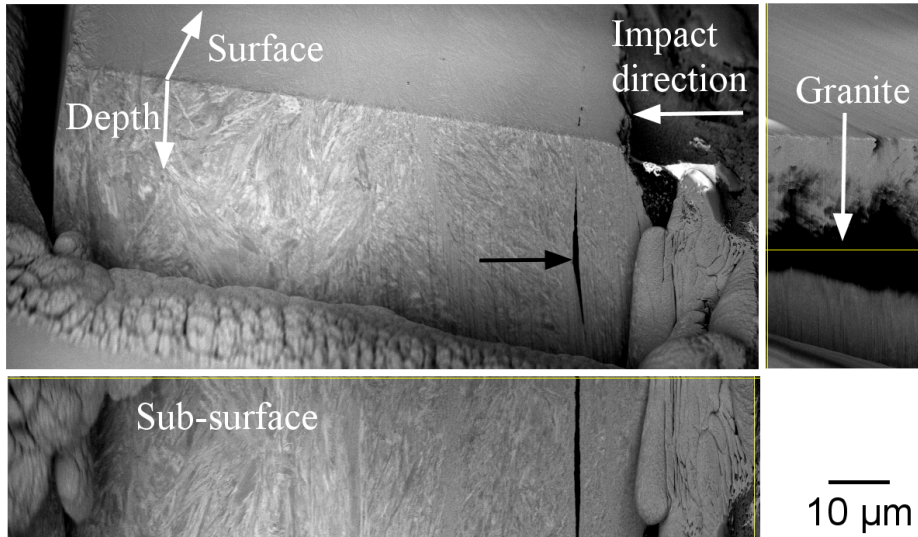
Fig. 6.3 3D SEM of the rolled sample. Top left: Section perpendicular to the impact direction. A crack can be noticed. Top Right: Cross section perpendicular to the crack as shown by black arrow. Bottom: Sub-surface structure showing crack.

Based on these observations, the wear mechanism can be summarised in a simplified form as follows (Figure 6.4):

- Cutting action that leads to cracks which propagate leading to the removal of material. Particle impacts may also cause direct fracture and it is likely that the same location is subjected to multiple impacts.

- Further removal of material by severe abrasion, including of the impact-roughened surface. Some partially fractured material may weld back to the sample due to collisions with granite. This is supported by the observation during three-dimensional serial sectioning of completely embedded granite particles.

6.3   Conclusions

In impact-abrasion, impact by abrasives results in cracks and creates asperity-like features, while abrasion removes the impact damaged material and further damages

(a)

(b)

(c)

(d)
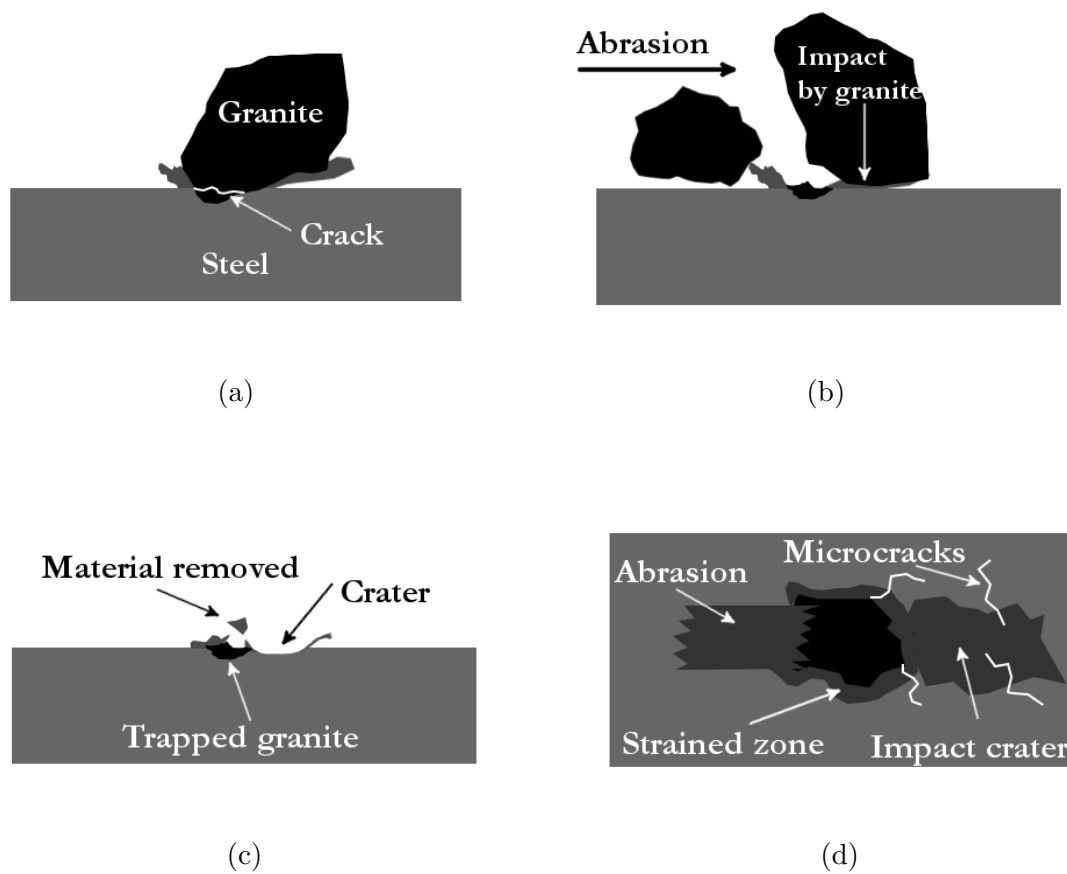
Fig. 6.4 Damage mechanism in impact-abrasion. (a) Granite impact causing crater and also causing protrusion of material, (b) abrasion and impact of the protruded material, (c) material removed due to either impact or abrasion and formation of crater, and (d) view of image (c) in the direction of impact.

the surface. Two major reasons for the increased wear resistance in the tough steel are: (a) surface crack density caused by impact is lower in the tough steel compared to the brittle steel, (b) the contact or friction layer is thinner and deformation layer is thicker in the tough steel compared to the brittle steel.

It was also found that fracture toughness increases wear resistance compared to hardness in high-hardness wear resistance materials. Toughness increases resistance to wear not only by the impact component but also by the abrasion component. Therefore focus on further development of steels should be on increasing fracture toughness of the hard wear-resistant steel for impact-abrasion applications.

An attempt has also been made to explain the impact-abrasion wear mechanism. The simple mechanism lays the foundation for the development of mathematical model to further understand the impact-abrasion and also to develop new wear resistance steels.

Chapter 7

Three-body abrasion wear of rolled, and quenched steels

7.1 Introduction

It would be interesting to subject the novel alloy studied in Chapter 5 to abrasion conditions that exclude impact damage. To evaluate the performance of rolled and quenched samples and their tempered variants under three-body abrasion conditions, wear tests were carried out consistent with ASTM G65 dry sand abrasion configuration as detailed earlier in Section 3.5.1. Working to this standard allows a comparison against published data. The test was carried for 16200 cycles of abrasion, corresponding to $\approx 11.62\,\text{km}$ of sliding distance. It was interrupted at $10\,\text{min}$ intervals to maintain the temperature of the sample and to measure the weight loss, to an accuracy of $\pm 0.0001\,\text{g}$. These test parameters match previous work [154]. The standard sand used in these experiments is referred to as 'Sand A'.

7.2 Test results

The results are presented in Figure 7.1 and in Table 7.1. The surface hardness values of the samples presented in the table are different from Table 5.2. The difference is attributed to removal of $1\,\text{mm}$ on testing surface by machining for this study to meet the requirement of the three-body abrasion wear. Low standard deviation in the present case can also be attributed to the removal of surface material. Further, the values have low standard deviation as the surface is removed All the samples showed

similar wear, except that quenched and tempered at 300 °C for 2 h. The wear rate was in all the cases worse than commercially available alloy of similar or lower hardness. In contrast, the relative wear loss of the rolled steel is significantly lower than that of the quenched steel during impact-tumbler wear test as discussed in Chapter 5. This shows that toughness has little role in increasing wear resistance when subjected to abrasion conditions.

Table 7.1 Specific wear rate of rolled, quenched and their tempered variants steels. Minimum ten surface hardness measurements were made on each sample.

Sample	Hardness / HV30 (kgf mm^{-2})	Specific wear rate (mm^3 N^{-1} m^{-1}/10^{-5})
Hot rolled	582 ± 5	58
Hot rolled and tempered at 190 °C for 2 h	593 ± 9	56
Hot rolled and tempered at 300 °C for 2 h	579 ± 5	58
Quenched	643 ± 7	55
Quenched and tempered at 190 °C for 2 h	568 ± 7	58
Quenched and tempered at 300 °C for 2 h	582 ± 5	68
Hardox 500 [70]	530	13
Hardox 400 [70]	473	32
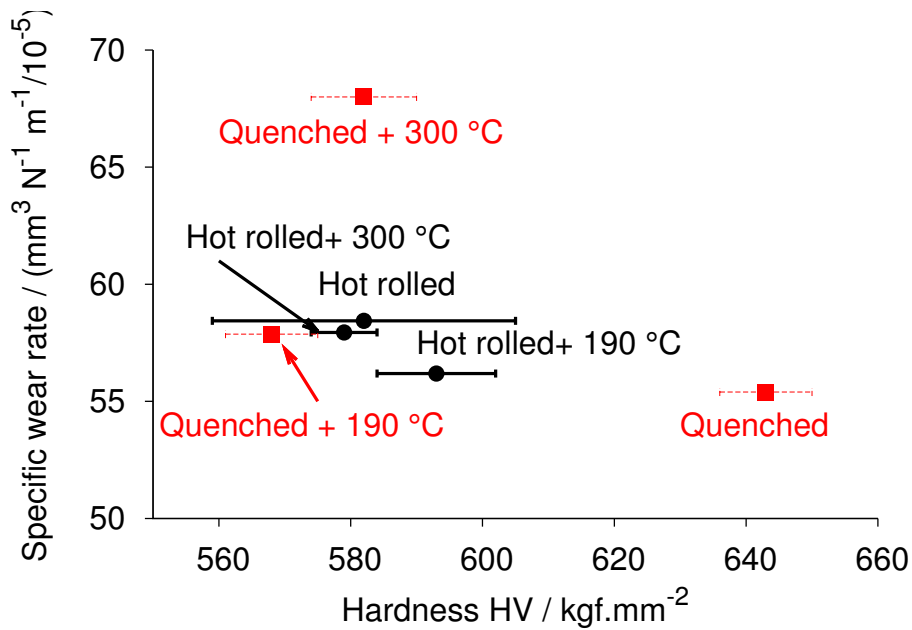
Fig. 7.1 Specific wear rate of rolled, quenched and their tempered variants with surface hardness of the tested samples using Sand A.

Though three-body abrasion test parameters are similar to previous studies, the specific wear rate of martensitic samples tested in [154] is quite different compared to the present work for a similar hardness level and microstructure. For instance, the wear rates of martensitic Hardox500 steel with hardness of 530 VHN and Hardox400 with hardness of 473 VHN are 12.7 and 31.5×10^{-5} mm^3 N^{-1} m^{-1}, respectively.

It seems that commercially available wear resistance steel with a hardness of about 500 performs exceptionally when compared to any of the steels in the present investigation. This called for the further investigation into the test procedure for abrasion wear.

Among all the parameters in three-body wear test, the sand used plays a key role [229]. Therefore, a different sand was used and keeping all the other parameters constant. The sand is from the same supplier under the same brand claiming similar properties but a different batch. This sand is referred to as 'Sand B '.
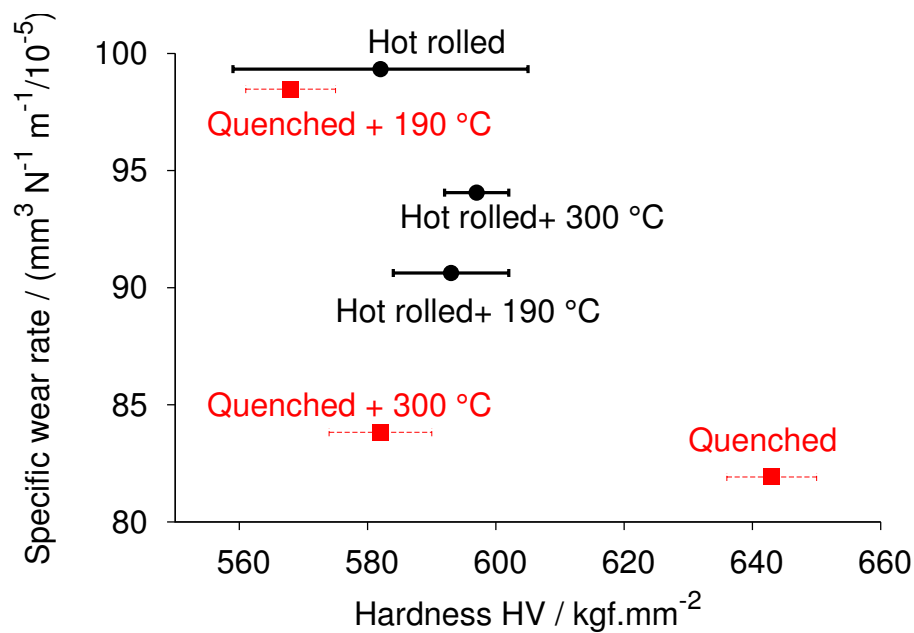
Fig. 7.2 Specific wear rate of rolled, quenched and their tempered variants with surface hardness of the tested samples. Sand B was used with similar testing parameters as for the data in Figure 7.1.

The test results of three-body abrasion with Sand B are shown in Figure 7.2. The specific wear rate with Sand B is about 40 to 50 % greater compared to data based on Sand A(Figure 7.1). Abrasion is a test of resistance to scratching and grooving where

hardness should be paramount so the quenched steels which are harder outperformed the other samples.
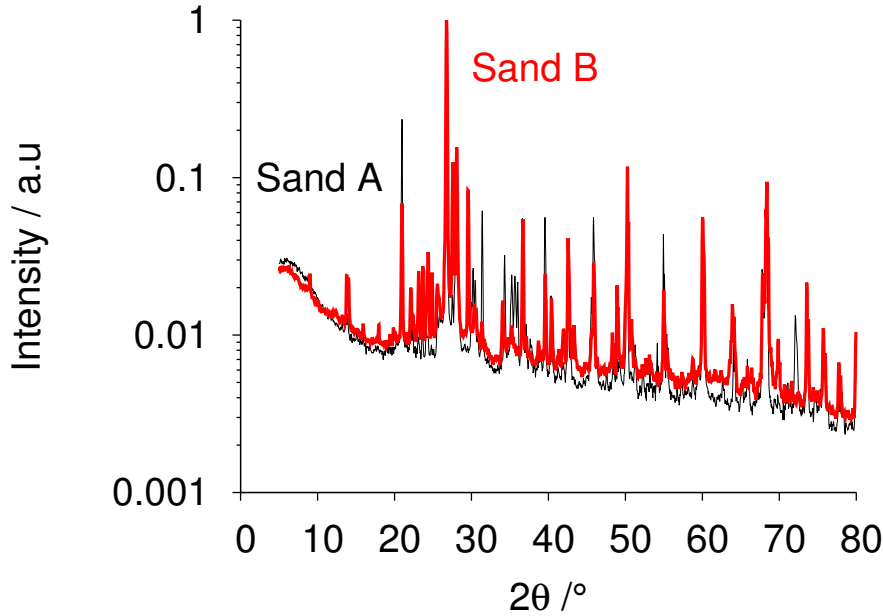
Fig. 7.3 Figure showing X-ray peak profile of two sands. The peaks correspond to quartz phase (SiO_2).

An attempt was made to understand what led to huge difference in wear rate when the samples are tested with different sands. Abrasive wear loss depends mainly on composition, hardness, toughness, particle size and shape of sand grains for a given set of testing parameters [230, 231]. The X-ray diffraction profiles of the sands are shown in Figure 7.3. The peaks are identified to be due to quartz (SiO_2) in sand. There is no appreciable difference between the two sands based on X-ray analysis.

Table 7.2 Particle size (diameter) and spike parameter quadratic fit (SPQ) of two different sands used in the testing.

	Sand A		Sand B	
	Before	After	Before	After
Size / µm	332 ± 122	318 ± 70	423 ± 144	418 ± 102
SPQ	0.8404 ± 0.0800	0.7924 ± 0.1000	0.8704 ± 0.0600	0.7587 ± 0.1000

The size and shape of sand particles was analysed to reveal any difference between the two sands. Unlike size, other than 'rounded'there is no specification in the ASTM
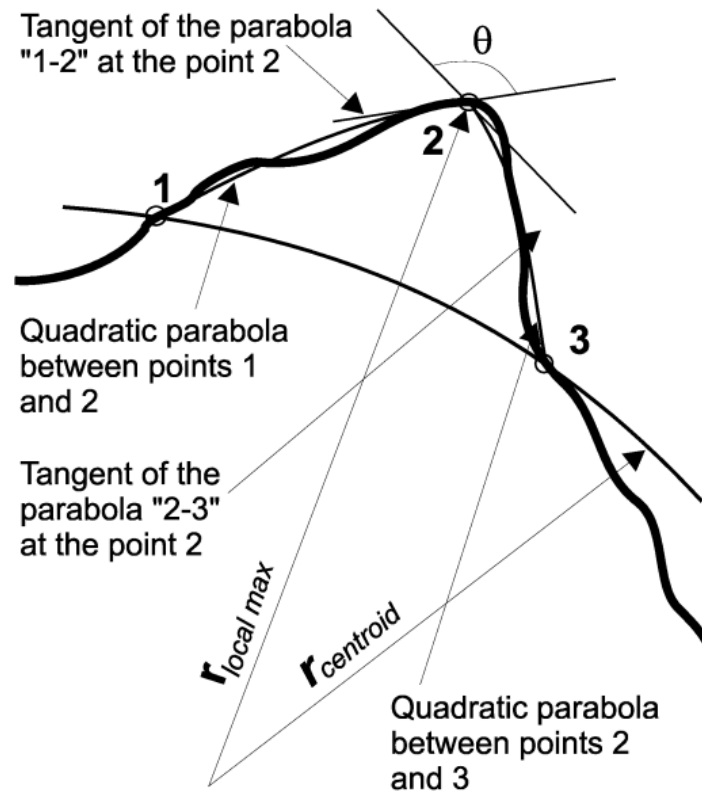
Fig. 7.4 Schematic illustration of a spike outside the circle and the basic principle in calculation of the spike value [233].

G65 standard on angularity or sharpness. Angularity parameter, SPQ, is selected in this study to compare the sands. Spike parameter quadratic fit (SPQ) is used to characterize particle angularity or sharpness of the sand particles. The SPQ quantifies spikes that are outside the circle with equal particle area centred over the particle centroid as shown in Figure 7.4. '2' in the figure is a spike outside the circle and the apex angle, θ, can be calculated by differentiating the polynomials at the point '2' and the spike value $SV = \cos \theta/2$. The final SPQ is an arithmetical mean of spike values: $SPQ = SV_{average}$. A lower SPQ value corresponds to spherical particles or lower angularity, while higher SPQ value represents high angularity or high aspect ratio [230–233]. Higher SPQ values in sand result in a greater extent of wear. Typical particles are shown in Figure 7.5 and the corresponding SPQ and average particle size data are presented in Table 7.2.

The standard size according to ASTM G65 is 50/70 mesh which corresponds to 210 to 290 µm. From the table it is evident that the particle size is relatively high compared to the standard size. Grit size of Sand B is about 100 µm higher compared

(a) Sand A: before testing

(b) Sand A: after testing

(c) Sand B: before testing

(d) Sand B: after testing
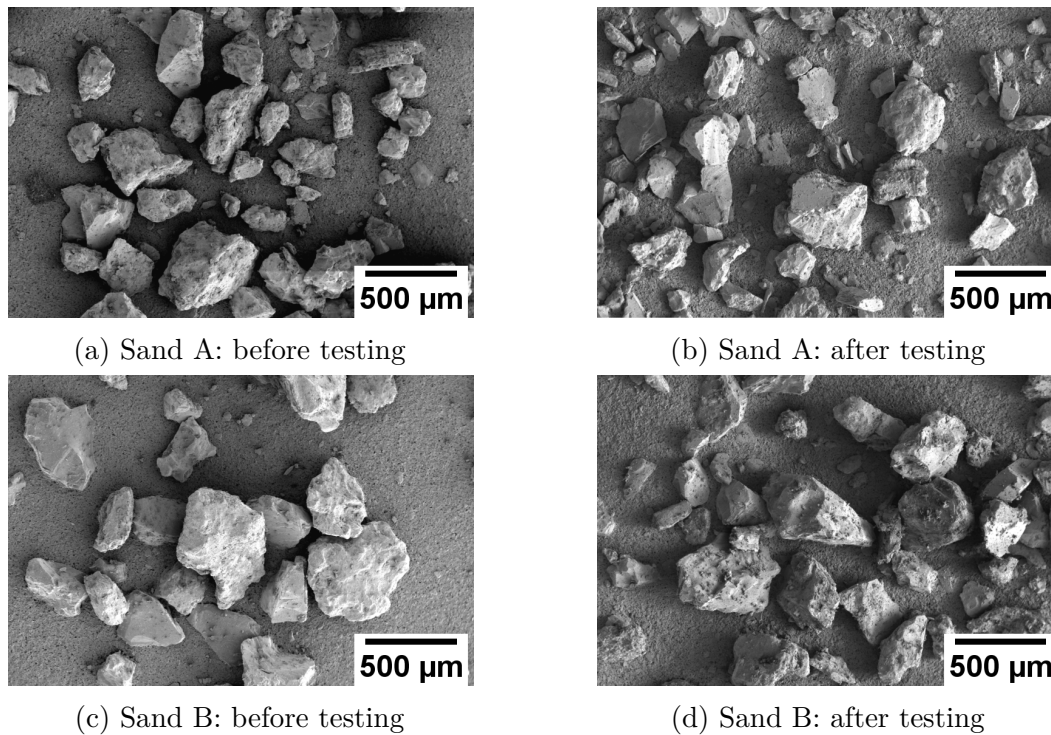
Fig. 7.5 Figures showing particles of sand before and after testing.

to Sand A. An increase in size in general increases wear rate [180]. As the tests were long duration experiments, the size difference could have resulted in high wear rate when tests were conducted with Sand B.

The SPQ values of the Sand B are reasonably identical to those for Sand A. The present values of SPQ in both the sands are high compared to ASTM G65 standard SPQ, 0.2 ± 0.1 which is near round as mentioned in the standard.

Based on the XRD profile, it can be assumed that the component in the sands is quartz, and from the shape analysis the sands are of similar sharpness or angularity. Only the size is the major difference among the sands and hence the difference in wear results when the sand was changed can be attributed to size [232].

The samples tested with Sand A were characterised to understand the damage mechanism and the results are presented in the following section. The low wear reported for the Hardox variants may be due to different test conditions or the sand used. Ideally, the comparison should include the commercial alloys under the conditions of the present work. Unfortunately, the commercial alloys could not purchased for the small quantities required here.

(a) Rolled   (b) Rolled and tempered at 190 °C   (c) Rolled and tempered at 300 °C

(d) Quenched   (e) Quenched and tempered at 190 °C   (f) Quenched and tempered at 300 °C
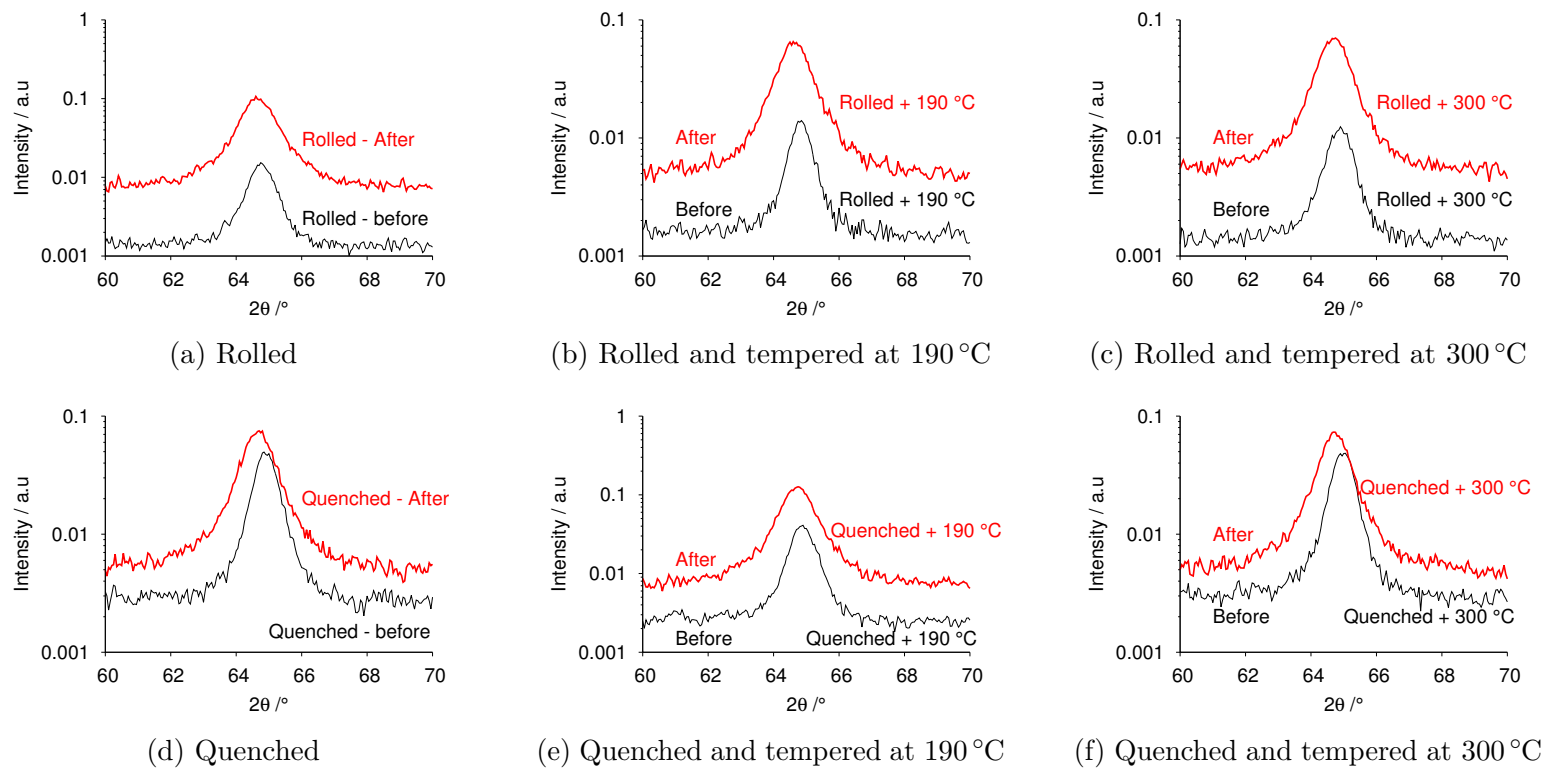
Fig. 7.6 X-ray diffraction profile of (002) peak of ferrite before and after abrasion testing

7.3 XRD of abraded surface

X-ray diffraction profiles were obtained before and after the abrasion to study the extent of damage caused in the vicinity of surface. Many factors such as instrument, crystallite size, microstrain, solid solution inhomogeneity, temperature factors, may contribute to the observed peak profile [234, 235]. The mcirostrain is elastic strain from non-uniform lattice distortions [236].

The FWHM of peaks (002) from both before and after abrasion are listed in Table 7.3 and their profiles are shown in Figure 7.6. In all the cases, the peak was, as expected, broadened following abrasion. Further the peaks are shifted to lower diffraction angle. It may be due to uniform residual strain [237].

Table 7.3 Full Width Half Maximum of (002) peak of the samples before and after testing.

Sample	Before (FWHM / 2θ)	After (FWHM / 2θ)	Difference (FWHM / 2θ)
Hot rolled	0.790 ± 0.003	1.040 ± 0.003	0.25
Hot rolled and tempered at 190 °C for 3 h	0.690 ± 0.003	1.090 ± 0.003	0.4
Hot rolled and tempered at 300 °C for 3 h	0.830 ± 0.003	1.050 ± 0.003	0.22
Quenched	0.760 ± 0.002	0.90 ± 0.01	0.14
Quenched and tempered at 190 °C for 3 h	0.760 ± 0.002	0.80 ± 0.02	0.04
Quenched and tempered at 300 °C for 3 h	0.50 ± 0.01	0.960 ± 0.003	0.46

Figure 7.7 shows the difference FWHM with specific wear rate. No correlation could be drawn between wear loss and peak broadening. It seems that the X-ray data do not differentiate sufficiently between the samples, resulting similar levels of residual stresses in the surface regions penetrated by the X-rays.

7.4 Damaged surface

Figure 7.8 shows the morphology of the abraded surfaces of rolled and its tempered variant at 190 °C, and quenched and its tempered variant at 190 °C tested using Sand A.

The mechanism of wear or removal of material during three-body abrasion should be somewhat similar to that during machining or grinding operations. The hard asperities of sand penetrate into the abraded surface under the normal contact pressure, and then they are ploughed and microscopically cut as the sand particles traverse across
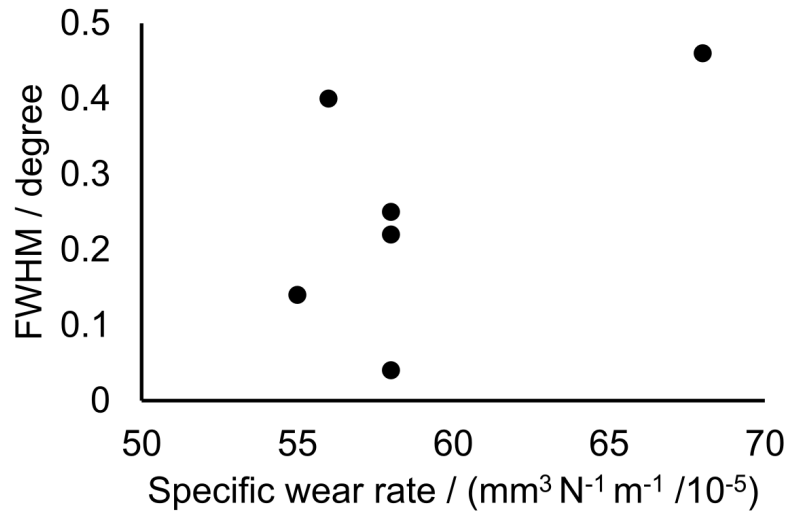
Fig. 7.7 Showing difference FWHM against sample's specific wear rate.

the substrate. As a result, the worn surface is generally characterised by grooves and scratches as illustrated in Figure 7.8.

The morphology of abraded surface reveals the pattern of movement of sand particles along the worn surface. The abrasive particles sometimes deviate from unidirectional, motion imposed by the rubber belt. This may be due to hindrance caused by the embedded particles. The worn surfaces also reveal wear scars, cracks, embedded debris, wear debris, delamination, damage area, shallow ploughing, deep ploughing, micro-cutting, micro-pitting and deep grooves due to the sharp edges of abraded particles. Except in the quenched and tempered at 190 °C sample, the abraded surfaces of the other samples look similar.

In order to understand the process better, the regions below were investigated as described in Section 6.2. Figure 7.9 shows the subsurface of rolled, and quenched variants. There are embedded particles with black contrast. An examination of the subsurface can better reveal the embedded particles which can then be quantified using image analysis given the sharp contrast between the particles and the substrate.

The area fraction of embedded particles in the rolled sample was measured to be 0.10 ± 0.05 compared to 0.05 ± 0.02 for the quenched sample. The embedded particles do get detached as the test progress, leaving a roughened surface that should be more susceptible to abrasion. The detachment can create voids that contribute to damage. This may explain the greater wear rate in rolled sample relative to quenched sample

(a) Rolled

(b) Rolled

(c) Rolled and tempered at 190 °C

(d) Rolled and tempered at 190 °C

(e) Quenched

(f) Quenched

(g) Quenched and tempered at 190 °C

(h) Quenched and tempered at 190 °C
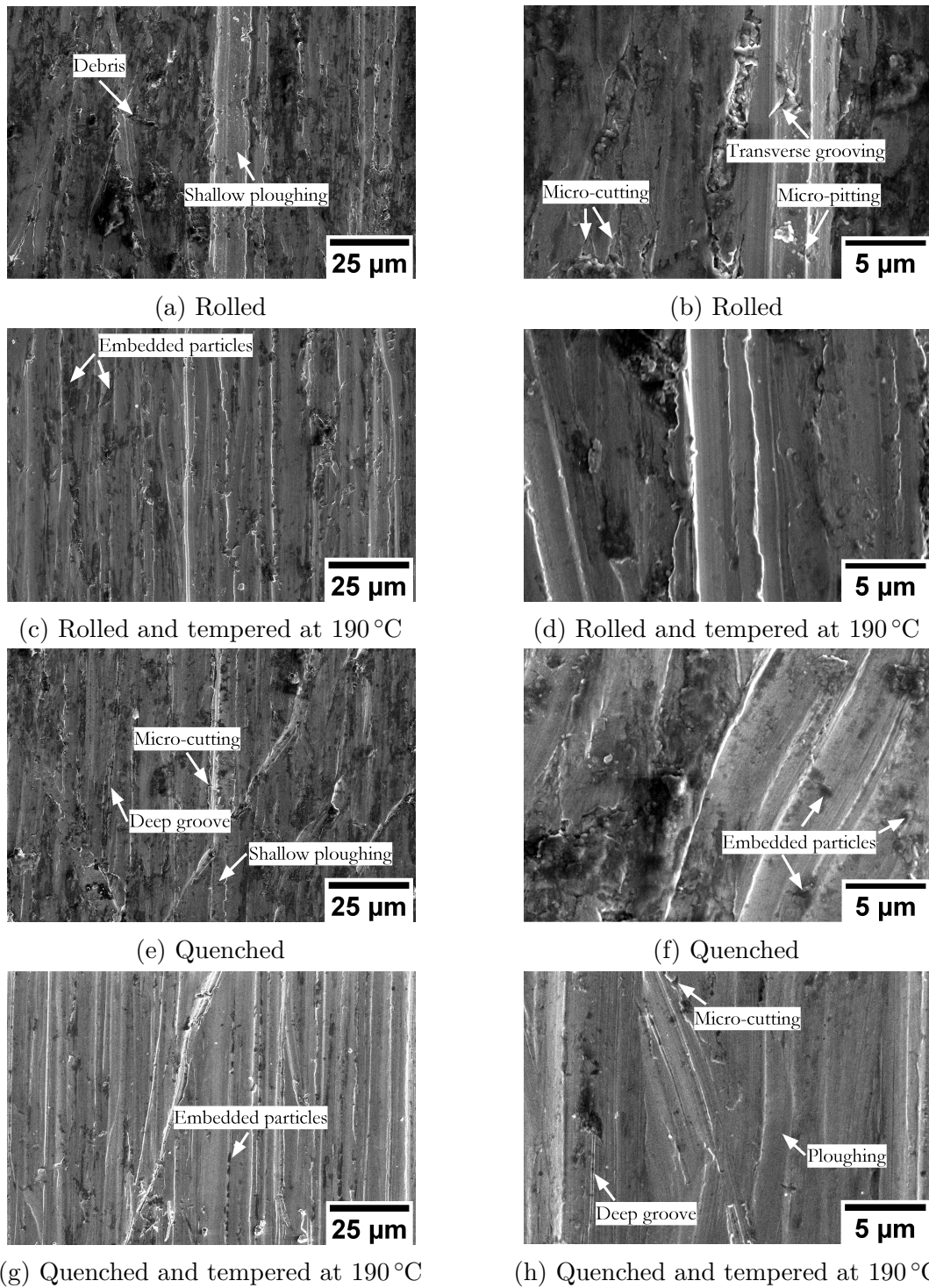
Fig. 7.8 Figures showing abraded surface of the tested samples: (a) & (b) for rolled, (c) & (d) for rolled and tempered at 190 °C, (e) & (f) for quenched and (g) & (h) for quenched and tempered at 190 °C .

(a) Rolled

(b) Rolled

(c) Quenched

(d) Quenched
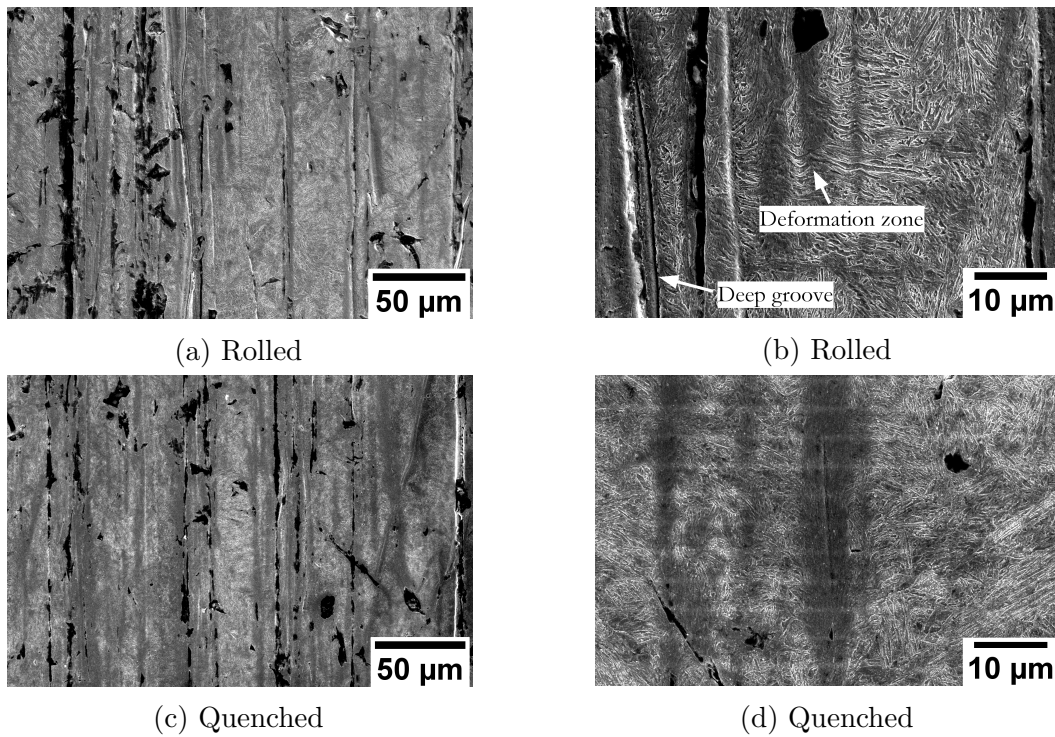
Fig. 7.9 Figures showing subsurface of the damaged surface of the tested samples.

which has high hardness. However, Figure 7.10 shows no strong correlation between area fraction of embedded particles and hardness of the substrate.

The study revealed that the three-body abrasion test is sensitive to abrasive properties. There is no specific relation that could be established between hardness or toughness and wear rate though high hardness steels performed better in quenched condition. A new method in analysing the subsurface revealed quantifiable information in differentiating rolled, and quenched steels.
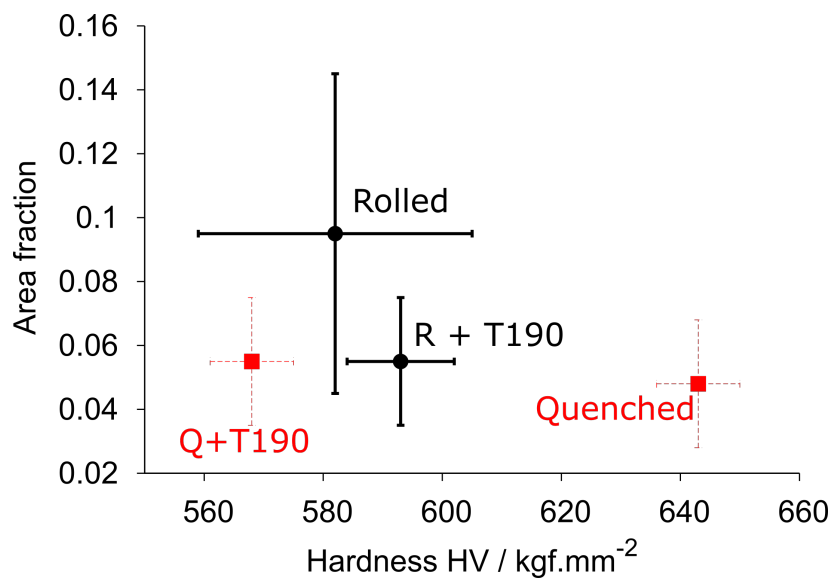
Fig. 7.10 Showing area fraction of embedded particles against steel hardness.

Chapter 8

Component level wear studies

On the basis of the impact-abrasion test data from the newly-developed steel in its various conditions, it is evident that toughness plays a prominent role in enhancing its performance when subjected to the combined wear mechanism. Nevertheless, the ultimate test must be during service, where the parameters are less controlled than in laboratory tests. In this context, full component level wear studies were initiated to study performance when the toughest variety is pitched against a current composite.

Table 8.1 Composition of elements present in the hardface in wt%.

C	Si	Cr	Nb	Mo	V	Al	Fe
3.46	0.47	22.95	0.035	0.022	0.07	0.018	Balance

Considerable wear and tear takes place in integrated steel plant due to the rapid movement of raw material as well as of finished goods. One such location is a chute of sinter plant where returns are collected from a blast furnace in Tata Steel Ltd., India. The blast furnace usually consumes sinter with an average diameter of about 6 to 30 mm and returns anything below 6 mm using a conveyor belt to drop the discards into a chute. At present, a low carbon steel plate with a thick overlay of a mixture of chromium carbide and austenite, deposited by arc welding, is used to resist impact as well as abrasion due to the sinter particles transfer. The composition of the overlay is given in Table 8.1. One of such plate is shown in Figure 8.1 after five years of use in the chute.

Before substituting the rolled steel in place of the existing plate, impact-abrasion tests were carried out to assess relative wear performance of the rolled steel and the existing composite plate used in chute. Samples from the undamaged part of the plate

<center>(a)   (b)</center>
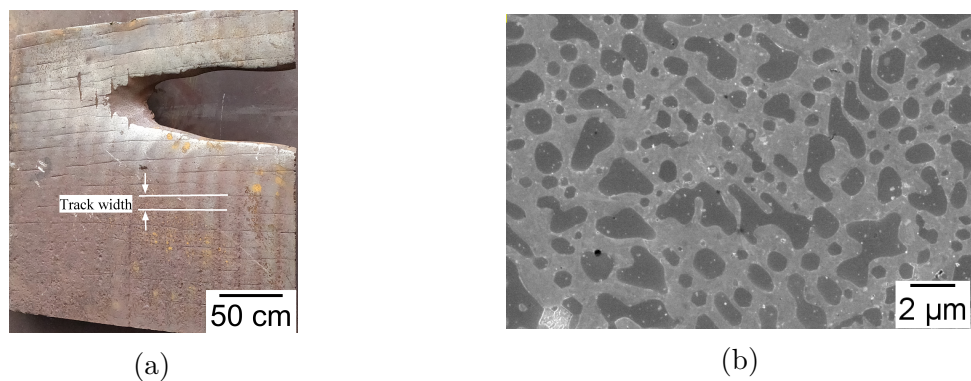
Fig. 8.1 (a) Worn out Cr based hardfaced plate. The lines indicates width of the weld track, (b) microstructure of the plate. Dark phase is carbides of Cr in austenite phase. Images courtesy Dr Subrata Mukherejee and Dr Durga Prasad Akula.

were cut for impact-abrasion testing using granite. The testing parameters are same as in Chapter 5.

Figure 8.2 shows wear loss relative to a standard sample that has a hardness of 400 BHN, and actual weight loss of the rolled, and hard-faced steel. They performed identically within the scatter expected, despite the greater hardness of the hard-faced steel (700 VHN). Therefore, the rolled steel can be a potential replacement to the existing composite for the following reasons:

1. The rolled plate is more economical to produce compared to the hard-faced steel.

2. Hard-facing is a cumbersome process as it involves deposition by welding.

3. Once the hard-facing is removed, the low carbon steel is exposed and can lead to rapid failure.

The tested surface has not revealed any useful information but the sub-surface revealed presence of cracks, in Figure 8.3. The bright phase is austenite, dark phase is carbides (M_7C_3) and some impact regions can be noticed in the figure. The cracks are mainly confined to carbides and the interface of carbide and austenite. A crack in black square in Figure 8.3b extended into austenite phase. An unsuccessful attempt was made using electron backscatter diffraction (EBSD) technique to investigate if the austenite was transformed to the more stable martensite due to strain caused by the crack. Due to difference in the hardness of phases and presence of embedded granite particles, good polishing required for EBSD could not be achieved. However, bulk X-ray diffraction data from the sub-surface revealed the presence of body centered
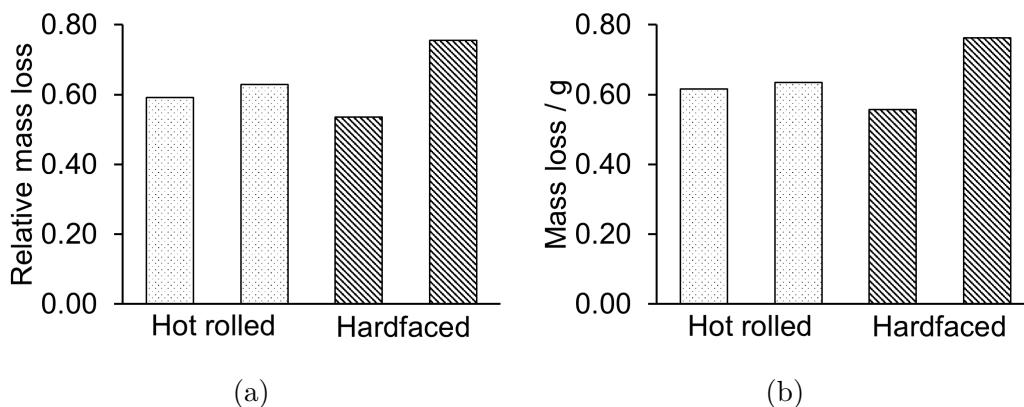
Fig. 8.2 (a) Relative wear loss of the rolled and the hardfaced samples in impact-tumbler tests. Relative wear loss is wear loss relative to the standard sample with hardness 400 VHN. The testing parameters are same as in Chapter 5, (b) actual wear loss of the samples.

cubic Structure (BCC) phase in small quantity, about 0.013 by volume fraction, subject to significant uncertainty.

The composition of the austenite at 1200 °C is given in the table calculated using commercial software Thermo-Calc with database TCFE10 [238], and given in Table 8.2. The same can be assumed at room temperature since the primary carbides are not expected to change significantly during cooling. Though the carbon content is only about 1 wt% in austenite, the presence of a substantial amount of Cr makes the phase highly stable. By increasing the percentage of Cr by 2.5 wt% from 0.1 wt%, the martensite start temperature dropped by 50 °C [239].

Table 8.2 Composition of elements present in the phases in wt% obtained using TCFE10.

Phase	C	Si	Cr	Mn	Fe
Austenite	1.04	0.6	9.83	2.09	Balance
M_7C_6	8.76	0	51.84	1.86	37.53

The rolled plates were placed in the chute to replace the existing hard-faced ones during April 2019. The condition of the plate after two months of usage is shown in Figure 8.4. There is no visible damage in the short time span but evaluations will continue. It is definite that there are no signs of visible damage after about a year in service.
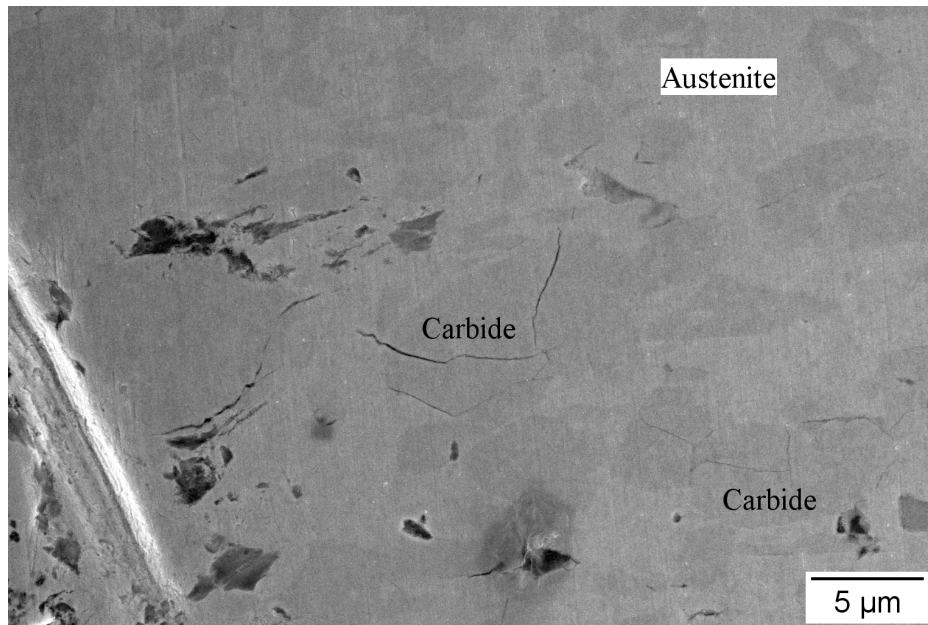
(a)
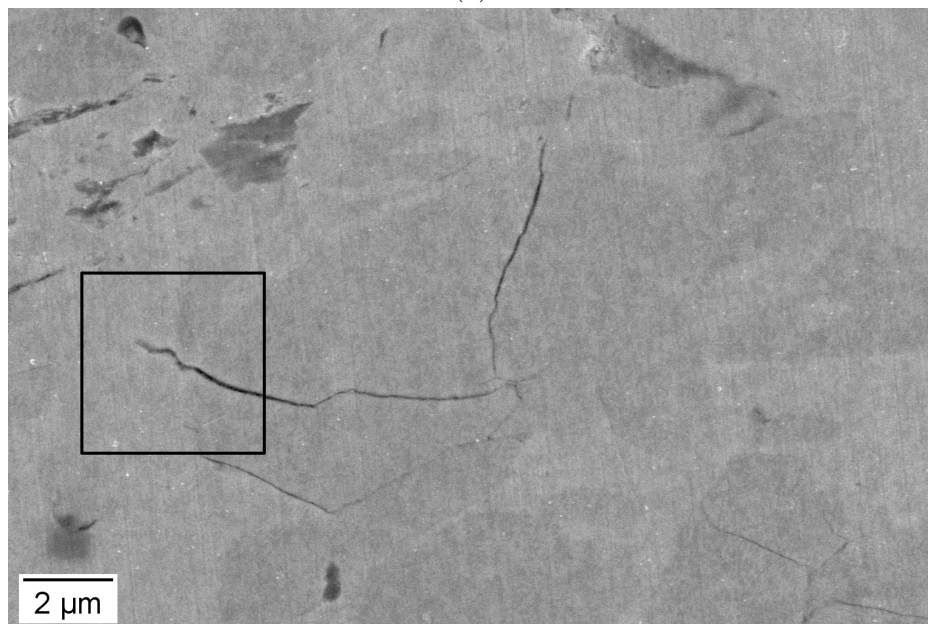
(b)

Fig. 8.3 (a) and (b) Sub-surface damage in overlay of impact-abrasion tested sample.
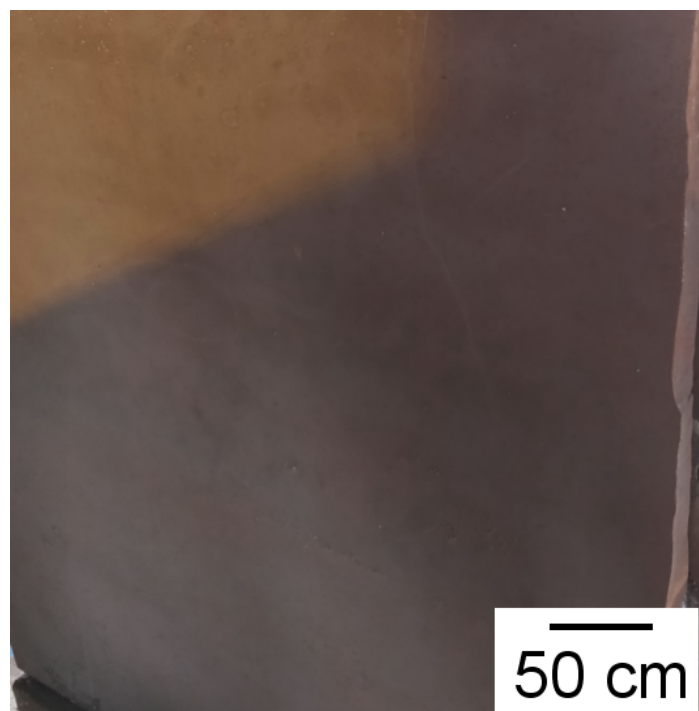
Fig. 8.4 The plate after two months of performance. Images courtesy Dr Subrata Mukherejee and Dr Durga Prasad Akula.

Chapter 9

Conclusions and Future work

9.1 Conclusions

Wear in the lifting and excavation industry is a complex phenomenon and steels designed for such applications must perform satisfactory and be economical to be commercially viable . One of the key requirements of such wear resistant steels is their bulk hardness. Indeed, commercially available steels are designed based on the principle their wear resistance increases with hardness. Due to the increased capacity of rolling mills in integrated steel plants and addition of micro-alloying solutes, thicker and harder wear resistance plates are being developed for complex wear environments. For example, commercial grades are marketed based on their Brinell hardness number. The developed steels are tested in abrasion environment according to an ASTM standard but used in a variety of wear resistance applications. The questions before taking up this work were:

1. Do steels developed based on hardness and tested at laboratory scale in abrasion environment perform well at component level?

2. The hardness of steels depends on their microstructure which in turn controls mechanical properties. Therefore, not only hardness but other mechanical properties and microstructure must play a role in controlling wear resistance. What is the role of mechanical properties other than hardness in increasing wear resistance?

3. Does microstructure and its substructure play a role in controlling wear rate?

In this context, a critical review of the published literature revealed the importance of toughness and work-hardening capacity in steels with hardness more than 500 VHN.

One of the important findings is that work-hardening capacity of steel decreases with its hardness and seems to have remained constant for the hardened steels with hardness above 500 VHN due to reduced ability of the steel to spread deformation to a greater depth. Another important finding is that surface hardness of the steel changes damage mechanism. When the steels are neither too soft nor brittle, fracture toughness controls wear resistance as critical strain to failure becomes smaller than the applied plastic deformation.

To increase wear resistance in high hardness steel, microstructural changes must be brought in to increase toughness and work-hardening capacity. The presence of retained austenite in martensitic steels and refining structural features, such as blocks and lath size, in martensite phase can improve wear resistance when they are exposed to complex wear environments. Though nanoscale and carbide free bainitic steels seem promising to increase wear resistance in variety of test conditions, commercial production through the existing mills in integrated steel plants is a challenge.

To examine the specific role of toughness in increasing wear resistance in high hardness steels, an attempt was made to study how toughness might influence the ability of a new steel, which is not only hard but also tough, to resist the combined effects of impact and abrasion. The experiments were controlled by comparison against an embrittled variety of the alloy.

The damaged surface was carefully polished to remove about 10 to 15 μm to study sub-surface of the damaged substrates and it revealed a wealth of information to quantify the damage and relate with microstructure and mechanical properties. It helped to understand the wear mechanism in abrasion as well as impact-abrasion. Based on sub-surface and cross-sectional microscopy a possible simple damage mechanism is proposed for impact-abrasion wear.

In the present impact-abrasion wear tests, it was revealed that the impact component mainly damages the surface while abrasion removes the accumulated damaged material. Therefore, both surface hardness and toughness are important to resist complex wear in impact-abrasion environment. Sub-surface damage revealed that presence of large number of radial cracks at granite impacts in low toughness steel. Presence of such cracks can entrap fractured granite particles which can act as wedge during the successive impacts and hence increased wear.

While in tough steel, a part of impact energy is dissipated by formation of deformation or shear bands in sub-surface extended up to 50 μm. Advanced characterisation studies revealed the refinement of microstructure in the bands to an extent that the

prior laths are completely fragmented with a large reduction in coherent regions. Deformation in the sub-surface, refinement of microstructure and presence of less number of cracks in the contact zone are possibly the major reasons for the increased wear resistance of the new tough steel.

In pure abrasion wear, it seems that particles embedded in the contact surface determine wear rate. The tough steel has more embedded particles possibly due to its ductility compared to brittle steels. The sand particles can be removed during process leaving a rough surface which is conducive for high wear loss due to increased friction.

The performance of materials can of course be evaluated at component level, but it can take considerably longer time to evaluate the performance and hence delay product development. For instance, in the present study a hardfaced composite was replaced by the tough steel but it may take more than two or three years as the former lasted for five years. Therefore, there is a need to develop a standard test to accommodate complex wear environments. For example, the present impact-tumbler wear test can be standardized by studying the wear of a standard steel (D2 tool steel) by varying test conditions like changing average granite size, weight, speed of the impeller and tumbler, and duration of the test. This test may not be sacrosanct but definitely better than the existing standard test when the in-service conditions are not mere abrasion.

9.2   Future work

Though this study indisputably proves the role of toughness in increasing the impact-abrasion wear resistance, there is more to be gained with further work as follows:

1. The weldability of the steel is important to the extent that steel must in some applications be incorporated into engineering structures. Though the steel has proven to have good weldability, the performance of welded joints under impact-abrasion conditions needs to be studied, because they could compromise the uniformity of the damage, uniform wear is more desirable than local attack because the latter occurs at weakened sites, therefore at a greater rate.

2. Wear resistance is a system property that depends on the conditions of the tribosystem. It is difficult to simulate the tribosystem at laboratory and evaluate the steels. The present tests have limited use as the final component level testing is necessary to fully evaluate the steels. As these tests are for empirical ranking of the materials, efforts should be to document and report all the mechanical

properties and microstructure of the steels tested to develop a neural network based model that can compliment the laboratory testing. For instance, recent regression analysis of large set of three-body abrasion correlates wear resistance with strength coefficient (K in $\sigma = K.\log\epsilon$) [240]. Such studies may assist in reducing number of tests to evaluate the steel and assist in developing new steels.

3. Wear is a surface damage process and hence it depends on surface and sub-surface properties of the material. Therefore, the techniques developed to improve surface properties, such as shot peening, carburization and hardening, can be exploited to increase wear resistance. Shot peening is a standard practice to increase fatigue life of materials. The process produces a significant increase in surface compressive stresses and hardening due to plastic deformation at the surface regions of the sample. However, the effect is limited to a maximum of $1\,mm$ depth so once the hardened layer is removed, the base material becomes exposed to exaggerated wear.

4. As the wear is not a material property, actual damage of wear component depends on tribosystem. The microstructural study of failed or in-service components helps to understand the damage. Advanced characterization of damaged surface can enhance our knowledge in design of steels for wear resistance applications. For example, it is not known if the retained austenite increasing wear resistance of Hardfaced steel. Studying the crack region in austenite by FIB, TEM and transmission Kikuchi diffraction (TKD) may provide insights on response of austenite to repeated impact loads.

5. The work-hardening capacity of the material increases wear resistance but how to increase work-hardening capacity in high hardness steels is a challenge. Retained austenite, about 0.1 volume fraction, may be one of the ways to increase the capacity. The composition of the steel can be designed in such a way that it retains considerable amount of retained austenite at room temperature. A novel approach could be exploiting banded microstructure in steels. Steels with considerable amount of Mn ($2\,wt\%$) without Si causes banding with alternative layers with difference in Mn content. Rolling and cooling can be designed in such a way that the banding is retained at room temperature that produces high amount of austenite in Mn rich regions. This composite structure may increase work-hardening capacity in high hardness steels.

6. It would be useful to model the impact-tumbler test in terms of sample and abrasive contacts, and the number of interactions as a function of test parameters. The model may help in the design of the experiment suited to a particular application. For instance, a discrete numerical model for granular assemblies, known as the discrete element method (DEM), was used to investigate particles interactions as in kilns and tumbler systems with great success [241]. A DEM is a numerical methods for computing the motion and effect of a large number of small particles interaction in a confined volume. The numerical technique is integrated with time to obtain particle velocity, position and interactions. High computing power and advanced numerical algorithms for nearest neighbor sorting made it possible to numerically simulate millions of particle interactions on a single processor. Therefore, the DEM can be used to simulate sample-abrasive and abrasive-abrasive interactions in impact-tumbler test to calculate forces responsible for impact and abrasion events.

Appendix A

X-ray computed tomography of tested sample

X-ray computed tomography (CT) has become a promising tool within material science for 3D characterization over several length scales [242]. This technique was used to obtain high resolution 3D topography of the damaged surface at a macro-level to understand the origin of the deformation bands and crack like features which were noticed in the cross-sectional microscopy. Zeiss VersaXRM-520 X-ray machine was used at the Henry Moseley X-ray Imaging Facility, The University of Manchester, to scan a large volume of the sample and to construct the 3D topography from the scan results.
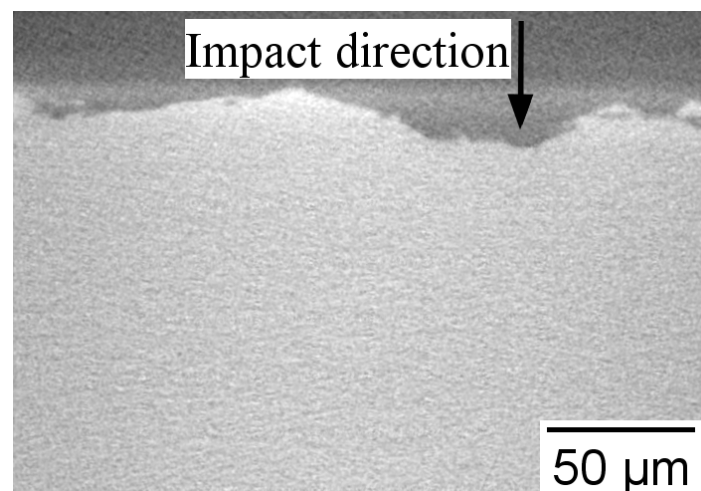
Fig. A.1 X-ray tomography of the rolled sample. One of the sections of the 3D volume obtained using voxel size of 0.6 µm.

Scanning was carried at various possible voxel sizes starting from $2.2\,\mu\text{m}$ to $0.6\,\mu\text{m}$. A voxel (a volume pixel) is the unit block of the 3D grid in space defining a volume, analogously to pixels in 2D images, and represents the spatial sampling. But it was found that no useful information was obtained after a scan. A typical 2D image of the large data obtained is shown in Figure A.1. The difficulty is that the intrinsic resolution and contrast mechanism of X-ray CT, renders this approach best at highlighting surface structure: the cracks and voids underneath the surface do not provide adequate contrast in the volume reconstruction.

Appendix B

TEM study of impact-abrasion tested rolled sample

A thin lamella was cut from the deformation band region of the rolled sample shown in Figure B.1a to study its microstructural features. The cut region 'A' in the figure is close to the crack like feature and also contains deformation bands. One of the bands is marked as '1' is in the contact zone, while the other, marked as '2', is spread in the deformation zone as explained in the cross-sectional microscopy studies in Chapter 6. The objective of this TEM study was to assess the extent of refinement in the deformation bands.

The cut TEM lamella was imaged with the FIB gallium ion beam giving higher orientation contrast to distinguish the laths as shown in Figure B.1b. Three important regions are identified in Figure B.1b. The microstructural features in the deformed regions, '1' and '2', are very fine compared to region '3'. Further, the neighbouring regions of '2' are also deformed but the features can be distinguished.

Figure B.2 shows the bright field images and selected area electron diffraction (SAED) patterns from '1', '2' and '3' locations marked in Figure B.1b . The two deformation regions ('1' and '2') show different microstructures from the '3', where laths can be seen in higher detail in Figure B.2e. From the diffraction pattern in Figure B.2f, it seems that relatively (1 0 -1) planes parallel to the incident beam of electrons are more in number compared to other planes in its family.

In the deformation bands, '1' and '2', the microstructure exhibited the presence of much finer crystallites as shown in Figure B.2a and B.2c. Moreover, the number of laths was qualitatively reduced due to the substantial refinement process. The refined crystallite were confirmed from the SAED pattern shown in Figure B.2b and B.2d.
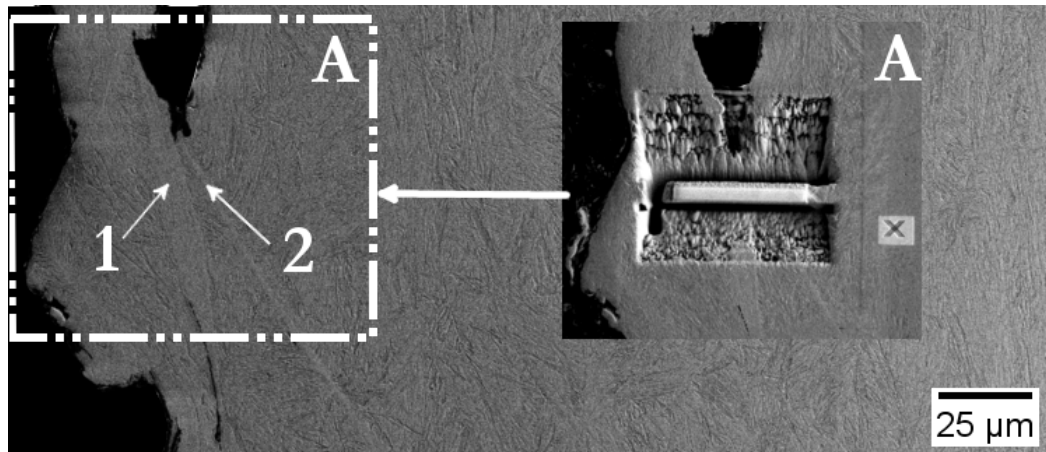
(a)
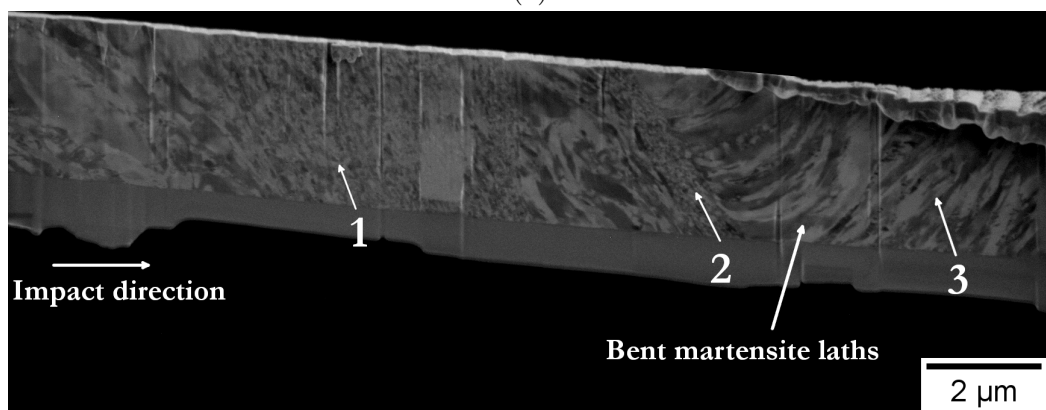
(b)

Fig. B.1 (a) Region, A, selected for TEM lamella. '1' and '2' indicate deformation bands. (b) TEM lamella. '1' and '2' show the deformation bands marked before cutting.
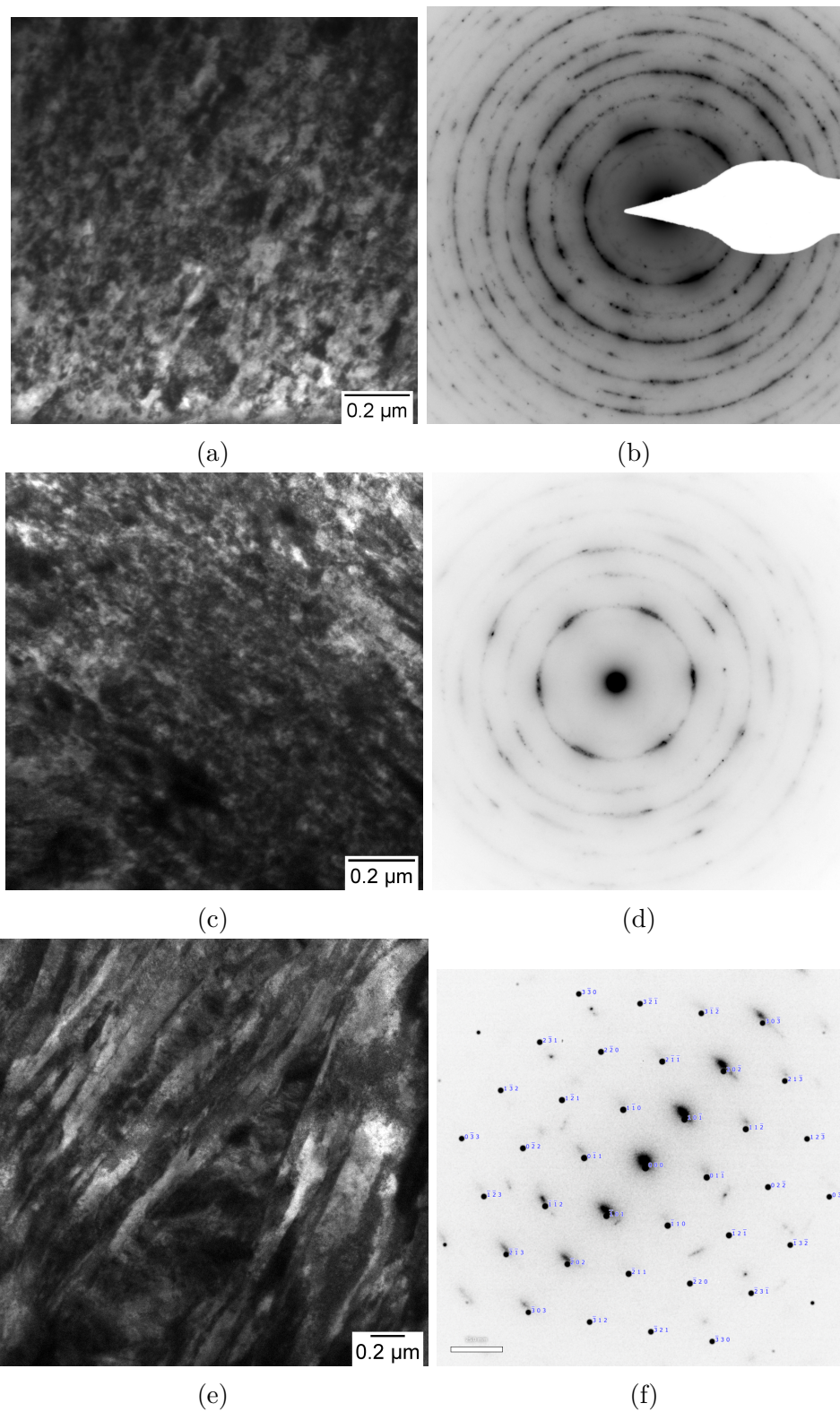
Fig. B.2 Showing images obtained at different regions in the TEM lamella and their diffraction. (a) and (b) from region '1', (c) and (d) from region '2', and (e) and (f) from region '3'.

The subsurface deformation bands, also known as shear bands or adiabatic shear bands, were noticed in previous investigations involving impact as well as sliding wear [57, 243–247]. One of the mechanisms explains that the cell or subgrain structures developed distinctly from the surface is due to shear instability at substructure boundaries below the surface due to loading conditions at the surface[244, 248]. It is possible because the contact zone is strongly hardened during the wear process and hence subsurface zone is exposed to the early impact or abrasive loads. It is also evident from the hardness of the tested surface that the hardness of the contact zone is increased (Figure 5.10).

References

[1] K. Bhansali and A. E. Miller. Resistance of pure metals to low stress abrasive wear. *Wear*, 71:375 – 379, 1981.

[2] K-H. Zum Gahr. Microstructure and wear of materials in Tribology series. volume 10, pages 1 – 7. Elsevier, 1987.

[3] Z. Guo, F. Xiao, S. Lu, H. Li, and B. Liao. Effects of heat-treatment on the microstructure and wear resistance of a high-chromium cast iron for rolls. *Advances in Materials Science and Engineering*, 2016, 2016.

[4] M. M. Khruschov. Principles of abrasive wear. *Wear*, 28:69 – 88, 1974.

[5] L. Qian, X. Xiao, Q. Sun, and T. Yu. Anomalous relationship between hardness and wear properties of a superelastic nickel–titanium alloy. *Applied Physics Letters*, 84:1076–1078, 2004.

[6] I. M. Hutchings. Wear-resistant materials: into the next century. *Materials Science and Engineering: A*, 184:185 – 195, 1994.

[7] E. Zdravecká, J. Tkáčová, M. Ondáč, et al. Effect of microstructure factors on abrasion resistance of high-strength steels. *Research in Agricultural Engineering*, 60:115–120, 2014.

[8] L. Fang, Q. D. Zhou, and Y. J. Li. An explanation of the relation between wear and material hardness in three-body abrasion. *Wear*, 151:313 – 321, 1991.

[9] JFESteel. Everhard™ abrasion resistance steel plate. http://www.jfe-steel.co.jp/en/products/plate/catalog/c1e-004.pdf, 2017. Accessed: 2018-12-06.

[10] ArcelorMittal. Wear resistant steels. http://industeel.arcelormittal.com/products/wear-resistant-steels/, 2017. Accessed: 2015-11-06.

[11] S. D. Bakshi, P. H. Shipway, and H. K. D. H. Bhadeshia. Three-body abrasive wear of fine pearlite, nanostructured bainite and martensite. *Wear*, 308:46 – 53, 2013.

[12] A. Ball. On the importance of work hardening in the design of wear-resistant materials. *Wear*, 91:201 – 207, 1983.

[13] W. Wang, R. Song, S. Peng, and Z. Pei. Multiphase steel with improved impact-abrasive wear resistance in comparison with conventional hadfield steel. *Materials & Design*, 105:96 – 105, 2016.

[14] B. Bhushan. *Wear*, pages 447–544. John Wiley & Sons, Ltd, 2013.

[15] C. Hatchett. IV. experiments and observations on the various alloys, on the specific gravity, and on the comparative wear of gold. being the substance of a report made to the right honourable the lords of the committee of privy council, appointed to take into consideration the state of the coins of this kingdom. *Philosophical Transactions of the Royal Society of London*, 93:43–194, 1803.

[16] G. Rennie. Experiments on the friction and abrasion of the surfaces of solids. In *Abstracts of the Papers Printed in the Philosophical Transactions of the Royal Society of London*, volume 2, pages 364–365. The Royal Society, 1833.

[17] N. Chand and M. Fahim. *An introduction to tribology of FRP materials.* Allied Publishers, 2000.

[18] R. G. Bayer. *Fundamentals of Wear Failures*, pages 901 – 905. ASM Handbook International, 2002.

[19] A. D. Sarkar. *Wear of Metals: International Series in Materials Science and Technology*, volume 18. Elsevier, 2013.

[20] J. R. Davis. *Surface Engineering for Corrosion and Wear Resistance.* Book (Institute of Materials (London, England)). ASM International, 2001.

[21] M. J. Neale and M. Gee. Chapter 2 - industrial wear problems. pages 3 – III, 2001.

[22] J. F. Archard. Contact and rubbing of flat surfaces. *Journal of Applied Physics*, 24:981–988, 1953.

[23] K. Kato and K. Adachi. chapter Wear Mechanisms. Mechanics & Materials Science. CRC Press, Dec 2000. 0.

[24] B. Bhushan. *Modern Tribology Handbook.* The mechanics and materials science series. CRC Press, 2001.

[25] A. W. Batchelor G. W. Stachowiak and B. Grazyna. *Chapter 4 Classification of Wear Processes*, volume 10, pages 80 – 131. 1987. Microstructure and Wear of Materials.

[26] N. P. Suh. The delamination theory of wear. *Wear*, 25:111 – 124, 1973.

[27] R. Aghababaei, D. H. Warner, and J-F. Molinari. Critical length scale controls adhesive wear mechanisms. *Nature communications*, 7, 2016.

[28] V. Vahid, G. S. David, T. T. Kevin, and C. W. Robert. Mechanics of interaction and atomic-scale wear of amplitude modulation atomic force microscopy probes. *ACS Nano*, 7:3221–3235, 2013. PMID: 23506316.

[29] C. A. Brockley and G. K. Fleming. A model junction study of severe metallic wear. *Wear*, 8:374 – 380, 1965.

[30] G. W. Stachowiak and A. W. Batchelor. Chapter 11 - abrasive, erosive and cavitation wear in Engineering tribology. pages 525 – 576, 2014.

[31] E. Rabinowicz, L.A. Dunn, and P.G. Russell. A study of abrasive wear under three-body conditions. *Wear*, 4:345 – 355, 1961.

[32] E. Rabinowicz, L. A. Dunn, and P. G. Russell. A study of abrasive wear under three-body conditions. *Wear*, 4:345–355, 1961.

[33] L. Fang, W. Liu, D. Du, X. Zhang, and Q. Xue. Predicting three-body abrasive wear using monte carlo methods. *Wear*, 256:685–694, 2004.

[34] A. Sundström, R. José, and M. Olsson. Wear behaviour of some low alloyed steels under combined impact/abrasion contact conditions. *Wear*, 250:744–754, 2001.

[35] A. R. Chintha, K. Valtonen, V-T. Kuokkala, S. Kundu, M.J. Peet, and H.K.D.H. Bhadeshia. Role of fracture toughness in impact-abrasion wear. *Wear*, 2019.

[36] J. T. Xi, Q. D. Zhou, S. H. Liu, and G. S. Song. Influence of retained austenite on the wear resistance of high chromium cast iron under various impact loads. *Wear*, 162:83 – 88, 1993. Wear of Materials: Proceedings of the 9th International Conference.

[37] P. L. Hurricks. Some metallurgical factors controlling the adhesive and abrasive wear resistance of steels. a review. *Wear*, 26:285 – 304, 1973.

[38] A. Misra and I. Finnie. A review of the abrasive wear of metals. *Journal of Engineering Materials and Technology*, 104:94–101, 1982.

[39] M. A. Moore. A review of two-body abrasive wear. *Wear*, 27(1):1–17, 1974.

[40] T. H. C. Childs. The sliding wear mechanisms of metals, mainly steels. *Tribology international*, 13(6):285–293, 1980.

[41] J. D. Gates. Two-body and three-body abrasion: a critical discussion. *Wear*, 214(1):139–146, 1998.

[42] A. A. Torrance. Modelling abrasive wear. *Wear*, 258(1-4):281–293, 2005.

[43] G. Pintaude, E. Albertin, and A. Sinatora. A review on abrasive wear mechanisms of metallic materials. *Anais do abrasion*, 2005.

[44] P. J. Blau. Fifty years of research on the wear of metals. *Tribology International*, 30(5):321–331, 1997.

[45] E. Miyoshi, K. Azumi, T. Katou, Y. Ohmori, and M. Nakagawa. On the abrasion properties of steels by sand. *Tetsu-to-Hagane*, 51:2322–2327, 1965.

[46] R. C. D. Richardson. The maximum hardness of strained surfaces and the abrasive wear of metals and alloys. *Wear*, 10:353–382, 1967.

[47] K-H Zum Gahr. Wear by hard particles. *Tribology International*, 31(10):587–596, 1998.

[48] E. Rabinowicz and A. Mutis. Effect of abrasive particle size on wear. *Wear*, 8:381–390, 1965.

[49] M. Naim and S. Bahadur. Work hardening in erosion due to single-particle impacts. *Wear*, 98:15–26, 1984.

[50] S. L. Rice, H. Nowotny, and S. F. Wayne. Characteristics of metallic subsurface zones in sliding and impact wear. *Wear*, 74:131–142, 1981.

[51] V. Ratia, I. Miettunen, and V. T. Kuokkala. Surface deformation of steels in impact-abrasion: The effect of sample angle and test duration. *Wear*, 301:94 – 101, 2013. Wear of Materials 2013.

[52] R. D. Wilson and J. A. Hawk. Impeller wear impact-abrasive wear test. *Wear*, 225–229, Part 2:1248 – 1257, 1999.

[53] O. Haiko, M. Somani, D. Porter, P. Kantanen, J. Kömi, N. Ojala, and V. Heino. Comparison of impact-abrasive wear characteristics and performance of direct quenched (dq) and direct quenched and partitioned (dq&p) steels. *Wear*, 400:21–30, 2018.

[54] S. L. Rice, H. Nowotny, and S. F. Wayne. Formation of subsurface zones in impact wear. *Asle Transactions*, 24:264–268, 1981.

[55] S. L. Rice. Variations in wear resistance due to microstructural condition in high strength steel under repetitive impact. *TRIBOLOGY international*, 12(1):25–29, 1979.

[56] V. G. Efremenko, K. Shimizu, T. Noguchi, A. V. Efremenko, and Y. G. Chabak. Impact–abrasive–corrosion wear of fe-based alloys: Influence of microstructure and chemical composition upon wear resistance. *Wear*, 305(1-2):155–165, 2013.

[57] V. Rastegar and A. Karimi. Surface and subsurface deformation of wear-resistant steels exposed to impact wear. *Journal of materials engineering and performance*, 23:927–936, 2014.

[58] O. Haiko, I. Miettunen, D. Porter, N. Ojala, V. Ratia, V. Heino, and A. Kemppainen. Effect of finish rolling and quench stop temperatures on impact-abrasive wear resistance of 0.35% carbon direct-quenched steel. *Tribologia-Finnish Journal of Tribology*, 35(1–2):5–21, 2017.

[59] V. Ratia, H. Rojacz, J. Terva, K. Valtonen, E. Badisch, and V-T. Kuokkala. Effect of multiple impacts on the deformation of wear-resistant steels. *Tribology Letters*, 57(2):15, 2015.

[60] K. Hokkirigawa and K. Kato. An experimental and theoretical investigation of ploughing, cutting and wedge formation during abrasive wear. *Tribology international*, 21:51–57, 1988.

[61] T. O. Mulhearn and L. E. Samuels. The abrasion of metals: A model of the process. *Wear*, 5:478 – 498, 1962.

[62] M. J. Murray, P. J. Mutton, and J. D. Watson. Abrasive wear mechanisms in steels. *Journal of Lubrication Technology*, 104(1):9–16, 1982.

[63] N. P. Suh. The delamination theory of wear. *Wear*, 25(1):111–124, 1973.

[64] V. Javaheri, D. Porter, and V-T. Kuokkala. Slurry erosion of steel–review of tests, mechanisms and materials. *Wear*, 408:248–273, 2018.

[65] Y. Wang and Zhen-Guo Z. Yang. Finite element model of erosive wear on ductile and brittle materials. *Wear*, 265(5-6):871–878, 2008.

[66] J. Halling. Tribological properties of solid materials. In *Principles of Tribology*, pages 128–146. Springer, 1978.

[67] J. Rendón and M. Olsson. Abrasive wear resistance of some commercial abrasion resistant steels evaluated by laboratory test methods. *Wear*, 267:2055–2061, 2009.

[68] V. Ratia. Behavior of martensitic wear resistant steels in abrasion and impact wear testing conditions, 2015.

[69] G. J. Gore and J. D. Gates. Effect of hardness on three very different forms of wear. *Wear*, 203:544 – 563, 1997. 11th International Conference on Wear of Materials.

[70] J. A. Hawk, R. D. Wilson, J. H. Tylczak, and Ö. N. Doğan. Laboratory abrasive wear tests: investigation of test methods and alloy correlation. *Wear*, 225–229, Part 2:1031 – 1042, 1999.

[71] J. H. Tylczak, J. A. Hawk, and R. D. Wilson. A comparison of laboratory abrasion and field wear results. *Wear*, 225–229, Part 2:1059 – 1069, 1999.

[72] Arcelormittal. Yellow goods. http://usa.arcelormittal.com/what-we-do/markets/yellow-goods, 2018. Accessed: 2018-12-06.

[73] Venturi. Earth Moving Machines | Venturi Acciai: Hardox Weldox Strenx Steel. https://venturiacciai.it/en/market/earthmoving-machinery/, 2015. Accessed: 2018-12-06.

[74] S. Talaş. The assessment of carbon equivalent formulas in predicting the properties of steel weld metals. *Materials & Design (1980-2015)*, 31(5):2649–2653, 2010.

[75] H. K. D. H. Bhadeshia. Wear bucket. https://www.phase-trans.msm.cam.ac.uk/2010/Alberta/d/Pages/7.html, 2015. Accessed: 2018-12-06.

[76] A. J. Marshall. Raex wear resistant steel. http://www.ajmarshall.com/wp-content/uploads/2017/01/RAEX-Wear-Resistant-Steel.pdf. Accessed: 2017-07-02.

[77] V. Ratia, K. Valtonen, A. Kemppainen, and V. T. Kuokkala. High-stress abrasion and impact-abrasion testing of wear resistant steels. *Tribology Online*, 8:152–161, 2013.

[78] V. M. Glazkov, Y. D. Novomeiskii, and K. V. Savitskii. Nature of resistance to abrasive wear. *Soviet Physics Journal*, 12:1441–1444, 1969.

[79] I. M. Hutchings and P. Shipway. 6 - wear by hard particles. In I. M. Hutchings and P. Shipway, editors, *Tribology (Second Edition)*, pages 165 – 236. Butterworth-Heinemann, second edition edition, 2017.

[80] J. O. Everhart. Special wear-resisting materials for clay machinery parts. *Journal of the American Ceramic Society*, 21:69–72, 1938.

[81] I. Jiro. Study on abrasion resistance material against sand and slime in a rapid current of water and their hardface-welding (1st report). *Welding Society Journal*, 24:480–486, 1955.

[82] I. Jiro. Study on abrasion resistance material against sand and slime in a rapid current of water and their hardface-welding (3rd report). *Welding Society Journal*, 27:81–85, 1958.

[83] K-H. Zum Gahr. *Microstructure and wear of materials.* Tribology series. Elsevier, Amsterdam ; New York, 1987.

[84] D. Tabor. Mohs's hardness scale-a physical interpretation. *Proceedings of the Physical Society. Section B*, 67(3):249, 1954.

[85] M. Lindroos, K. Valtonen, A. Kemppainen, A. Laukkanen, K. Holmberg, and V. Kuokkala. Wear behavior and work hardening of high strength steels in high stress abrasion. *Wear*, 322–323:32 – 40, 2015.

[86] J. Rendón and M. Olsson. Abrasive wear resistance of some commercial abrasion resistant steels evaluated by laboratory test methods. *Wear*, 267:2055 – 2061, 2009. {ICAP} 2008.

[87] AE Giannakopoulos, P-L Larsson, and R Vestergaard. Analysis of vickers indentation. *International journal of solids and structures*, 31(19):2679–2708, 1994.

[88] P. J. Mutton and J. D. Watson. Some effects of microstructure on the abrasion resistance of metals. *Wear*, 48:385–398, 1978.

[89] K. S. Al-Rubaie. Equivalent hardness concept and two-body abrasion of iron-base alloys. *Wear*, 243:92–100, 2000.

[90] H. Sin, N. Saka, and N. P. Suh. Abrasive wear mechanisms and the grit size effect. *Wear*, 55:163–190, 1979.

[91] K. H. Z. Gahr and V. D. Doane. Optimizing fracture toughness and abrasion resistance in white cast irons. *Metallurgical Transactions A*, 11:613–620, Apr 1980.

[92] M. A. Moore. Abrasive wear. *International Journal of Materials in Engineering Applications*, 1:97–111, 1978.

[93] L. Xu, C. Vose, and D. S. John. Abrasive wear study of selected white cast irons as liner materials for the mining industry. *Wear*, 162:820 – 832, 1993.

[94] S. F. Sciezka and K. Filipowicz. An integrated testing method for cermet abrasion resistance and fracture toughness evaluation. *Wear*, 216:202 – 212, 1998.

[95] R. G. Bayer. Fundamentals of wear failures. *Materials Park, OH: ASM International, 2002.*, pages 901–905, 2002.

[96] A. A. Torrance. Modelling abrasive wear. *Wear*, 258:281 – 293, 2005. Second International Conference on Erosive and Abrasive Wear.

[97] H. Uetz and J. Föhl. Wear as an energy transformation process. *Wear*, 49:253–264, 1978.

[98] E. Hornbogen. The role of fracture toughness in the wear of metals. *Wear*, 33:251–259, 1975.

[99] M. A. Moore and R. M. Douthwaite. Plastic deformation below worn surfaces. *Metallurgical Transactions A*, 7:1833–1839, 1976.

[100] V. S. Popov, P. L. Nagornyi, A. B. Shumikin, V. A. Guk, and S. M. Popov. Relation between the energy capacity of metals and alloys and their resistance to abrasive wear. *Strength of Materials*, 3:1114–1119, 1971.

[101] K-H. G. Gahr and G. T. Eldis. Abrasive wear of white cast irons. *Wear*, 64:175–194, 1980.

[102] A. Leiro, E. Vuorinen, K. G. Sundin, B. Prakash, T. Sourmail, V. Smanio, F. G. Caballero, C. G. Mateo, and R. Elvira. Wear of nano-structured carbide-free bainitic steels under dry rolling–sliding conditions. *Wear*, 298:42–47, 2013.

[103] W. M. Garrison Jr and R. A. Garriga. Ductility and the abrasive wear of an ultrahigh strength steel. *Wear*, 85:347–360, 1983.

[104] N. Ojala, K. Valtonen, V. Heino, M. Kallio, J. Aaltonen, P. Siitonen, and V. T. Kuokkala. Effects of composition and microstructure on the abrasive wear performance of quenched wear resistant steels. 317:225–232.

[105] H. Nakayo and H. Kuniji. Surfaces of carbon steel worn by foundry sand. *Casting*, 36:102–111, 1964.

[106] C. Chattopadhyay, S. Sangal, K. Mondal, and A. Garg. Improved wear resistance of medium carbon microalloyed bainitic steels. *Wear*, 289:168–179, 2012.

[107] S. L. Rice. The role of microstructure in the impact wear of two aluminum alloys. *Wear*, 54(2):291–301, 1979.

[108] S. F. Wayne, S. L. Rice, K. Minakawa, and H. Nowotny. The role of microstructure in the wear of selected steels. *Wear*, 85(1):93–106, 1983.

[109] F. Hu, K. M. Wu, and P. D. Hodgson. Effect of retained austenite on wear resistance of nanostructured dual phase steels. *Materials Science and Technology*, 32(1):40–48, 2016.

[110] G. H. Yang and W. M. Garrison Jr. A comparison of microstructural effects on two-body and three-body abrasive wear. *Wear*, 129(1):93–103, 1989.

[111] T. Jian-Min, Z. Yi-Zhong, S. Tian-Yi, and D. Hai-Jin. The influence of retained austenite in high chromium cast iron on impact-abrasive wear. *Wear*, 135(2):217–226, 1990.

[112] L. C. Cheng, T. B. Wu, and C. T. Hu. The role of microstructural features in abrasive wear of a d-2 tool steel. *Journal of materials science*, 23(5):1610–1614, 1988.

[113] J. Siepak. The influence of contact stress on the wear of a carburized steel case with a high content of retained austenite. *Wear*, 80(3):301–305, 1982.

[114] X. Jun-Tong, Z. Qing-De, L. Shi-Hui, and S. Guang-Shun. Influence of retained austenite on the wear resistance of high chromium cast iron under various impact loads. *Wear*, 162:83–88, 1993.

[115] V. F. Da Silva, L. F. Canale, D. Spinelli, W. W. Bose-Filho, and O. R. Crnkovic. Influence of retained austenite on short fatigue crack growth and wear resistance of case carburized steel. *Journal of materials engineering and performance*, 8(5):543–548, 1999.

[116] L. C. Chang. The rolling/sliding wear performance of high silicon carbide-free bainitic steels. *Wear*, 258(5-6):730–743, 2005.

[117] K. Hyung-Jun and K. Young-Gak. The effects of retained austenite on dry sliding wear behavior of carburized steels. *Wear*, 193(1):8–15, 1996.

[118] V. Ratia, I. Miettunen, and V. T. Kuokkala. Surface deformation of steels in impact-abrasion: the effect of sample angle and test duration. *Wear*, 301:94–101, 2013.

[119] W. Wang, R. Song, S. Peng, and Z. Pei. Multiphase steel with improved impact-abrasive wear resistance in comparison with conventional hadfield steel. *Materials & Design*, 105:96–105, 2016.

[120] Weilin Yan, Liang Fang, Kun Sun, and Yunhua Xu. Effect of surface work hardening on wear behavior of hadfield steel. *Materials Science and Engineering: A*, 460:542–549, 2007.

[121] H. Chen, D. Zhao, Q. Wang, Y. Qiang, and Ji. Qi. Effects of impact energy on the wear resistance and work hardening mechanism of medium manganese austenitic steel. *Friction*, 5(4):447–454, 2017.

[122] J. Jae-Eun and L. Young-Kook. Strain hardening behavior of a fe–18mn–0.6 c–1.5 al twip steel. *Materials Science and Engineering: A*, 527(1-2):157–161, 2009.

[123] A. Leiro, A. Kankanala, E. Vuorinen, and B. Prakash. Tribological behaviour of carbide-free bainitic steel under dry rolling/sliding conditions. *Wear*, 273:2 – 8, 2011. Selected papers from 14th Nordic Symposium on Tribology, {NORDTRIB} 2010.

[124] S. Hernandez, A. Leiro, M. R. Ripoll, E. Vuorinen, K. G. Sundin, and B. Prakash. High temperature three-body abrasive wear of 0.25c 1.42si steel with carbide free bainitic (cfb) and martensitic microstructures. *Wear*, 360:21 – 28, 2016.

[125] H. K. D. H. Bhadeshia. *Bainite in steels: theory and practice.* Maney Publishing, 2015.

[126] T. Sourmail, F. G. Caballero, C. García-Mateo, V. Smanio, C. Ziegler, M. Kuntz, R. Elvira, A. Leiro, E. Vuorinen, and T. Teeri. Evaluation of potential of high si high c steel nanostructured bainite for wear and fatigue applications. *Materials Science and Technology*, 29(10):1166–1173, 2013.

[127] S. D. Bakshi, A. Leiro, B. Prakash, and H. K. D. H Bhadeshia. Dry rolling/sliding wear of nanostructured bainite. *Wear*, 316:70–78, 2014.

[128] P. H. Shipway, S. J. Wood, and A. H. Dent. The hardness and sliding wear behaviour of a bainitic steel. *Wear*, 203:196–205, 1997.

[129] R. Devanathan and P. Clayton. Rolling-sliding wear behavior of three bainitic steels. *Wear*, 151:255 – 267, 1991.

[130] L. Ambrosini and S. Bahadur. Erosion of aisi 4140 steel. *Wear*, 117:37–48, 1987.

[131] E. Vuorinen, N. Ojala, V. Heino, C. Rau, and C. Gahm. Erosive and abrasive wear performance of carbide free bainitic steels – comparison of field and laboratory experiments. *Tribology International*, 98:108 – 115, 2016.

[132] A. M. Gola, M. Ghadamgahi, and S. W. Ooi. Microstructure evolution of carbide-free bainitic steels under abrasive wear conditions. *Wear*, 376:975–982, 2017.

[133] R. Rementeria, I. García, M. M. Aranda, and F. G. Caballero. Reciprocating-sliding wear behavior of nanostructured and ultra-fine high-silicon bainitic steels. *Wear*, 338–339:202 – 209, 2015.

[134] R. Rementeria, M. M. Aranda, C. Garcia-Mateo, and F. G. Caballero. Improving wear resistance of steels through nanocrystalline structures obtained by bainitic transformation. *Materials Science and Technology*, 32(4):308–312, 2016.

[135] E. Vuorinen, N. Ojala, V. Heino, C. Rau, and C. Gahm. Erosive and abrasive wear performance of carbide free bainitic steels–comparison of field and laboratory experiments. *Tribology International*, 98:108–115, 2016.

[136] L. C. Chang. The rolling and sliding wear performance of high silicon carbide-free bainitic steels. *Wear*, 258:730 – 743, 2005.

[137] A. Ninham. The effect of mechanical properties on erosion. *Wear*, 121:307–324, 1988.

[138] A. M. El-Rakayby and B. Mills. The role of primary carbides in the wear of high speed steels. *Wear*, 112:327–340, 1986.

[139] L. Xu, S. Wei, F. Xiao, H. Zhou, G. Zhang, and J. Li. Effects of carbides on abrasive wear properties and failure behaviours of high speed steels with different alloy element content. *Wear*, 376:968–974, 2017.

[140] E. Wen, R. Song, and W. Xiong. Effect of tempering temperature on microstructures and wear behavior of a 500 hb grade wear-resistant steel. *Metals*, 9(1):45, 2019.

[141] X. T. Deng, T. L. Fu, Z. D. Wang, R. D. K. Misra, and G. D. Wang. Epsilon carbide precipitation and wear behaviour of low alloy wear resistant steels. *Materials Science and Technology*, 32:320–327, 2016.

[142] W. J. Salesky and G. Thomas. Medium carbon steel alloy design for wear applications. *Wear*, 75:21–40, 1982.

[143] L. M. Clarebrough, M. E. Hargreaves, and M. H. Loretto. The influence of grain size on the stored energy and mechanical properties of copper. *Acta Metallurgica*, 6:725–735, 1958.

[144] M. A. Moore, R. C. D. Richardson, and D. G. Attwood. The limiting strength of worn metal surfaces. *Metallurgical transactions*, 3:2485–2491, 1972.

[145] K. S. Cheoul, L. J. Young, and K. D. Youg. Abrasion resistance study of austenite high mn steel. *Journal of Materials Science*, 14:241–249, 1976.

[146] V. N. Kashcheev. Some aspects of improving abrasive resistance. *Wear*, 89:265–272, 1983.

[147] S. Gündüz, R. Kaçar, and H. S. Soykan. Wear behaviour of forging steels with different microstructure during dry sliding.

[148] Y. Prawoto, N. Jasmawati, and K. Sumeru. Effect of prior austenite grain size on the morphology and mechanical properties of martensite in medium carbon steel. *Journal of Materials Science & Technology*, 28(5):461–466, 2012.

[149] S. Chatterjee and H. K. D. H. Bhadeshia. Trip-assisted steels: cracking of high-carbon martensite. *Materials Science and Technology*, 22:645–649, 2006.

[150] J. Kömi, P. Karjalainen, and D. Porter. Direct-quenched structural steels. In *Encycl. Iron, Steel Their Alloy*, pages 1109–1125. CRC Press Boca Raton, 2016.

[151] T. Hanamura, S. Torizuka, S. Tamura, S. Enokida, and H. Takechi. Effect of austenite grain size on transformation behavior, microstructure and mechanical proper ties of 0.1 C–5Mn martensitic steel. *ISIJ international*, 53:2218–2225, 2013.

[152] J. Hidalgo and M. J. Santofimia. Effect of prior austenite grain size refinement by thermal cycling on the microstructural features of as-quenched lath martensite. *Metallurgical and Materials Transactions A*, 47:5288–5301, 2016.

[153] H. F. Lan, LX. Du, Q. Li, C. L. Qiu, J. P. Li, and R. D. K. Misra. Improvement of strength-toughness combination in austempered low carbon bainitic steel: The key role of refining prior austenite grain size. *Journal of Alloys and Compounds*, 710:702–710, 2017.

[154] S. D. Bakshi. Wear of fine pearlite, nanostructured bainite and martensite. *PhD Thesis*, 2016.

[155] I. R. Sare, J. I. Mardel, and A. J. Hill. Wear-resistant metallic and elastomeric materials in the mining and mineral processing industries—an overview. *Wear*, 250:1–10, 2001.

[156] K. Singh, R. K. Khatirkar, and S. G. Sapate. Microstructure evolution and abrasive wear behavior of d2 steel. *Wear*, 328:206–216, 2015.

[157] MASTEEL. Mas ar abrasion resistant steel. https://masteel.co.uk/2017/01/31/mas500-ar/. Accessed: 2018-12-06.

[158] Voestalpine. Durostata wear resistance steels. http://www.voestalpine.com/stahl/en/Products/Brand-names/durostat-R. Accessed: 2018-12-06.

[159] Chapelsteel. Wear resistance steels. https://www.chapelsteel.com/ar400-ar360.html. Accessed: 2018-12-06.

[160] Matweb. Wear resistance steels. http://www.matweb.com/. Accessed: 2018-12-06.

[161] Dillinger. Wear resistance steels. https://www.dillinger.de. Accessed: 2018-12-06.

[162] SSAB. Wear resistance steels. http://www.ssab.co.uk. Accessed: 2018-12-06.

[163] Thyssenkrupp. Wear resistance steels. https://www.thyssenkrupp-steel.com/en/products/heavy-plate/wear-resistant-steel/xar/productpage-xar.html. Accessed: 2018-12-06.

[164] Quard400. Wear resistance steels. https://jola.nl. Accessed: 2018-12-06.

[165] Wear resistance steels. https://www.tatasteeleurope.com. Accessed: 2018-12-06.

[166] C. Rimando. Everhard steel. http://www.australiansteel.com.au/wear-plates/everhard-steel/. Accessed: 2018-12-06.

[167] Brownmac. Abrasion resistant steel - brown mcfarlane. https://www.brownmac.com/en/products/abrasion-resistant-steel. Accessed: 2018-12-06.

[168] Wear resistance steels. http://www.abrexplates.com/. Accessed: 2018-12-06.

[169] J. Kalousek, D. M. Fegredo, and E. E. Laufer. The wear resistance and worn metallography of pearlite, bainite and tempered martensite rail steel microstructures of high hardness. *Wear*, 105:199 – 222, 1985.

[170] P. Clayton and R. Devanathan. Rolling/sliding wear behavior of a chromium-molybdenum rail steel in pearlitic and bainitic conditions. *Wear*, 156:121 – 131, 1992.

[171] H. K. D. H. Bhadeshia and Institute Of Materials. *Bainite in steels*. Institute of Materials London, 1992.

[172] Y. L. Yang, C. H. Yang, S. N. Lin, C. H. Chen, and W. T. Tsai. Effects of Si and its content on the scale formation on hot-rolled steel strips. *Materials Chemistry and Physics*, 112:566–571, 2008.

[173] F. Hanguang, X. Qiang, and Y. Li. A study of the microstructures and properties of fe–v–w–mo alloy modified by rare earth. *Materials Science and Engineering: A*, 395:281 – 287, 2005.

[174] A. K. Bhakat, A. K. Mishra, and N. S. Mishra. Characterization of wear and metallurgical properties for development of agricultural grade steel suitable in specific soil conditions. *Wear*, 263:228–233, 2007.

[175] A. K. Bhakat, A. K. Mishra, N. S. Mishra, and S. Jha. Metallurgical life cycle assessment through prediction of wear for agricultural grade steel. *Wear*, 257:338–346, 2004.

[176] J. Xu and Y. T. Yang. Comprehensive influence of cr and si on hardness and wear resistance of cold roll steel. In *Advanced Materials Research*, volume 476, pages 334–339. Trans Tech Publ, 2012.

[177] Y. J. Kang, J. C. Oh, H. C. L., and S. Lee. Effects of carbon and chromium additions on the wear resistance and surface roughness of cast high-speed steel rolls. *Metallurgical and Materials Transactions A*, 32(10):2515–2525, 2001.

[178] B. W. E Avient, J. Goddard, and H. Wilman. An experimental study of friction and wear during abrasion of metals. *Proc. R. Soc. Lond. A*, 258:159–180, 1960.

[179] I. I. Garbar. Abrasion resistance as a function of substructural changes in steel. *Wear*, 258:275–280, 2005.

[180] G. K. Nathan and W. J. D. Jones. The empirical relationship between abrasive wear and the applied conditions. *Wear*, 9:300–309, 1966.

[181] J. Larsen-Badse. Influence of grit size on the groove formation during sliding abrasion. *Wear*, 11:213–222, 1968.

[182] J. Larsen-Badse. Abrasion resistance of some sap-type alloys at room temperature. *Wear*, 12:357–368, 1968.

[183] J. E. Goodwin, W. Sage, and G. P. Tilly. Study of erosion by solid particles. *Proceedings of the Institution of Mechanical Engineers*, 184:279–292, 1969.

[184] S. W. Date and S. Malkin. Effects of grit size on abrasion with coated abrasives. *Wear*, 40:223–235, 1976.

[185] H. H. Tian and G. R. Addie. Experimental study on erosive wear of some metallic materials using coriolis wear testing approach. *Wear*, 258:458–469, 2005.

[186] A. Misra and I. Finnie. On the size effect in abrasive and erosive wear. *Wear*, 65:359 – 373, 1981.

[187] A. Misra and I. Finnie. Some observations on two-body abrasive wear. *Wear*, 68:41–56, 1981.

[188] J. Jiang, F. Sheng, and F. Ren. Modelling of two-body abrasive wear under multiple contact conditions. *Wear*, 217:35–45, 1998.

[189] T. Sasada, M. Oike, and N. Emori. The effect of abrasive grain size on the transition between abrasive and adhesive wear. *Wear*, 97:291–302, 1984.

[190] R. Gåhlin and S. Jacobson. The particle size effect in abrasion studied by controlled abrasive surfaces. *Wear*, 224:118–125, 1999.

[191] I. Sevim and I. B. Eryurek. Effect of fracture toughness on abrasive wear resistance of steels. *Materials & Design*, 27:911 – 919, 2006.

[192] D. V. De Pellegrin, A. A. Torrance, and E. Haran. Wear mechanisms and scale effects in two-body abrasion. *Wear*, 266:13–20, 2009.

[193] G. Tressia, J. J. Penagos, and A. Sinatora. Effect of abrasive particle size on slurry abrasion resistance of austenitic and martensitic steels. *Wear*, 376:63–69, 2017.

[194] I. Sevim and I. B. Eryurek. Effect of abrasive particle size on wear resistance in steels. *Materials & design*, 27:173–181, 2006.

[195] J. Goddard and H. Wilman. A theory of friction and wear during the abrasion of metals. *Wear*, 5:114–135, 1962.

[196] J. Goddard, H. J. Harker, and H. Wilman. A theory of the abrasion of solids such as metals. *Nature*, 184:333, 1959.

[197] S. Malkin, K. L. Wiggins, M. Osman, and R. W. Smalling. Size effects in abrasive processes. In *Proceedings of the Thirteenth International Machine Tool Design and Research Conference*, pages 291–296. Springer, 1973.

[198] M. R. Thakare, J. A. Wharton, R. J. K. Wood, and C. Menger. Effect of abrasive particle size and the influence of microstructure on the wear mechanisms in wear-resistant materials. *Wear*, 276:16–28, 2012.

[199] A. Misra and I. Finnie. On the size effect in abrasive and erosive wear. *Wear*, 65(3):359–373, 1981.

[200] I. Finnie. Some reflections on the past and future of erosion. *Wear*, 186:1–10, 1995.

[201] H. M. Clark and R. B. Hartwich. A re-examination of the 'particle size effect'in slurry erosion. *Wear*, 248(1-2):147–161, 2001.

[202] R. S. Lynn, K. K. Wong, and H. M. Clark. On the particle size effect in slurry erosion. *Wear*, 149(1-2):55–71, 1991.

[203] D. J. O'Flynn, M. S Bingley, M. S. A Bradley, and A. J Burnett. A model to predict the solid particle erosion rate of metals and its assessment using heat-treated steels. *Wear*, 248:162 – 177, 2001.

[204] G. E. Dieter. *Mechanical Metallurgy*. McGraw-Hill, London, UK, 1988.

[205] K-H Zum Gahr. Modelling of two-body abrasive wear. *Wear*, 124(1):87–103, 1988.

[206] A. A. Torrance. A three-dimensional cutting criterion for abrasion. *Wear*, 123(1):87–96, 1988.

[207] A. Khellouki, J. Rech, and H. Zahouani. Micro-scale investigation on belt finishing cutting mechanisms by scratch tests. *Wear*, 308:17–28, 2013.

[208] A. S. Geoffrey. Hardness tests research: Some practical aspects of the scratch test for hardness. *Proceedings of the Institution of Mechanical Engineers*, 108:647–687, 1925.

[209] H. R. Shetty, T. H. Kosel, and N. F. Fiore. A study of abrasive wear mechanisms using diamond and alumina scratch tests. *Wear*, 80:347–376, 1982.

[210] A. J Sedriks and T. O. Mulhearn. Mechanics of cutting and rubbing in simulated abrasive processes. *Wear*, 6:457–466, 1963.

[211] A. J. Sedriks and T. O. Mulhearn. The effect of work-hardening on the mechanics of cutting in simulated abrasive processes. *Wear*, 7:451–459, 1964.

[212] M. Peet and H. K. D. H. Bhadeshia. Development of very hard and tough steel ever produced. *Unpublished work*, 2015.

[213] K. G. Budinski. *Guide to friction, wear and erosion testing*. ASTM International West Conshohocken, PA, 2007.

[214] *ASTM G65-16 Standard Test Method for Measuring Abrasion Using the Dry Sand/Rubber Wheel Apparatus ASTM International, West Conshohocken, PA*. 2016.

[215] J. A. Hawk and R. D. Wilson. chapter 35 tribology of earthmoving mining and minerals processing, modern tribology handbook, editor b. bhusan, volumes 1-2, 2001.

[216] E. Badisch, S. Ilo, and R. Polak. Multivariable modeling of impact-abrasion wear rates in metal matrix-carbide composite materials. *Tribology Letters*, 36:55–62, 2009.

[217] H. K. D. H. Bhadeshia. *Bainite in steels: theory and practice.* CRC Press, 2019.

[218] V. A. Yardley. *Magnetic detection of microstructural change in power plant steels.* PhD thesis, University of Cambridge, 2003.

[219] J. W. Morris Jr, C. Kinney, K. Pytlewski, and Y. Adachi. Microstructure and cleavage in lath martensitic steels. *Science and technology of advanced materials*, 14(1):014208, 2013.

[220] A-F Gourgues-Lorenzon. Application of electron backscatter diffraction to the study of phase transformations. *International Materials Reviews*, 52:65–128, 2007.

[221] M. Peet. Program MAP_steel_ms_empirical_2014. *Phase Transformations & Complex Properties Research Group.*

[222] D. P. Koistinen and R. E. Marburger. A general equation prescribing the extent of the austenite-martensite transformation in pure iron-carbon alloys and plain carbon steels. *Acta Metallurgica*, 7:59 – 60, 1959.

[223] V. Ratia, K. Valtonen, and V. T. Kuokkala. Impact-abrasion wear of wear-resistant steels at perpendicular and tilted angles. *Proceedings of the Institution of Mechanical Engineers, Part J: Journal of Engineering Tribology*, 227:868–877, 2013.

[224] K. Valtonen. Relevance of Laboratory Wear Experiments for the Evaluation of In-Service Performance of Materials. Tampere University of Technology, 11 2018.

[225] K. Valtonen, V. Ratia, N. Ojala, and V-T Kuokkala. Comparison of laboratory wear test results with the in-service performance of cutting edges of loader buckets. *Wear*, 388:93–100, 2017.

[226] N. P. Suh. An overview of the delamination theory of wear. *Wear*, 44:1–16, 1977.

[227] B. S. Chahar and A. K. P. Siddhartha. Erosion wear of ductile materials: A review.

[228] V. Heino, K. Valtonen, P. Kivikytö-Reponen, P. Siitonen, and V-T. Kuokkala. Characterization of the effects of embedded quartz layer on wear rates in abrasive wear. *Wear*, 308(1-2):174–179, 2013.

[229] M. Woldman, E. van der Heide, D. J. Schipper, T. Tinga, and M. A. Masen. Investigating the influence of sand particle properties on abrasive wear behaviour. *Wear*, 294-295:419 – 426, 2012.

[230] G. B. Stachowiak and G. W. Stachowiak. The effects of particle characteristics on three-body abrasive wear. *Wear*, 249(3-4):201–207, 2001.

[231] G. W. Stachowiak. Numerical characterization of wear particles morphology and angularity of particles and surfaces. *Tribology International*, 31(1-3):139–157, 1998.

[232] A. A. Torrance. The effect of grit size and asperity blunting on abrasive wear. *wear*, 253(7-8):813–819, 2002.

[233] P. Kulu, V. Mikli, H. Kaerdi, and M. Besterci. Angularity evaluation of milled wc-co powder. *International Journal of Materials and Product Technology*, 22(4):289–298, 2005.

[234] D. Balzar, N. Audebrand, M. R. Daymond, A. Fitch, A. Hewat, J. I. Langford, A. L. Bail, D. Louër, O. Masson, C. N. McCowan, et al. Size–strain line-broadening analysis of the ceria round-robin sample. *Journal of Applied Crystallography*, 37(6):911–924, 2004.

[235] T. Ungár and J. Gubicza. Grain size, size-distribution and dislocation structure from diffraction peak profile analysis. 2002.

[236] S. A. Speakman. Estimating crystallite size using xrd. *MIT Center for Materials Science and Engineering*, pages 03–08, 2014.

[237] E. Sakher, N. Loudjani, M. Benchiheub, and M. Bououdina. Influence of milling time on structural and microstructural parameters of ni50ti50 prepared by mechanical alloying using rietveld analysis. *Journal of Nanomaterials*, 2018, 2018.

[238] J-O. Andersson, T. Helander, L. Höglund, P. Shi, and B. Sundman. Thermo-calc & dictra, computational tools for materials science. *Calphad*, 26(2):273–312, 2002.

[239] R. Hossain, F. Pahlevani, and V. Sahajwalla. Effect of small addition of cr on stability of retained austenite in high carbon steel. *Materials Characterization*, 125:114–122, 2017.

[240] X. Xu, F. H. Ederveen, S. v. d. Zwaag, and W. Xu. Correlating the abrasion resistance of low alloy steels to the standard mechanical properties: A statistical analysis over a larger data set. *Wear*, 368–369:92 – 100, 2016.

[241] P. A. Cundall and O. D. Strack. A discrete numerical model for granular assemblies. *geotechnique*, 29(1):47–65, 1979.

[242] E. Maire and P. J. Withers. Quantitative x-ray tomography. *International materials reviews*, 59(1):1–43, 2014.

[243] L. H. Chen. Deformation, transfer and debris formation during sliding wear of metals. *Scripta Metallurgica et Materialia*, 24:827–832, 1990.

[244] A. R. Rosenfield. A shear instability model of sliding wear. *Wear*, 116:319–328, 1987.

[245] P. L. Menezes, S. V Kailas, et al. Subsurface deformation and the role of surface texture—a study with cu pins and steel plates. *Sadhana*, 33:191, 2008.

[246] Hüseyin Çimenoğlu. Subsurface characteristics of an abraded low carbon steel. *Wear*, 210:204–210, 1997.

[247] D. A. Rigney. Viewpoint set on materials aspects of wear—introduction. *Scripta Metallurgica et Materialia*, 24:799–803, 1990.

[248] A. R. Rosenfield. A dislocation theory approach to wear. *Wear*, 72:97–103, 1981.